

# Gauge fixing for the simulation of black hole spacetimes

Dissertation  
zur Erlangung des Grades eines Doktors  
der Naturwissenschaften  
der Fakultät für Mathematik und Physik  
der Eberhard-Karls-Universität zu Tübingen

vorgelegt von  
Erik Schnetter  
aus Letmathe

2003

Tag der mündlichen Prüfung: 13. Juni 2003  
Dekan: Prof. Dr. Herbert Mütter  
1. Berichterstatter: Prof. Dr. Hanns Ruder  
2. Berichterstatter: Priv.-Doz. Dr. Jörg Frauendiener

# Abstract

I consider the initial-boundary-value-problem of nonlinear general relativistic vacuum spacetimes, which today cannot yet be evolved numerically in a satisfactory manner. Specifically, I look at gauge conditions, classifying them into gauge evolution conditions and gauge fixing conditions. In this terminology, a gauge fixing condition is a condition that removes all gauge degrees of freedom from a system, whereas a gauge evolution condition determines only the time evolution of the gauge condition, while the gauge condition itself remains unspecified. I find that most of today's gauge conditions are only gauge evolution conditions.

I present a system of evolution equations containing a gauge fixing condition, and describe an efficient numerical implementation using constrained evolution. I examine the numerical behaviour of this system for several test problems, such as linear gravitational waves or nonlinear gauge waves. I find that the system is robustly stable and second-order convergent. I then apply it to more realistic configurations, such as Brill waves or single black holes, where the system is also stable and accurate.



# Acknowledgements

I have greatly enjoyed all the research that has gone into this thesis. This enjoyment comes not least from the interaction that I have had with my supervisors and colleagues, and the liberal and inspiring atmospheres that they created in their departments.

It was certainly luck that brought me to the Institut für Theoretische Astrophysik in Tübingen. In countless discussions with my colleagues I there learned the joy that lies in academic discourse and in the discovery of new and old ideas. My supervisor Hanns Ruder has the rare ability of capturing his listeners' whole attention by explaining physics in a most interesting manner. He also encouraged me to spend some time abroad.

The Deutsche Akademische Austauschdienst then granted me a stipend that allowed me to spend one year with Pablo Laguna at the Department of Astronomy in Penn State. He introduced me to numerical relativity, his research inspired the topic of this thesis, and his Latin mentality taught me how to defend my ideas. Mijan Huq and Deirdre Shoemaker patiently answered my questions, and I had many interesting discussions with my fellow students Bernard Kelly and Ken Smith, especially on Thursdays.

After returning to Tübingen, Hanns Ruder gave me very generous financial support, and also gave me the paternal nudging that is necessary to finish a thesis. I would also like to thank Jörg Frauendiener and Ute Kraus for their competent advice, and Daniel Kobras and Stefan Kunze for making the important hardware in our department work.

It is almost by their nature that these acknowledgements are incomplete, and I apologise to the many people whom I have to thank in person instead.



# Contents

<b>Abstract</b>	<b>3</b>
<b>Acknowledgements</b>	<b>5</b>
<b>Table of contents</b>	<b>7</b>
<b>1 Introduction</b>	<b>11</b>
<b>2 Simulating spacetimes</b>	<b>13</b>
2.1 The ADM formalism . . . . .	13
2.2 Constrained evolution . . . . .	14
2.3 Picturing spacetimes . . . . .	14
2.4 Interpreting the quantities . . . . .	17
2.5 Instabilities . . . . .	18
2.6 My goal in this thesis . . . . .	19
<b>3 Gauge conditions</b>	<b>21</b>
3.1 Common gauge conditions . . . . .	21
3.2 Gauge evolution and gauge fixing . . . . .	22
3.3 Good gauge fixing conditions . . . . .	23
3.4 My gauge fixing condition . . . . .	24
<b>4 The system of equations</b>	<b>27</b>
4.1 The variables . . . . .	27
4.2 Enforcing the gauge and the constraints . . . . .	28
<b>5 Boundary conditions</b>	<b>29</b>
5.1 Outer boundary . . . . .	29
5.1.1 Location of the outer boundary . . . . .	29
5.1.2 Physical boundary conditions . . . . .	29
5.1.3 Periodicity . . . . .	30
5.1.4 Gauge and constraint boundary conditions . . . . .	31
5.2 Excision boundary . . . . .	32
5.2.1 Location and shape of the excision boundary . . . . .	33
5.2.2 Boundary conditions . . . . .	34

## Contents

<b>6</b>	<b>Initial data</b>	<b>37</b>
6.1	Data without black holes . . . . .	37
6.1.1	Minkowski metric (flat space) . . . . .	37
6.1.2	Weak Bondi wave (linear planar wave) . . . . .	37
6.1.3	Gauge pulse (nonlinear planar gauge wave) . . . . .	38
6.1.4	Brill wave . . . . .	39
6.2	Single black hole data . . . . .	39
6.2.1	Kerr–Schild coordinates . . . . .	39
6.2.2	Painlevé–Gullstrand coordinates . . . . .	40
6.2.3	Harmonic coordinates . . . . .	41
6.2.4	Coordinate transformations . . . . .	41
6.3	Multiple black hole data . . . . .	43
6.3.1	Brill–Lindquist data . . . . .	43
6.3.2	Superposed Kerr–Schild data . . . . .	43
<b>7</b>	<b>Code</b>	<b>45</b>
7.1	The Tiger code . . . . .	45
7.2	Initial data . . . . .	46
7.3	Constraint solvers . . . . .	46
7.4	Time integration . . . . .	47
7.5	Boundary conditions . . . . .	47
7.5.1	Outer boundary . . . . .	47
7.5.2	Excision boundary . . . . .	47
7.6	Analysis routines . . . . .	48
<b>8</b>	<b>Results</b>	<b>49</b>
8.1	Convergence tests . . . . .	49
8.1.1	Static and stationary tests: black holes . . . . .	49
8.1.2	Dynamic linear test: weak Bondi wave . . . . .	54
8.1.3	Dynamic nonlinear test: gauge pulse . . . . .	57
8.2	Stability test . . . . .	59
8.3	Brill wave . . . . .	61
8.4	Kerr–Schild black hole . . . . .	71
<b>9</b>	<b>Conclusion</b>	<b>75</b>
<b>A</b>	<b>Equations</b>	<b>77</b>
A.1	The ADM formalism . . . . .	77
A.1.1	Variables . . . . .	77
A.1.2	Time evolution . . . . .	78
A.1.3	Ricci tensor . . . . .	78
A.1.4	Constraints . . . . .	78
A.2	The TGR system . . . . .	79
A.2.1	Variables . . . . .	79
A.2.2	Time evolution . . . . .	79
A.2.3	Constraints . . . . .	81
A.2.4	Enforcing the constraints . . . . .	81



A.2.5	Gauge condition . . . . .	81
A.2.6	Enforcing the gauge condition . . . . .	82
A.2.7	Determining lapse and shift . . . . .	82
<b>B</b>	<b>Numerics</b>	<b>83</b>
B.1	Spatial discretisation . . . . .	83
B.2	Time integration . . . . .	83
B.2.1	Artificial viscosity . . . . .	84
B.3	Elliptic integration . . . . .	84
B.3.1	Variable transformations . . . . .	85
B.3.2	Elliptic solvers . . . . .	86
B.4	Coding equations . . . . .	86
<b>C</b>	<b>Definitions</b>	<b>89</b>
C.1	Glossary of terms . . . . .	89
C.2	Abbreviations . . . . .	90
C.3	Symbols . . . . .	90
	<b>Bibliography</b>	<b>93</b>

*Contents*

# 1 Introduction

I want to simulate spacetimes containing black holes.

I am not alone with this project; it has a long history. This was the goal of the Binary Black Hole Coalescence Grand Challenge in the USA, and is also part of the programme of the SFB 382 in Germany which pays my salary. One wants to numerically simulate spacetimes that contain singularities, where the spacetimes are time-dependent and have no symmetries that reduce the dimensionality, and where no approximations are possible to simplify the nonlinear equations.

Such calculations are often justified by referring to gravitational wave detectors such as GEO 600, LIGO, or LISA, which will soon produce data which then need to be compared to theoretical calculations. I, however, think that the ability to and the knowledge how to simulate fully generic spacetimes have value in itself and need no further justification.

The two major problems that one encounters today when simulating spacetimes are the computational expense and numerical instabilities. Three-dimensional time-dependent simulations always produce much data, and always need supercomputers to run on. Supercomputers are awkward to use, and it is time-consuming to experiment and try new ideas.

The numerical instabilities that are encountered in spacetime simulations are a problem of a different kind. For many years now, simulations have been plagued by instabilities of unknown origin. Simulations run fine for some time, but in many cases they encounter an unphysical and poorly understood unbounded growth.

Many approaches have been tried to find a cure for these instabilities. People have blamed the formulation of the equations, the boundary conditions, the gauge conditions, and the discretisation methods. It is clear that errors in any of these can cause a simulation to fail. The only successful methods to remove the instabilities known today rely on a combination of several steps that seem to be random, looking like a magician's recipe, and can only be justified after the fact. While it is now possible e.g. to evolve a static black hole for a long time, or to run a black hole collision for a reasonable time, the overall situation is still far from satisfactory (see e.g. [SY02]).

In this thesis I look at gauge conditions, which are one of the possible causes of instabilities mentioned above. I distinguish between *gauge fixing* and *gauge evolution* conditions. Gauge fixing conditions are "real" gauge conditions, whereas the weaker gauge evolution conditions describe only the time evolution of an (unspecified) gauge condition. The majority of today's gauge conditions are only gauge evolution conditions in this terminology. I propose a set of gauge fixing conditions, and show that their additional power can lead to a stable evolution, even without using any magic ingredients.

While experimenting with different formalisms, I am willing to sacrifice speed. I do believe that it is enough to have a formulation that can at least in principle be implemented efficiently. Computers become faster every year, and run time on supercomputers is rather easy to obtain for research purposes. It is better to start with a slow, but stable formulation, and optimise later on, than trying to find stability among fast implementations. It is also better to have a simple scheme for doing things, than having to follow a long recipe containing many steps, each of which is necessary.

## *1 Introduction*

This thesis is structured as follows. I start with a general introduction to simulating vacuum spacetimes and the problems encountered therein (chapter 2). I then explain gauge fixing conditions in general and the condition I chose in particular (chapter 3), as well as a system of evolution equations that is suited to this kind of condition (chapter 4). After that I discuss some boundary conditions (chapter 5) and initial data (chapter 6) that I use later on. I briefly mention some facts about the code that I developed (chapter 7) and move on to present in some detail the test cases and their results that demonstrate the properties of my gauge fixing conditions (chapter 8). I make some concluding remarks (chapter 9), and add some appendices containing equations and explanations that are likely not of general interest.

## 2 Simulating spacetimes

A spacetime can be characterised by its four-metric  $g_{\mu\nu}$ , which has to satisfy the Einstein equation  $G_{\mu\nu} = 8\pi T_{\mu\nu}$ . I will restrict myself in this thesis to the vacuum case where  $T_{\mu\nu} = 0$ . (The notational conventions are explained in appendix C.3.) The four-formalism couples the spatial and temporal degrees of freedom. The astrophysical interpretation, however, calls for an initial-boundary-value formulation.

### 2.1 The ADM formalism

One commonly used way of transforming the Einstein equations into such a system of time evolution equations is the so-called ADM formalism [ADM62]. This is one form of a so-called 3 + 1 split into 3 spatial and 1 temporal dimensions. It leads to the primary variables three-metric  $\gamma_{ij}$  and extrinsic curvature  $K_{ij}$ . The time evolution equations contain the freely specifiable quantities lapse  $\alpha$  and shift  $\beta^i$ . The three-metric and extrinsic curvature have to satisfy two constraints, the Hamiltonian constraint  $H$  and the momentum constraint  $M_i$ .

In order to evolve a spacetime in an ADM-like formalism, one needs initial data, boundary conditions, and a choice of lapse and shift. Additionally, one can choose to enforce the constraints or a gauge. For reference, the ADM variables are given in appendix A.1.1, the ADM evolution equations in appendix A.1.2, and the ADM constraints in appendix A.1.4.

At first sight, the primary variables of an ADM system (three-metric  $\gamma_{ij}$  and extrinsic curvature  $K_{ij}$ ) seem to contain six physical degrees of freedom, i.e. twelve independent quantities. However, only four of those twelve have a true physical meaning. Out of the twelve apparent independent quantities, the constraints eliminate four, and the choice of gauge eliminates another four. Thus there are only four independent quantities left, corresponding to the two degrees of freedom for gravitational waves.

These days<sup>1</sup>, the original ADM system has gone out of fashion in the numerical relativity community. Instead, one uses extended ADM-like systems, often called ctADM (“conformal traceless ADM”) systems. They have two more variables, a conformal factor  $\psi$  for the three-metric and the trace  $K$  of the extrinsic curvature. The three-metric is replaced by a conformal three-metric  $\tilde{\gamma}_{ij}$ , and the extrinsic curvature by a conformally rescaled traceless extrinsic curvature  $\tilde{A}_{ij}$ . These systems also have two additional constraints, namely  $\det \tilde{\gamma}_{ij} = 1$  and  $\text{trace } \tilde{A}_{ij} = 0$ .

Both the ADM and the ctADM systems exist in multiple variations. The constraint equations are of the form  $C = 0$ , and it is therefore possible to add arbitrary multiples of the constraints  $C$  to the right hand sides of the time evolution equations. Doing this can dramatically change the behaviour of a system.

The ctADM systems have the advantages that the new variables  $\psi$  and  $K$  have a direct interpretation as constraint and gauge quantities.  $\psi$  is closely related to the Hamiltonian constraint  $H$ ,

---

<sup>1</sup>I write this in 2002

## 2 Simulating spacetimes

while  $K$  is related to the lapse  $\alpha$ . These relations make it easier to influence the time evolution of these quantities. It also makes it potentially easier to enforce the constraints with the York–Lichnerowicz method, which also relies on a conformal traceless decomposition.

Both the Maya [Pen, LS02, KLL<sup>+</sup>01] and the AEI variants of the BSSN systems [NOK87, NO89, SN95, BS99] are variants of ctADM systems, where certain derivatives of the conformal three-metric have additionally been made independent variables, which leads to three additional constraints. The additional variables capture gauge degrees of freedom that are closely related to the shift, and thus allow further control over the system.

### 2.2 Constrained evolution

Sometimes it is necessary or convenient to enforce the constraints explicitly. This can either be a part of a scheme to obtain initial data, or it can be part of an evolution scheme, e.g. to prevent deviation from the constraint hypersurface due to accumulated numerical errors. Enforcing the constraints can also help stability, as e.g. described by Evans [Eva89] or Marsha and Choptuik [MC96]. The constraint equations contain no time derivatives, and also do not contain the lapse or the shift. They connect the three-metric and extrinsic curvature only.

When spherical or axial symmetry is assumed, then some constraint equations are algebraic conditions for some of the evolved variables. That means that these constraints can be enforced rather easily. This is unfortunately not the case in three dimensions. There, the constraint equations are not suitable for enforcing in their ADM form. However, they can be rewritten so that they are elliptic equations in certain quantities that are connected to the three-metric and the extrinsic curvature. In the York–Lichnerowicz formalism [Yor73, Yor74] [Coo02, section 2.2.1], a ctADM system is extended to include a vector potential  $V_i$  for the conformal traceless extrinsic curvature. The constraints determine the conformal factor and this vector potential. This requires variable transformations before and after solving.

As it is somewhat expensive to solve elliptic equations, it has become customary to perform *unconstrained evolution* for three-dimensional simulations, i.e. to evolve without regard to the constraints, monitoring the constraints only as a measure of quality for the time evolution. Given initial data that satisfy the constraints, the Bianchi identities then guarantee that the constraints will be satisfied at all times, of course only modulo numerical errors. Choptuik [Cho91] argues that the order of accuracy of an unconstrained evolution will not be worse than that of a constrained evolution.

### 2.3 Picturing spacetimes

There are two fundamentally different points of view that one can take to interpret a spacetime. In the following, I use the terms *grid points* and *coordinate system* in an equivalent manner. One can think of coordinate lines forming a grid, and the intersections of these coordinate lines are then the grid points.

**The coordinate based view** treats the primary variables similar to hydrodynamic or electrodynamic field quantities. One pictures a non-physical background grid, containing regularly spaced grid points forming the numerical grid. On each grid point, or in each grid cell, live

the primary variables, i.e. the three-metric and extrinsic curvature. The background grid has nothing to do with the evolved spacetime, it exists only in a flat coordinate space.

Time evolution consists of updating the evolved quantities through source and advection terms. The boundary of the grid stays in a fixed place in the coordinate space. This picture is the one that is most often used when quantities are plotted or displayed. Instabilities show up as certain metric coefficients becoming negative or some quantity growing without bound. In this picture, the apparent horizon of a static black hole can move across the grid.

**In the physically based view**, one looks at the location of the coordinate grid points in the physical spacetime. It is not always easy to picture (let alone draw or plot) a curved spacetime, but much of general relativity has to do only with strange coordinate systems, and applies even in a flat spacetime. It is instructive to use this picture to look at a time evolution of flat space in a nontrivial, time-dependent coordinate system.

In this picture, time evolution consists of choosing the locations of the next layer of coordinate grid points. That is, it is the grid that is constructed layer by layer, while the (unknown) spacetime is not evolved, but only discovered. Instabilities show up as grid points getting too close or too far apart, grid cells becoming too elongated, or grid lines crossing. In this picture, the apparent horizon of a static black hole stays fixed, while the grid points can move across it.

The coordinate based view is much easier to draw or display, and is hence what is usually presented. The physically based view is much more difficult to display, and requires in general some (artificial) embedding. However, the physically based point of view makes it also much easier to interpret gauge modes. For gauge modes, the embedding stays the same, only the grid points move.

As an example, consider the time-dependent metric

$$ds^2 = -\frac{1}{(1+Ax^2)^2} dt^2 + 2\frac{2Atx}{(1+Ax^2)^3} dt dx + \left[1 - \frac{(2Atx)^2}{(1+Ax^2)^4}\right] dx^2 + dy^2 + dz^2 \quad (2.1)$$

with the free parameter  $A$ . For  $A = 0$ , this metric is identical to the Minkowski metric. This metric happens to describe a flat spacetime for all values of  $A$ , which is not obvious to see. Figure 2.1 shows the graphs of the three-metric, extrinsic curvature, lapse, and shift for the case  $A = 1/2$ . This figure uses the coordinate based view.

Assume now that this deviation from the Minkowski metric is due to an unwanted gauge mode. It is possible to arrive at the conclusion that this metric is identical to the Minkowski metric after a gauge transformation by looking at the field quantities shown in figure 2.1. Yet it is not trivial to do so, nor can the nature of the gauge transformation (i.e. the gauge mode) easily be found out. However, one wants to know what gauge transformation was applied so that the gauge mode can be counteracted in a numerical evolution.

Figure 2.2 shows the same metric, but now uses the physically based view. That is, shown are the grid points of the coordinate system described by the metric (2.1), using a Cartesian coordinate system (i.e. the Minkowski metric) as reference. This graph is only possible because the spacetime is flat; otherwise one would need an embedding. It is obvious from this graph that the gauge

## 2 Simulating spacetimes

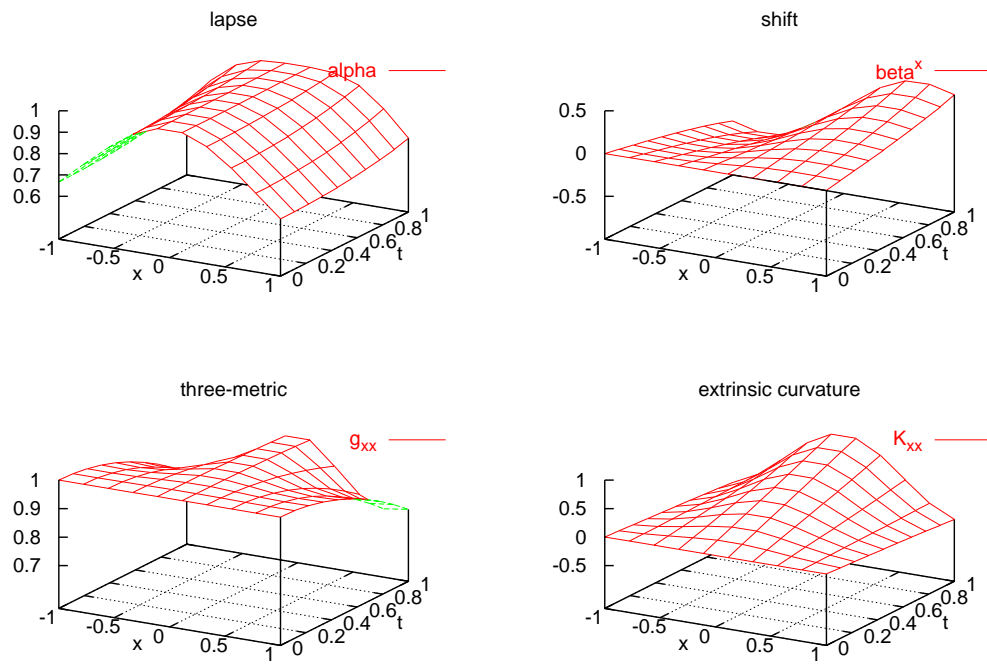


Figure 2.1: Evolved field quantities vs. time and space



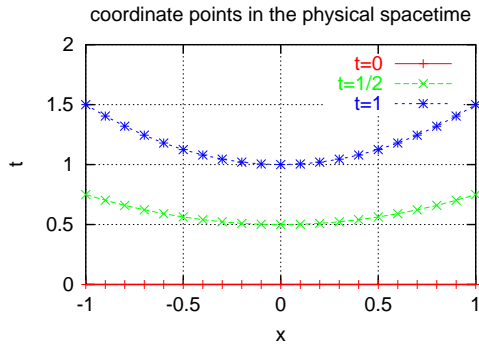


Figure 2.2: Location of the coordinate grid points in the (flat) physical spacetime

transformation is a very simple one, namely just  $t' = t(1 + Ax^2)$  with  $A = 1/2$ . Knowing this, one could e.g. choose a different lapse to prevent the time slices from curling up. While this can in principle also be deduced by looking only at the primary field variables, it is certainly easier in the physically based view.

## 2.4 Interpreting the quantities

It is quite useful to have a mental picture of what the quantities in an ADM or ctADM system mean:

- The conformal factor determines the volume that is contained in a grid cell; the volume is given by  $\sqrt{\det \gamma_{ij}} = \psi^6$ .
- The diagonal elements of the three-metric determine the physical length of the coordinate lines between grid points within a time slice. The off-diagonal elements determine the angles between the coordinate lines.
- The trace of the extrinsic curvature determines the mean curvature of the layer of grid points forming the current time slice. It is closely related to the time derivative of the conformal factor. It is also closely connected to the lapse, as it is mostly the lapse that determines the change of the mean curvature in time.
- I have found no immediately useful interpretation of the extrinsic curvature tensor. One can view it as the time derivative of the three-metric.
- The lapse is the physical distance between two time slices, measured in proper time of an observer that is at rest in those slices. It is thus the ratio between proper and coordinate time for such an observer. When the lapse is zero, coordinate time increases, but no proper time elapses.
- The shift determines the difference between the spatial coordinate systems of two neighbouring time slices. It is the velocity of the coordinate system with regard to a resting observer.

## 2 Simulating spacetimes

Given the three-metric and extrinsic curvature of a time slice, there is no direct way of knowing just where in a given spacetime the current time slice is located. One has to work out how the time slice is embedded in the spacetime, and then compare the resulting three-metrics and extrinsic curvatures. This is in general a difficult matching process, and I know of no attempts to try this in four dimensions (but see the Lazarus project [BCL02]). An efficient algorithm for this problem would surely be very useful for comparing results of runs with different formulations, or of runs with different coordinate conditions [Sal02, Haw02, app].

### 2.5 Instabilities

Three-dimensional numerical simulations of nonlinear general relativistic spacetimes have been plagued by instabilities. To date, it is still safe to say that these instabilities are not well understood. There are many ideas about on how to remove these instabilities, but none have truly succeeded so far.

I use the term *instability* here in a rather loose manner. I take it to mean that a certain quantity grows exponentially (or faster) and without bound. I want to use this term here not for a theoretical argument, but only to describe empirical results from simulation runs.

I do not want to use the definition of instability from the theory of hyperbolic systems. I think that this definition is not too useful in this case, as it considers an exponential growth to be stable. (On the other hand, it introduces the concept of resolution independence, which is crucial for numerical simulations.)

Jeffrey Winicour has introduced the very practical definition of *robust stability* [SGBW00, SSW02], which allows for at most polynomial growth even when arbitrary noise is continuously injected into the system. This can easily be tested in a numerical implementation.

Apart from being stable, a system must also be convergent. That is, it must be able to track a given solution arbitrarily closely, where the deviation should depend on the resolution e.g. in a quadratic manner. I will concentrate on stability, rather than convergence, in the following section. That does, of course, not mean that I believe convergence to be unimportant.

Let me try to classify the possible instabilities of a system implementing the Einstein equations in a  $3 + 1$  split:

**Physical instabilities** have their cause in the spacetime itself. A spacetime can contain singularities, and if the part of the spacetime that is described by the numerical metric gets close to or contains such a singularity, there will be a physical instability. There is not much one can do against such a singularity. Possible approaches include choosing a slicing that does not intersect the singularity, or excising that part of the spacetime, or trying to “subtract” the singularity and treating it analytically.

**Constraint-violating instabilities** occur because the constraints are not exactly satisfied in a numerical simulation. Many theorems about general relativity hold only when the constraints are satisfied. It is not known what happens when the constraints are not satisfied, and it is quite possible that such a constraint violation would grow exponentially. Constraint violating modes may also propagate faster than light; they do not have to follow causality. The constraint violation can be easily monitored. It is possible to enforce the constraints at any time by e.g. solving elliptic equations, but this is expensive.

**Gauge instabilities** result from a bad choice of coordinates. With a gauge evolution condition, i.e. a choice of lapse and shift, one does not choose the coordinate system directly, but rather only its time evolution. Especially when lapse and shift are themselves the result of a time evolution equation with its associated boundary conditions, the relationship between them and the quality of the coordinate system becomes complicated. Gauge instabilities can theoretically always be cured by a different choice of coordinates, but this is difficult in practice. There is no clear-cut distinction between physical and gauge degrees of freedom, which makes it difficult to separate between physical and gauge instabilities.

Instead of classifying instabilities by the affected quantities, one can also try to classify them by their sources:

**Instabilities in the formulation** are another name for an ill-posed problem. The prototype of an ill-posed problem is the backward heat equation  $\dot{u} = -u''$ . While the (forward) heat equation has a smoothing property, the backward heat equation amplifies any perturbation exponentially. The amplification time scale depends on the length scale of the perturbation, where smaller perturbations are amplified more quickly.

**Instabilities due to boundaries** are caused by inappropriate boundary conditions. The advection equation  $\dot{u} = u'$  on the unit interval  $[0; 1]$  needs a boundary condition at  $x = 1$ , but cannot have one arbitrarily imposed at  $x = 0$ . This follows from the characteristic of the equation. However, characteristics for more complicated, nonlinear equations that are not given in a first-order form are difficult to find. The characteristics also depend on the formulation and the gauge conditions, so that expressing the same physical system with different variables or with a different gauge will lead to different characteristics.

**Instabilities in the discretisation** are introduced by an unsuitable discretisation scheme. A prototypical example of such an unsuitable scheme for e.g. the advection equation  $\dot{u} = u'$  is combining centred differencing with an explicit first order time integrator. Suitable schemes for this equation are e.g. using upwind differencing, adding artificial diffusion, using an implicit time integrator, or using interpolation instead of finite differencing and time integration.

## 2.6 My goal in this thesis

In this thesis, I am not attempting to find a well-posed formulation for the Einstein equations. I am instead using a simple, straightforward formulation that might well not be well-posed (although I do not know this). I am adding artificial diffusion to counteract problems caused by this. This artificial diffusion cures the discretisation instabilities.

Also, in this thesis I am not trying to find an especially suited discretisation scheme for the Einstein equations. I am using centred differencing and a second order explicit time integrator, which are among the most simple tools that can be used for this. First order artificial diffusion makes my overall discretisation scheme first order accurate only.

Instead, in this thesis, I use the first classification of instabilities, and discuss gauge modes. I introduce generic gauge fixing conditions which apply in ways equivalent to the constraints. That allows gauge modes and gauge instabilities to be identified, and also to be removed by enforcing the gauge.

## 2 *Simulating spacetimes*

## 3 Gauge conditions

The ADM evolution equations contain the free quantities lapse  $\alpha$  and shift  $\beta^i$ , which need to be specified prior to a time evolution. Lapse and shift determine how the coordinate system in the spacetime is constructed, starting from the current time slice. Such a choice of lapse and shift is also commonly called a *gauge condition*. Unfortunately, the simplest gauge choices will in general lead to coordinate singularities, so that more involved conditions are necessary.

The gauge choice also influences the properties of the system of evolution equations. Hyperbolicity, and the stability properties in general, do crucially depend on the gauge condition. The search for good gauge choices forms an important part of the current efforts to obtain stable evolutions.

Below, I list several gauge choices that are or were commonly used, and mention some of the classifications for gauge conditions that have proven useful in numerical relativity. I discuss the difference between *gauge evolution conditions* and *gauge fixing conditions*, and point out the properties that a good gauge fixing condition needs to have.

I then describe such a gauge fixing condition that has these properties, and that I will use in the following chapters. I also examine the behaviour of its induced coordinate systems and compare it to existing gauge conditions.

### 3.1 Common gauge conditions

Clearly the easiest way to specify lapse and shift is by prescribing them as functions of space and time, i.e. as functions of the coordinates  $x^i$  and  $t$ . Doing so might be called using an *exact gauge condition*<sup>1</sup>. Again the simplest possible way to do this is to prescribe  $\alpha = 1$  and  $\beta^i = 0$  everywhere, which is called geodesic slicing and normal coordinates, respectively. For other exact gauge conditions, one often uses a known solution of Einstein's equations to obtain expressions for the lapse and shift. As mentioned above, such a simple gauge choice usually leads to unstable evolutions. The intuitive explanation for these instabilities is that numerical errors accumulate, creating gauge modes or a gauge drift, while the gauge condition does not compensate.

An only slightly more complicated way to specify lapse and shift is by taking the values of the primary variables into account. This is often called an *analytic gauge condition*. In an ADM-like system, one specifies lapse and shift as functions of the coordinates  $x^i$  and  $t$ , the three-metric  $\gamma_{ij}$ , and the extrinsic curvature  $K_{ij}$ . Thus analytic gauges are a superset of exact gauges. The additional freedom in choosing lapse and shift can be used to counteract instabilities. It is also possible to solve time evolution equations for lapse and shift. For example, harmonic slicing [BM88] can be implemented by setting  $\partial_t \alpha = -\alpha^2 K$ . Harmonic slicing has singularity avoiding properties similar to maximal slicing (see below).

The most expensive gauge conditions are *elliptic gauge conditions*, consisting of elliptic equations for lapse or shift. They are a subset of analytic gauge conditions. The prototype for this is maximal

---

<sup>1</sup>I think that this expression was coined by Manuel Tiglio.

### 3 Gauge conditions

slicing [SY78]. This gauge condition prescribes  $K = 0$ , which leads to the condition  $\Delta\alpha = \alpha R$  for the lapse. Other well-known elliptic gauge conditions are minimal strain and minimal distortion [SY78], and the Gamma-freezing shift derived from  $\partial_t \tilde{\Gamma}^i = 0$  [Pol01] in the BSSN system.

The gauge conditions currently en vogue in the community are analytic gauges with time evolution equations. Elliptic conditions have desirable properties, but are considered to be too expensive. Harmonic slicing and variations thereof can be seen as *driver conditions*. Instead of solving an elliptic equation for lapse or shift, one transforms the elliptic equation into a parabolic or hyperbolic time evolution equation. These evolution equations drive the lapse or shift towards the desired value. A parabolic equation acts as a diffusive mechanism that disperses the difference, and a hyperbolic equation acts as a (damped) radiative system that transports the difference away.

Hyperbolic driver gauge conditions have been successful to some extent for the BSSN system, and also for the KST system [KST<sup>+</sup>00] with a densitised lapse.

As mentioned in the introduction, I do not share the belief that elliptic gauge equations are too expensive. While it is obviously true that they are inconveniently expensive, it is often possible to optimise them for speed, such as e.g. solving only every  $n$  time steps, and using some approximation in between. Furthermore, stability is more important than speed.

## 3.2 Gauge evolution and gauge fixing

A gauge condition is in four-space a condition that is applied to the four-metric  $g_{\mu\nu}$ . A choice of lapse and shift corresponds to a specific choice of  $g_{00}$  and  $g_{0i}$  and is thus a true gauge condition there.

However, in an ADM-like system, the primary variables are not the four-metric, but rather the three-metric and the extrinsic curvature. A gauge condition thus has to be applied to these quantities. A choice of lapse and shift does not restrict the primary variables, and should therefore not quite be called a gauge condition. Because I do not want to break with tradition too much, I call it a *gauge evolution condition* in this text. While a choice of lapse and shift does not eliminate the gauge freedom present in the initial data, it does determine how the gauge condition is evolved in time. A gauge evolution condition can be obtained from an evolution equation of a primary variable, e.g. from  $\partial_t K = \dots$  or  $\partial_t \tilde{\Gamma}^i = \dots$ .

A “true” gauge condition is what I call a *gauge fixing condition* here. A gauge fixing condition is a direct restriction on the possible values of the primary variables. This will implicitly also lead to a choice for lapse and shift. Maximal slicing ( $K = 0$ ) is an example of a gauge fixing condition; it not only selects a lapse, but also restricts the possible sets of values for the primary variables.

(Gauge fixing is not a new idea. In fact, gauge fixing is the way in which gauge conditions are applied in other fields. Calling a choice of lapse and shift a gauge condition seems to be a relatively new convention in general relativity, which was used by Smarr and York in [SY78].)

Most of the gauge conditions mentioned above and used today are only gauge evolution conditions. This fact does not make them inferior per se, but using them can easily lead to (coordinate) singularities, which show up as instabilities. Let me consider, as an example, geodesic slicing ( $\alpha = 1$ ) in a flat spacetime, and let me disregard the shift for now. In Minkowski coordinates, geodesic slicing works fine. With different initial data for a flat spacetime, geodesic slicing can lead to coordinate singularities, while of course the spacetime is still flat. This is numerically a problem when one starts out close to Minkowski coordinates, with the difference being only due to numerical errors.

Unexpected gauge singularities, i.e. gauge instabilities, cannot happen with a gauge fixing condition. A gauge fixing condition imposes a condition on a primary variable, e.g. specifies the values for  $K$ , and then selects a lapse so that this condition continues to hold. Because  $K$  is specified, it is impossible to accidentally select a lapse that makes  $K$  diverge, as in the example above. The only way to produce a gauge singularity is by specifying a diverging  $K$  to begin with.

This does not prevent accumulated numerical errors, which could still make  $K$  diverge. But the gauge fixing condition can be monitored during the evolution, so that one can judge the quality of the simulation. This is equivalent to the way one handles the constraints. Furthermore, a gauge fixing condition can also be directly enforced when numerical errors have accumulated, eliminating gauge instabilities altogether.

The interplay between lapse and shift and gauge singularities is further complicated by the boundary conditions. One needs boundary conditions for the primary variables, and also for lapse and shift if they are evolved in time. Without a proper gauge fixing condition to start from it is prohibitively difficult to ensure that a certain choice of lapse and shift does not, under the influence of numerical errors, lead to a gauge singularity at the boundary. With a gauge fixing condition, such instabilities are not possible, or can at least be easily detected.

The only gauge fixing condition that is in use today in nonlinear three-dimensional numerical relativity is maximal slicing.

A close candidate is AEI's Gamma freezing, which sets  $\partial_t \tilde{\Gamma}^i = 0$  and derives an elliptic shift condition from that. Placing a condition on a time derivative is not directly a gauge fixing condition, which requires placing a condition on the variable itself. But setting a time derivative to zero can be viewed as fixing the variable at its initial value, and I therefore want to count it as gauge fixing. However, Gamma freezing does not try to keep the value of  $\tilde{\Gamma}^i$  consistent with  $\tilde{\gamma}_{ij}$ , i.e. the new constraints arising from introducing  $\tilde{\Gamma}^i$  as additional primary variable [BS99] are not controlled. (These constraints seem to be important, because they seem to be growing without bound when they are not controlled.) Re-calculating  $\tilde{\Gamma}^i$  from  $\tilde{\gamma}_{ij}$  destroys the gauge fixing properties of Gamma freezing.

Minimal distortion is not a gauge fixing condition. This condition minimises the distortion, which is the *change* of shape during a time step. It does not try to attain any specific coordinate shape (e.g. for a sphere), and is therefore not a gauge fixing condition. It restricts only the time derivative of the three-metric, and not the three-metric itself.

One interesting case of a gauge fixing condition is area locking. Area locking was introduced in spherically symmetric situations, and it leads to very stable evolutions in this case. It sets  $\partial_t \gamma_{\theta\theta} = 0$ , which leads to a condition for the shift component  $\beta^r$ . As above, I count this as gauge fixing. Unfortunately, area locking was never successfully generalised to three dimensions.

### 3.3 Good gauge fixing conditions

A gauge fixing condition is a condition that acts directly on the primary variables, i.e. the three-metric and the extrinsic curvature for an ADM-like system. It has thus properties similar to the constraints. Gauge fixing conditions are a superset of gauge evolution conditions which select a lapse and a shift only.

A good gauge fixing condition has to have several properties:

1. Of course, it has to leave enough degrees of freedom so as to not constrain any physics, even in the full nonlinear case. No physical degree of freedom must be removed from the system.

### 3 Gauge conditions

2. It has to lead to a unique prescription for lapse and shift, so that the gauge condition will also hold for the neighbouring time slices.
3. It should be easy to evaluate, so that one knows whether the gauge condition still holds, or by how far one has left this gauge.
4. There should be a reasonable way to enforce this gauge, so that one can counteract numerical errors that have accumulated over time, or create initial data in this gauge.
5. It should be independent of the constraints. That is, the condition should be independent of the variables that are changed when the constraints are enforced, so that one can at the same time enforce the gauge condition and the constraints.
6. It should have an understandable physical interpretation, so that the physicist can apply his or her intuition.
7. It should be general enough so that many kinds of initial data can be prepared with this gauge, and many spacetimes can be described in it.

I do count solving elliptic equations as being “reasonable” in the context of the above. There are kinds of equations that are much more unwieldy than elliptic ones. And there exist efficient methods for solving elliptic equations with a cost that grows only linearly with the problem size. I do not strive for the fastest possible implementation here, I only want something “reasonable”.

Maximal slicing almost satisfies these properties, but it is not a complete gauge choice. It selects a slicing, but does not determine the three-coordinate system. Additionally, the condition  $K = 0$  is too constraining in practice — it does e.g. not permit a horizon-penetrating static slicing of a static black hole (see e.g. [Coo02, section 3.1.1]).

### 3.4 My gauge fixing condition

My goal in this thesis is to present a gauge fixing condition that can be used to simulate black hole spacetimes. This condition has to have the properties that I list above. As mentioned in the introduction, I also want a simple system. The currently promising systems (e.g. the BSSN variants) all contain many subtle rules that have to be followed closely. The gauge condition should be conceptually as simple as possible, even if it is expensive to use.

For my gauge condition, I choose as gauge variables the trace  $K$  of the extrinsic curvature and certain combinations of partial derivatives of the conformal three-metric, which I call  $F_i$  after Shibata and Nakamura [SN95]. My gauge condition then consists of prescribing, in advance, values for these quantities as functions of space and time, i.e. depending on  $x^i$  and  $t$  only.

Prescribing the trace of the extrinsic curvature leads to an elliptic equation for the lapse (see appendix A.2.2). Given that, it is clear that a choice of  $K$  has all of the above properties. Interpreting  $K$  as a gauge variable is a common choice. It is a straightforward generalisation of maximal slicing [SY78], and I think that this gauge variable needs no further justification.

My gauge condition acting on the metric is a bit more involved. I first define (for technical reasons) the traceless conformal three-metric  $\bar{h}_{ij}$  as

$$\bar{h}_{ij} = \tilde{\gamma}_{ij} - \frac{1}{3}\delta_{ij}\delta^{kl}\tilde{\gamma}_{kl} \quad . \quad (3.1)$$



### 3.4 My gauge fixing condition

The bar  $\bar{\cdot}$  indicates here that the indices are to be raised and lowered with the coordinate metric  $\delta_{ij}$ . My gauge variable  $F_i$  is then defined by

$$F_i = \bar{h}_{ij,j} . \quad (3.2)$$

That is, my gauge quantity  $F_i$  is closely related to the divergence of the conformal three-metric  $\tilde{\gamma}_{ij}$ . The fact that I use the traceless part only has only technical reasons, having to do with the method used to enforce the gauge condition, which is explained further down.

This gauge condition is similar to the transverse-traceless gauge used in linearised general relativity, where one often requires of the metric perturbation the condition  $h_{ij,j} = 0$ . (Here  $h_{ij}$  is a three-metric perturbation, which is different from the variable  $\bar{h}_{ij}$  above.) However, I do not require that  $F_i = 0$ , but only that it be prescribed in advance.

This gauge variable is also very similar to, but slightly different from the auxiliary variable  $F_i$  introduced by Shibata and Nakamura [SN95] as  $F_i = \tilde{\gamma}_{ij,j}$ . The BSSN system has instead  $\tilde{\Gamma}^i = \tilde{\gamma}^{jk} \tilde{\Gamma}_{jk}^i$  [BS99], which is also closely related to the Shibata–Nakamura  $F_i$ .

It is by design that the gauge condition is not covariant. The gauge defines the coordinate system, and the use of a specific coordinate system is what makes a calculation be not covariant. That means that it does not make sense to speak of a covariant gauge condition — such a gauge condition could not single out a specific coordinate system.

The choice of the gauge variable  $F_i$  constrains the possible shapes of the three-coordinate system. The gauge condition judges the quality of the current coordinate system, and prevents a deterioration by placing the grid points appropriately.

As described in section 2.4, the metric components  $\gamma_{ii}$  (no summation implied) describe the physical distance between grid points in the  $i$  direction, while the components  $\gamma_{ij}$  (with  $i \neq j$ ) describe the physical angle between the  $i$  and  $j$  coordinate directions. The direct metric divergence  $\gamma_{ij,j}$  hence describes the spatial change of the behaviour of the grid lines in the  $i$  direction — the change in length, plus the change in the angles with the other grid lines.

The physical meaning of the components of the conformal traceless metric  $\bar{h}_{ij}$  is more complex, but will be similar in nature. Hence enforcing a certain  $\bar{h}_{ij,j}$  means to enforce a certain spatial rate of change of the coordinate system. Enforcing the gauge changes the metric, and therefore effectively moves the grid points until they have the “right” location with respect to their neighbours.

As one can set the quantity  $F_i$  to an arbitrary function, this gauge choice can be used for all initial data. Fixing  $F_i$  leads, via the time evolution equation of  $\tilde{\gamma}_{ij}$ , to an elliptic equation defining the shift (see appendix A.2.7), so that using this shift preserves the gauge condition. That means that this gauge condition is generic, can be used for all spacetimes, and does not constrain any physical degrees of freedom.<sup>2</sup>

The resulting elliptic equations for the lapse  $\alpha$  and the shift  $\beta^i$  also require boundary conditions. These boundary conditions are part of the gauge condition. One can use the boundary conditions for the lapse to slow down or speed up the time evolution, or to tilt the time slice. The boundary conditions for the shift can be used to move the boundary further in or out, or to move or rotate the whole simulation domain. This can be used to set up co-rotating coordinate systems, for example.

By introducing a vector potential  $W_i$  for the traceless conformal metric  $\bar{h}_{ij}$ , one can enforce this gauge condition in a manner equivalent to enforcing the momentum constraint on the extrinsic

<sup>2</sup>In this I assume that this elliptic equation has a solution. This depends e.g. also on the boundary conditions. For the cases I am interested in, one can assume that the domain is simply connected and has Dirichlet boundaries. I have not proven that a solution exists, but numerical tests support my assumption.

### 3 Gauge conditions

curvature.<sup>3</sup> One can reconstruct the conformal metric  $\tilde{\gamma}_{ij}$  from its traceless part through the condition  $\det \tilde{\gamma}_{ij} = 1$ , which determines its trace. Furthermore, as enforcing the constraints in the York–Lichnerowicz formalism (see section 4.2) does not change the conformal metric or the trace of the extrinsic curvature, it preserves this gauge conditions.

This means that this gauge has all the properties (1)–(7) above for a good gauge fixing condition. I will use it in the following chapters and examine its numerical properties.

Another, potentially more elegant gauge condition on the metric could be  $F_i = \tilde{\gamma}_{ij,j}$ . Another, potentially more elegant way of enforcing the gauge condition could be to apply a four-dimensional coordinate transformation. A coordinate transformation would have the advantage that the constraints are not influenced. I did not investigate these alternatives.

---

<sup>3</sup>The existence and uniqueness properties of the York–Lichnerowicz method thus are trivially valid for this method as well.

## 4 The system of equations

### 4.1 The variables

I chose not to use the standard ADM system to represent a spacelike hypersurface, but rather a variant of a conformal traceless ADM (ctADM) system. Such a system can more easily be used to enforce the constraints, and furthermore it also already makes the gauge degrees of freedom more explicit.

My primary variables are

- the conformal factor  $\psi$ , with  $\psi^{12} = \det \gamma$
- the conformal three-metric  $\tilde{\gamma}_{ij}$ , with  $\psi^4 \tilde{\gamma}_{ij} = \gamma_{ij}$
- the trace  $K$  of the extrinsic curvature, with  $K = \gamma^{ij} K_{ij}$
- the traceless conformal extrinsic curvature  $\tilde{A}_{ij}$ , with  $\psi^{-2} \tilde{A}_{ij} = A_{ij}$ . Here  $A_{ij}$  is the traceless extrinsic curvature, i.e.  $A_{ij} = K_{ij} - \frac{1}{3} \gamma_{ij} K$
- the divergence  $F_i$  of the traceless conformal three-metric, with  $F_i = \tilde{h}_{ij,j}$ . Here  $\tilde{h}_{ij}$  is the traceless conformal three-metric, i.e.  $\tilde{h}_{ij} = \tilde{\gamma}_{ij} - \frac{1}{3} \delta_{ij} \delta^{kl} \tilde{\gamma}_{kl}$

In the above,  $\gamma_{ij}$  and  $K_{ij}$  are the three-metric and extrinsic curvature of the standard ADM system. This system implicitly fulfils the constraints  $\det \tilde{\gamma}_{ij} = 1$  and  $\text{trace } \tilde{A}_{ij} = \tilde{\gamma}^{ij} \tilde{A}_{ij} = 0$ . I use a tilde  $\tilde{\phantom{x}}$  for quantities that are connected to the conformal metric  $\tilde{\gamma}_{ij}$  rather than the physical metric  $\gamma_{ij}$ , and a bar  $\bar{\phantom{x}}$  for quantities that are connected to the coordinate metric  $\delta_{ij}$ . The time evolution equations for this system are derived in appendix A.2.2, the constraints in these variables in appendix A.2.3.

This system, which I call the *TGR system*, is similar to the BSSN [NOK87, NO89, SN95, BS99] system. The main differences are that it has the conformal factor  $\psi$  instead of its logarithm  $\phi = \log \psi$  as primary variable, and that the traceless conformal extrinsic curvature is scaled with a different power of the conformal factor; while the TGR system uses the scaling factor  $\psi^{-2}$ , the BSSN system uses the same factor  $\psi^4$  as for the conformal metric. It also has  $F_i$  instead of  $\tilde{\Gamma}^i$ , which is similar but different.

Compared to the original ADM system, the TGR system has the advantage that it can more easily be used to enforce the constraints. Enforcing the constraints using the York–Lichnerowicz formalism [Yor73, Yor74] [Coo02, section 2.2.1] requires a decomposition into a system with a conformal metric and a traceless conformal extrinsic curvature. With the standard ADM system, this requires variable transformations before and after each enforcing, which leads to additional discretisation errors. In fact, the very system used by Cook in [Coo02, section 2.2.1] motivated my choice of variables. The BSSN system would also be suitable for solving the constraint equations, although only with a slightly different method.

## 4.2 Enforcing the gauge and the constraints

In order to enforce the constraints with the York–Lichnerowicz method, one introduces a vector potential  $V_i$  for the traceless conformal extrinsic curvature. This transforms the constraint equations into a set of coupled nonlinear elliptic equations for the conformal factor and this vector potential, which can then be solved. This is described in appendix A.2.4. The gauge condition can be enforced in a similar way by introducing a vector potential  $W_i$  for the traceless conformal metric. This is described in appendix A.2.6.

With given initial data, boundary, and gauge conditions, the time evolution of a physical system is defined by the time evolution equations for the above system. The constraint and the gauge equations can also be used to enforce the constraints and the gauge, i.e. to create initial data, or to counteract numerical errors during the time evolution.

Enforcing the constraints and the gauge conditions has to happen in a certain order. This order is necessary, because e.g. enforcing the gauge condition for  $F_i$  on  $\tilde{\gamma}_{ij}$  changes the constraints. Therefore, the gauge condition for  $F_i$  has to be enforced before the constraints are enforced. Lapse and shift are calculated after all enforcing. One possible order is the following:

1. Enforce gauge, part I: set  $K = K^*$
2.  $\det \tilde{\gamma}_{ij}$ : Rescale  $\tilde{\gamma}_{ij}$  such that  $\det \tilde{\gamma}_{ij} = 1$
3. Enforce gauge, part II: change  $\tilde{\gamma}_{ij}$  such that  $F_i = F_i^*$ , preserving  $\det \tilde{\gamma}_{ij}$
4. trace  $\tilde{A}_{ij}$ : Change  $\tilde{A}_{ij}$  such that  $\text{trace } \tilde{A}_{ij} = 0$  (depends on  $\tilde{\gamma}_{ij}$ )
5. Enforce constraints: change  $\psi$  and  $\tilde{A}_{ij}$  such that  $H = 0$  and  $M_i = 0$  (depends on  $\tilde{\gamma}_{ij}$ ,  $K$ , and  $\tilde{A}_{ij}$ )
6. Calculate lapse  $\alpha$  and shift  $\beta^i$  (depends on  $\psi$ ,  $\tilde{\gamma}_{ij}$ ,  $K$ , and  $\tilde{A}_{ij}$ )

In the above, values marked with an asterisk  $\cdot^*$  are values prescribed by the gauge condition.

In principle, enforcing the gauge and the constraints is not necessary for a perfect time evolution. In practice, it is necessary or advantageous to counteract numerical errors. It might be possible to change these elliptic equations into hyperbolic ones which would be much cheaper to solve; I have not tried this.

## 5 Boundary conditions

Boundary conditions are necessary while integrating the evolution equations in time, and for solving the elliptic gauge and constraint equations. They are needed at the outer boundary, and if excision (see below) is used, also at the excision boundary.

### 5.1 Outer boundary

Most astrophysically interesting spacetimes are asymptotically flat [Wal84, chapter 11]. That means that at large distances from the origin, the spacetime is flat plus some perturbation that falls off at least with  $1/r$ . Of the spacetimes considered in this thesis, only some numerical test problems are not asymptotically flat.

For single black hole and binary black hole collision simulations, the outer boundary should ideally be located at spatial or null infinity. In that case, no gravitational radiation will enter or leave the simulation domain, which makes the boundary condition easy to implement.

#### 5.1.1 Location of the outer boundary

In a numerical simulation, the outer boundary will be at a finite location (and not at spatial infinity), where the four-metric is not flat.<sup>1</sup> It can usually be assumed to consist of a known background metric that is superposed with small perturbations. These perturbations can be gravitational waves, or can be gauge modes, or can be constraint violating modes that arise from numerical errors.

It is theoretically possible to put the outer boundary indeed at spatial infinity by choosing a suitable coordinate system. However, one would have to get there with a finite number of grid points, and the gravitational waves would be backscattered by the change in resolution. One would have to make sure that the gravitational waves have been absorbed or dissipated before they reach a region where they cannot be resolved any more. Given this, there seems to be no real advantage in putting the outer boundary at spatial infinity.

#### 5.1.2 Physical boundary conditions

Astrophysically, one wants an outgoing radiation boundary condition at the outer boundary. All gravitational radiation that reaches the outer boundary should be let out, and no gravitational radiation should be sent in or reflected back. This means that the outer boundary has to be in a region where one can meaningfully speak of gravitational radiation “on top of something else”, i.e. one needs to be close to a known background solution, and the radiation amplitude has to be small.

---

<sup>1</sup>It is possible to put the outer boundary at null infinity or beyond by using a conformal approach [Fra98]. I will not consider this here.

## 5 Boundary conditions

A true radiative boundary condition would require splitting the quantities at the boundary into a background solution containing the total mass and spin, plus a linearised perturbation representing the gravitational waves, separated into their incoming and outgoing modes. This would be a rather complex and time consuming process. People have instead contemplated matching a perturbative formulation to the nonlinear formulation at the outer boundary [Win02]. This should in principle lead to a very clean boundary condition, but is hampered in practice by the coordinate transformations necessary to match the formulations. I know of no stable implementation using this approach.

One approximation is to use some kind of sponge layer near the outer boundary. Within this layer, one introduces an increasing absorption coefficient. It emits no radiation by itself, absorbs the waves reaching the layer, and reflects almost nothing back. On the outer side of this sponge layer one imposes a Dirichlet boundary condition. Penn State uses a blending zone [BCG<sup>+</sup>00], which is similar to this approach.

One other approximation is to assume that the waves are spherical about the origin. AEI uses conditions like this. Such radiative boundary conditions assume that the evolved quantity is an outgoing radial wave, satisfying  $f(t, r) = f_\infty + u(r - t)/r$ , where the constant  $f_\infty$  is given, and the function  $u$  is determined implicitly at each boundary point.

For elliptic equations, the usual boundary condition is a Robin boundary condition, which enforces a certain falloff towards infinity, i.e. a condition  $f(r) = f_\infty + C/r^n$  with given  $f_\infty$  and  $n$ . Here  $f_\infty$  is the desired value at infinity, and  $n$  is the falloff power. The constant  $C$  is determined implicitly at each boundary point.

If the solution at the outer boundary is known, which is usually not the case, then one can use Dirichlet boundary conditions. For waves, a constant-in-time Dirichlet boundary is a reflective boundary, so that waves cannot leave the simulation domain. This makes Dirichlet boundaries unsuitable for realistic applications, but also well suited for test problems, e.g. to study the stability of a formulation.

### 5.1.3 Periodicity

It is, especially for test problems, sometimes convenient to assume periodicity. Periodicity means that there are no real boundary conditions; this allows one to examine the system of evolution equations independent of any problems that might be caused by the boundary conditions. For example, the first two stages of Winicour's robust stability test [SGBW00, SSW02] involve periodic boundaries. Additionally, periodicity allows one to more easily examine the long-term behaviour of dynamic systems, because the interesting features cannot leave the simulation domain.

Unfortunately, periodicity poses a severe problem for elliptic equations. Their solution is determined by the boundary condition, and without a boundary their solution is not unique any more, or might cease to exist. If the solution is not unique any more, then one can impose a pseudo "boundary condition" at a single point in the domain to select a solution.

The elliptic equations arising in the TGR system seem in fact to be ill-posed when given periodic boundaries. That is, they do not admit a solution any more. This can already be seen at the example of the Poisson equation  $\Delta\phi = \rho$  with periodic boundaries. For  $\rho = 0$ , one needs to define  $\phi$  at one point to make the solution unique. For  $\rho \neq 0$ , the shape of  $\phi$  is a parabola, and is therefore clearly not periodic. Similarly, the Hamiltonian constraint equation in the York-Lichnerowicz formalism with periodic boundaries seems to be ill-posed when  $K_{ij}$  is not zero. For  $K_{ij} = 0$ , a solution exists, but is not unique.

This prevents many interesting test cases from being run while enforcing the gauge conditions and constraints. It is in some cases possible to convert these test cases into almost equivalent ones with Dirichlet boundaries. A travelling wave with periodic boundaries can e.g. be changed into a standing wave with periodic boundaries, and that system is then very similar to a standing wave with Dirichlet boundaries at the wave knots. And fortunately, test cases with Dirichlet boundaries are often considered to be more difficult to pass than those with periodic boundaries, i.e. they form stronger test cases.

#### 5.1.4 Gauge and constraint boundary conditions

A physical boundary condition does not define how to handle the gauge and constraint violating degrees of freedom. Physically, the constraints have to be satisfied. Numerically, there will always be errors. One has to try to reduce the violation of the constraints in some way, and this mechanism will interact with the boundary condition.

Similarly, after fixing the gauge, the gauge will numerically only be satisfied approximately. The boundary conditions have to deal with violations of the gauge and the constraints, meaning that there also has to be a boundary condition for the gauge and constraint violations. Unfortunately it is not clearly defined just which (combination) of the evolved or solved-for quantities contain these gauge and constraint violating degrees of freedom.

In my system, the variables  $\psi$ ,  $\tilde{\gamma}_{ij}$ , and  $\tilde{A}_{ij}$ , are evolved in time, while  $K$  and  $F_i$  are prescribed in advance by the gauge condition. It is not necessary to evolve the conformal factor  $\psi$  in time, as it can also be calculated from the Hamiltonian constraint. I do evolve it only to have a better initial guess for enforcing the Hamiltonian constraint, and in order to have more freedom in choosing the boundary conditions. Depending on the problem, I use either Dirichlet or radiative boundary conditions for the time evolution of these evolved variables.

It is clear that a Dirichlet boundary condition, even if it is consistent with the equations, is not suitable for an astrophysical problem. The radiation that is reflected at the outer boundary makes the result unphysical. But as such reflected radiation is considered to introduce instabilities, a Dirichlet boundary is actually a stronger stability test. I would use a sponge layer or a radiative boundary condition if I were to run a simulation with a domain large enough and a resolution fine enough to permit meaningful extraction of gravitational radiation.

The variables  $W_i$ ,  $\psi$ , and  $V_i$  need boundary conditions when the gauge and the constraints are enforced by solving elliptic equations. I use either Dirichlet or Robin boundary conditions for them. I impose  $W_i = 0$  and  $V_i = 0$  on the vector potentials. For the conformal factor  $\psi$  I distinguish between initial data and time evolution. For initial data I use either a Dirichlet or a Robin boundary condition. During time evolution, I use a Dirichlet or a radiative boundary condition.

I also apply Dirichlet or Robin boundary conditions to the lapse  $\alpha$  and the shift  $\beta^i$ . When using a Dirichlet boundary condition, I retain the boundary values from the initial data.

The lapse and the shift determine the coordinate system that is constructed for the spacetime during time evolution, and therefore their boundary values are important and have a clear meaning. Their boundary condition is part of the gauge condition, as described in section 3.4.

## 5.2 Excision boundary

Black hole spacetimes contain singularities. These singularities can, of course, not be directly treated numerically. Several methods have been used to treat them in a  $3 + 1$  split.

The likely oldest and mathematically most elegant ansatz is *maximal slicing* [SY78]. For this, one chooses the coordinate time in such a way that it reaches the singularity only for  $t \rightarrow \infty$ . The relation between the coordinate time  $t$  and the proper time  $\tau$  of an observer can be chosen almost arbitrarily through a suitable lapse function. With maximal slicing it is nevertheless the case that the whole spacetime is eventually covered by the time coordinate.

This elegant ansatz has the disadvantage that the time coordinate in the neighbourhood of the singularity proceeds more and more slowly, which eventually leads to a distortion of the coordinate system (“grid stretching”). Although the coordinate system stays well defined all the time, certain metric components start to grow without bound. This can in the end not be treated numerically any more. Maximal slicing can thus describe a black hole only for a certain amount of coordinate time before a code crashes for numerical reasons. There are also different slicings, such as harmonic [BM88] or  $1 + \log$  [ACM<sup>+</sup>95] slicings, with similar singularity-avoiding properties, and which also have similar disadvantages.

A different ansatz was developed at the AEI and is called *punctures* [BB97]. At the singularity, certain metric components are infinite. This behaviour can be described by decomposing the three-metric  $\gamma_{ij}$  into a conformal factor  $\psi$  and a conformal three-metric  $\tilde{\gamma}_{ij}$ . For certain initial data (such as e.g. Brill–Lindquist black holes; see section 6.3.1), the conformal three-metric remains finite over the singularity, and only the conformal factor diverges. The conformal factor for the initial data is known analytically, and by certain gauge choices (maximal slicing ( $K = 0$ ) and normal coordinates ( $\beta^i = 0$ ) at the punctures), the time derivative of the conformal factor can be set to zero. Additionally, one chooses a numerical grid such that the singularity does not coincide with a grid point. Through that, the code never has to calculate any diverging quantities. The conformal factor and its spatial derivatives are known analytically and can be provided with arbitrarily high accuracy.

However, the restriction on the gauge conditions has certain disadvantages; e.g. the position of the singularity cannot change in time. When two black holes coalesce, their physical distance decreases, while the coordinate distance stays constant with this method. This leads to similar problems as with maximal slicing. But a single black hole, which is an important test problem in numerical relativity, can in principle be described without problems with punctures.

Another way to treat singularities is *excision*. It consists of removing a certain region around the singularity from the simulation domain. Because there is, under certain reasonable assumptions, always an event horizon enclosing a singularity, this excising is possible without influencing the part of the domain outside the horizon. In the language of hydrodynamics, the excision or inner boundary is a supersonic outflow boundary for the physical degrees of freedom. Outflow means here “out of the simulation domain”, i.e. in the direction towards the singularity, further into the black hole.

In spherical coordinates, excision is quite customary, and it poses no problems, as the boundary can be put at an  $r = \text{const}$  coordinate plane. Unfortunately, spherical coordinates are not suitable for describing two coalescing black holes, which is why one usually uses Cartesian coordinates for that. The excised region on a Cartesian grid can not be spherical any more, but will rather look like a sphere that has been built from Lego blocks (see figure 5.1). This irregular shape leads to problems when implementing the excision boundary condition.



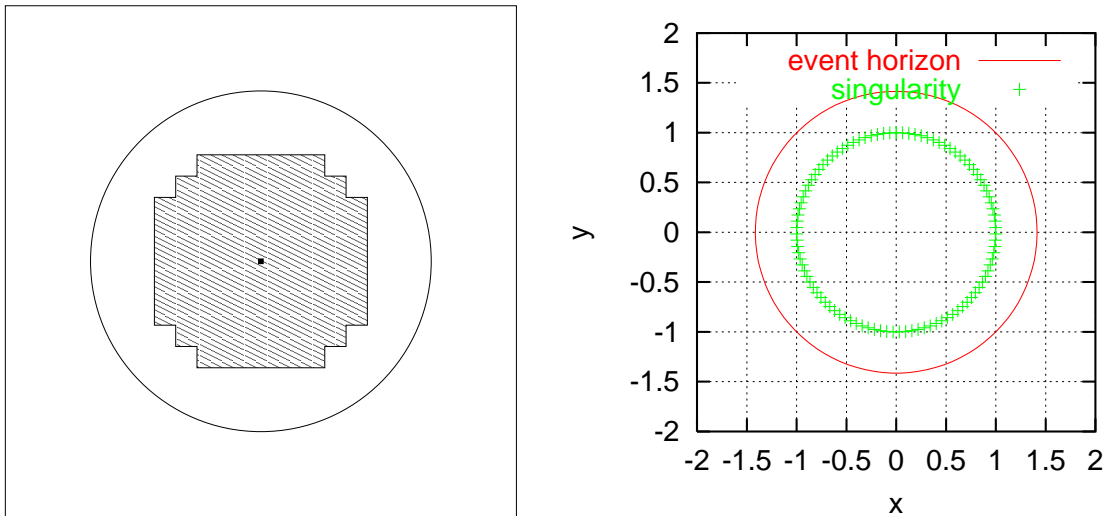


Figure 5.1: Left: Schematic picture of an excision region. The circle depicts the apparent horizon. The grey grid cells are excised. The excision boundary has to follow the grid cell boundaries. Right: A cut through the equatorial plane for an  $M = 1$ ,  $a = 1$  black hole in Kerr–Schild coordinates. There is not much coordinate space between the event horizon and the ring-shaped singularity.

It is generally assumed that excision is the most promising way to treat singularities, and that it will be widely used as soon as good boundary conditions are known for the excision region.

I will only consider excision boundaries in the remainder of this chapter. I will not consider punctures at all, and in order to use maximal slicing, one needs of course no special treatment of the singularity.

### 5.2.1 Location and shape of the excision boundary

In order to excise a region of space, one generally has to find a closed two-surface that is guaranteed to be both within the event horizon, and away from the singularity. One surface that is guaranteed to be within or on an event horizon is an apparent horizon (see section 7.6). For numerical reasons, one wants to stay several layers of grid points away from the event horizon, and also sufficiently far (as far as possible) from the singularity. It is thus necessary to locate apparent horizons to define or at least check the location of the excision boundary.

Choosing the right shape for the boundary is another rather difficult issue. Spherical or elliptic shapes are difficult to handle, because they do not have a normal direction that is aligned with the grid. Such normal directions are necessary for extrapolations. On the other hand, using a cubic boundary is not always possible. For example, the singularity of a rotating black hole in Kerr–Schild coordinates (see section 6.2.1) is ring-shaped, and the space available between the ring-shaped singularity and the elliptic horizon shape is too small to permit using a cubic boundary (see figure 5.1). One thus has to deal with boundary shapes that are not aligned with the computational grid. Some possible shapes include boxes “with the corners cut off”, which are polyhedra with 18

or 26 faces.<sup>2</sup>

### 5.2.2 Boundary conditions

Excision boundaries are very different from outer boundaries. Apart from the fact that they are more difficult to handle numerically because of their irregular shape, they are located in the strong field regime, and hence one cannot assume that any approximation holds. Luckily, there is an event horizon present, and the fact that no physical information can escape from the horizon means that one has some freedom in managing this boundary. As long as one stays within the limits of physics, one can choose any boundary condition without influencing the physics of the spacetime outside the horizon.

Yet there are things that do escape from the horizon. Information about the gauge and about constraint violations does not carry physical information. It can propagate faster than light, and can also leave the horizon. There is *a priori* no reason to assume that it would not do so. Care has to be taken in separating the individual quantities, which is much more difficult than at the outer boundary, where everything can be assumed to be a small perturbation of a known background. The inner boundary is a place where a hyperbolic formulation would definitively be of help.

While solving elliptic equations, it is consistent to use (arbitrary, constant in time) Dirichlet boundary conditions for the quantities  $V_i$ ,  $W_i$ ,  $\alpha$ , and  $\beta^i$ . Here the boundary values of the shift have to prevent the grid boundary from falling further into the black hole and getting too close to the singularity, or from rising out of it and leaving the event horizon (see also section 2.3). The latter would invalidate the assumption underlying excision and must therefore not be permitted.

While integrating in time, the boundary value for the conformal factor  $\psi$  has to be determined by a Dirichlet boundary condition from a known solution, or by extrapolation. The quantities  $\tilde{\gamma}_{ij}$  and  $\tilde{A}_{ij}$  carry a mixture of physical, gauge, and constraint information. The physical information has to be advected out of the simulation domain. Using a Dirichlet boundary condition for the physical degrees of freedom is consistent only if one uses the correct values. Of course, the correct values are only known if one tests the code with an analytic solution, so this is not possible for real-world cases.

A supersonic outflow boundary condition can be realised by extrapolation. Unfortunately, extrapolating the conformal metric causes problems, because the extrapolated conformal metric will normally not satisfy the constraint  $\det \tilde{\gamma}_{ij} = 1$  any more. It is not a good idea to enforce this constraint by rescaling the whole metric, because this will change certain gauge degrees of freedom in unpredictable ways. Allowing for arbitrary gauge changes at the excision boundary might allow gauge modes to appear.

Instead, the gauge degrees of freedom have to be fixed, according to the plan I set out in section 3.2. The obvious gauge degree of freedom to fix at the inner boundary is the location of the boundary itself. That is, I want to clearly define how the inner boundary moves inward or outward (again, see also section 2.3). Therefore I decompose the metric components  $\tilde{\gamma}_{ij}$  into those parallel to and those normal to the boundary. I enforce the constraint  $\det \tilde{\gamma}_{ij} = 1$  by rescaling only those components that are normal to the boundary. This is also consistent with the fact that gravitational waves cause transverse length changes only, because these lengths will not be changed by the rescaling.

The traceless conformal extrinsic curvature happens to be less critical. It does not contain any gauge degrees of freedom. By extrapolating  $\tilde{A}_{ij}$  one violates the constraint  $\tilde{A}_i^i = 0$ , especially

<sup>2</sup>I think this was first suggested by Miguel Alcubierre in 2000.

because the conformal metric used to calculate that trace is also extrapolated, and hence changes as well. Both the extrapolation of  $\tilde{A}_{ij}$  and enforcing  $\tilde{A}_i^i = 0$  later on will change the boundary condition for the constraints. However, the constraints can be enforced no matter what the boundary values. Numerical experiments show that the handling of the traceless conformal extrinsic curvature is not critical and does not lead to instabilities.

I assume that the constraint violation error that is introduced by extrapolating  $\tilde{A}_{ij}$  is less malevolent than the gauge error introduced by extrapolating  $\tilde{\gamma}_{ij}$ . This gauge error has the ability to change the extent of the simulation domain, and that is not acceptable. On the other hand, the constraint error could lead to certain components of  $\tilde{A}_{ij}$  growing without bound, although the constraints would stay satisfied. Luckily, that seems to not happen.

With the the above boundary conditions for the excision boundary, the time evolution of the TGR system is consistent, and all degrees of freedom are fixed.

## 5 *Boundary conditions*

## 6 Initial data

It is a nontrivial task to generate initial data for a black hole simulation. There are many analytic solutions for single black holes, but the proposed methods to construct spacetimes with two or more black holes either restrict the possible configurations, or require solving elliptic equations. Multiple black hole initial data usually need to be interpreted in terms of their ADM mass and spin [Wei72, chapter 6.6], and the apparent horizons (see chapter 7.6) that can be found.

Initial data are usually presented in the ADM variables  $\gamma_{ij}$  and  $K_{ij}$ , even if they are actually calculated in other variables. This has the advantage that the form of the initial data is independent of the formulation used in the evolution, and facilitates exchanging initial data between different formulations. The transformation between the ADM and other variables is usually straightforward.

I present three major kinds of initial data in this chapter. I start with data without black holes. These data often have an analytic solution for all times and can thus be easily used as test cases. I then present various coordinate systems for static or stationary single black holes. They are also mostly test cases of little astrophysical relevance. Last I present initial data for multiple black holes, for which no closed form solution exists for later times.

I follow the convention of giving names not to spacetimes, but rather to coordinate systems. This is motivated by the fact that different coordinate systems behave very differently numerically. On the other hand, the fact that two different coordinate systems might describe the same physical spacetime is largely irrelevant for me, because it cannot easily be tested. I also hope that this helps to prevent confusion. I thus distinguish between flat space (a spacetime) and a Minkowski metric (one possible coordinate system for it). Similarly, there are static black holes, of which Schwarzschild is just one possible metric, with zero-spin Kerr–Schild and Painlevé–Gullstrand being others.

### 6.1 Data without black holes

#### 6.1.1 Minkowski metric (flat space)

The Minkowski metric is the simplest case. It describes flat space in Cartesian coordinates. It has  $g_{\mu\nu} = \eta_{\mu\nu}$ , or  $\gamma_{ij} = \delta_{ij}$ ,  $K_{ij} = 0$ ,  $\alpha = 1$ , and  $\beta^i = 0$ .

#### 6.1.2 Weak Bondi wave (linear planar wave)

A weak Bondi wave is a planar gravitational wave with a small amplitude. This is a solution to the linearised Einstein equations, presented e.g. in [MTW73, chapter 35.9, eqn. (35.32)]. Assuming that the wave propagates in the  $z$  direction, the ADM quantities are given by

$$\gamma_{xx} = 1 + b \tag{6.1}$$

$$\gamma_{yy} = 1 - b \tag{6.2}$$

## 6 Initial data

$$\gamma_{zz} = 1 \quad (6.3)$$

$$K_{xx} = -\frac{1}{2}\dot{b} \quad (6.4)$$

$$K_{yy} = \frac{1}{2}\dot{b} \quad (6.5)$$

$$K_{zz} = 0 \quad (6.6)$$

where all other components of  $\gamma_{ij}$  and  $K_{ij}$  are zero, and  $\alpha = 1$  and  $\beta^i = 0$ . The free parameter function  $b(t, z)$  can e.g. be chosen as

$$b = A \sin k(z - t) \quad (6.7)$$

$$\dot{b} = \partial_t b = -k A \cos k(z - t) \quad (6.8)$$

for a wave propagating in the  $z$  direction, or as

$$b = A \sin kz \cos kt \quad (6.9)$$

$$\dot{b} = \partial_t b = -k A \sin kz \sin kt \quad (6.10)$$

for a standing wave, where in all cases  $|b| \ll 1$  has to hold. The parameters  $A$  and  $k$  determine the amplitude and wave number of the weak Bondi wave. This metric is a solution of the Einstein equations only for  $|A| \ll 1$ .

### 6.1.3 Gauge pulse (nonlinear planar gauge wave)

A gauge pulse is a planar nonlinear gauge wave. This is a solution to the full vacuum Einstein equations which does not contain gravitational waves. It represents a flat spacetime in a strange coordinate system. Assuming that the wave propagates in the  $z$  direction, the ADM quantities are given by

$$\gamma_{xx} = 1 \quad (6.11)$$

$$\gamma_{yy} = 1 \quad (6.12)$$

$$\gamma_{zz} = \exp\{b\} \quad (6.13)$$

$$K_{zz} = -\frac{1}{2} \exp\left\{\frac{b}{2}\right\} \dot{b} \quad (6.14)$$

$$\alpha = \exp\left\{\frac{b}{2}\right\} \quad (6.15)$$

where all other components of  $\gamma_{ij}$ ,  $K_{ij}$ , and  $\beta^i$  are zero. The free parameter function  $b(t, z)$  can e.g. be chosen as

$$b = A \sin k(z - t) \quad (6.16)$$

$$\dot{b} = \partial_t b = -k A \cos k(z - t) \quad (6.17)$$

for a wave propagating in the  $z$  direction, or as

$$b = A \sin kz \cos kt \quad (6.18)$$

$$\dot{b} = \partial_t b = -k A \sin kz \sin kt \quad (6.19)$$

for a standing wave. The parameters  $A$  and  $k$  determine the amplitude and wave number of the gauge pulse. The amplitude  $A$  can be arbitrarily large.

### 6.1.4 Brill wave

A Brill wave is a nonlinear, axially symmetric gravitational wave [Bri59]. A Brill wave can be strong enough to form a black hole. This is an interesting test case, insofar as a black hole can form from scratch, without a singularity or matter being present in the beginning.

In contrast to the solutions presented above, which are valid for all times, the Brill wave metric given below describes only initial data at  $t = 0$ . The metric can be written as

$$ds^2 = \psi^4 \left[ e^{2q} (d\rho^2 + dz^2) + \rho^2 d\phi^2 \right] \quad (6.20)$$

with the free function  $q(\rho, z)$  than can e.g. be chosen as

$$q = A \rho^2 e^{-r^2} \quad (6.21)$$

with the amplitude  $A$ .  $\rho$  is the cylindrical radial coordinate with  $\rho^2 = x^2 + y^2$ .

These initial data are then chosen to be time-symmetric with  $\partial_t \gamma_{ij} = 0$ . Together with the gauge choice  $\beta^i = 0$  this leads to the extrinsic curvature  $K_{ij} = 0$ , satisfying the momentum constraint identically. The conformal factor  $\psi$  has to be chosen (solved for) so that the Hamiltonian constraint is satisfied. One usually uses a Robin type boundary condition for this.

One usually uses maximal slicing ( $K = 0$ ) and normal coordinates ( $\beta^i = 0$ ) when simulating a Brill wave. One also usually uses a Robin boundary condition for the lapse.

## 6.2 Single black hole data

There are many coordinate systems that describe single black holes. I chose to test my formulation with three, namely Kerr–Schild coordinates, Painlevé–Gullstrand coordinates, and harmonic coordinates. The original Schwarzschild coordinates are not suitable here, because they do not penetrate the horizon. That would not allow me to use an excision boundary condition (see section 5.2), which has to be applied inside the event horizon.

### 6.2.1 Kerr–Schild coordinates

For single black hole test runs I prefer the Kerr–Schild coordinates<sup>1</sup>. This is a static (or stationary, when there is a nonzero spin) solution with a spin that can be specified freely. The slicing does intersect the singularity, and the singularity in the time slice is a point for a non-spinning, and is ring-shaped for a spinning black hole. The singularity diverges with  $1/r^2$  only, which still allows reasonable numerical resolutions to be used.

Kerr–Schild coordinates [Coo02, section 3.3.1] are usually expressed in an elliptic coordinate system, where the  $r$  coordinate is given by

$$\rho^2 = r^2 + a^2 \left( 1 - \frac{z^2}{r^2} \right) \quad (6.22)$$

---

<sup>1</sup>For some historic reason, these coordinates are sometimes also called “ingoing Eddington–Finkelstein coordinates” in the community, although the real iEF coordinates are different.

## 6 Initial data

with the usual radial coordinate  $\rho$ , i.e.  $\rho^2 = x^2 + y^2 + z^2$ . The four-metric can be written as

$$g_{\mu\nu} = \eta_{\mu\nu} + 2Hl_\mu l_\nu \quad (6.23)$$

where  $\eta_{\mu\nu}$  is the Minkowski metric,  $H$  is a scalar, and  $l_\mu$  is a null vector, which are given by

$$H = \frac{Mr^3}{r^4 + a^2 z^2} \quad (6.24)$$

$$l_t = 1 \quad (6.25)$$

$$l_x = \frac{rx + ay}{r^2 + a^2} \quad (6.26)$$

$$l_y = \frac{ry - ax}{r^2 + a^2} \quad (6.27)$$

$$l_z = \frac{z}{r} \quad (6.28)$$

where  $M$  is the black hole mass, and  $a$  is its spin about the  $z$  axis. The three-metric, lapse, and shift then follow as

$$\gamma_{rr} = 1 + \frac{2Mr}{\rho^2} \quad (6.29)$$

$$\gamma_{r\phi} = -a \left[ 1 + \frac{2Mr}{\rho^2} \right] \sin^2 \theta \quad (6.30)$$

$$\gamma_{\theta\theta} = \rho^2 \quad (6.31)$$

$$\gamma_{\phi\phi} = \left[ r^2 + a^2 + \frac{2Mr}{\rho^2} a^2 \sin^2 \theta \right] \sin^2 \theta \quad (6.32)$$

$$\alpha = \frac{1}{\sqrt{1 + \frac{2Mr}{\rho^2}}} \quad (6.33)$$

$$\beta^r = \alpha^2 \frac{2Mr}{\rho^2} . \quad (6.34)$$

The event horizon is located at  $r = M + \sqrt{M^2 - a^2}$ .

The extrinsic curvature is defined implicitly via  $\gamma_{ij}$ ,  $\alpha$ ,  $\beta^i$ , and their derivatives through the ADM time evolution equation for  $\gamma_{ij}$  (see eqn. (A.5)).

### 6.2.2 Painlevé–Gullstrand coordinates

Painlevé–Gullstrand coordinates [Coo02, section 3.3.3] are interesting because they have a flat three-metric  $\gamma_{ij} = \delta_{ij}$ . However, it seems empirically that their time evolution leads to higher discretisation errors. The spacetime is described by

$$\gamma_{ij} = \delta_{ij} \quad (6.35)$$

$$K_{ij} = \sqrt{\frac{2M}{\rho^3}} \left[ \delta_{ij} - \frac{3}{2} q^i q^j \right] \quad (6.36)$$

$$\alpha = 1 \quad (6.37)$$



$$\beta^i = \alpha^2 \sqrt{\frac{2M}{\rho}} q^i \quad (6.38)$$

where the parameter  $M$  is the mass of the black hole. The auxiliary quantity  $q^i$  is defined as  $q^i = x^i/\rho$ . I do not allow for spin.  $\rho$  is the usual radial coordinate with  $\rho^2 = x^2 + y^2 + z^2$ .

### 6.2.3 Harmonic coordinates

Harmonic coordinates follow from the coordinate conditions  $\square x^{(\mu)} = 0$  [Coo02, section 3.3.2]. A black hole in harmonic coordinates is described by

$$\gamma_{ij} = \delta_{ij} + (v + v^2 + v^3) q^i q^j \quad (6.39)$$

$$\alpha = \frac{1}{\sqrt{1 + v + v^2 + v^3}} \quad (6.40)$$

$$\beta^i = \alpha^2 v^2 q^i \quad (6.41)$$

where  $v = 2M/\rho$ , and  $q^i = x^i/\rho$ .  $\rho$  is the usual radial coordinate with  $\rho^2 = x^2 + y^2 + z^2$ , and  $M$  is the mass of the black hole. I do not allow for spin. The extrinsic curvature is defined implicitly via  $\gamma_{ij}$ ,  $\alpha$ ,  $\beta^i$ , and their derivatives through the ADM time evolution equation for  $\gamma_{ij}$  (see eqn. (A.5)).

### 6.2.4 Coordinate transformations

In order to have access to a larger class of initial data and analytic solutions, I allow for a generic coordinate transformation to be applied to the initial data.<sup>2</sup> This transformation is applied to the solution's four-metric, making it automatically covariant. The transformation can e.g. be used to rotate a black hole to point the spin into any direction, boost the black hole, deform the black hole in various more or less useful ways, and change to a moving coordinate system.

Such a generic coordinate transformation is defined by the usual  $x^\mu = T_\nu^\mu \hat{x}^\nu$  with the transformation tensor  $T_\nu^\mu = \partial x^\mu / \partial \hat{x}^\nu$ . I also allow for a coordinate translation  $x^\mu = \hat{x}^\mu + C^\mu$ . This makes for altogether  $16 + 4 = 20$  free parameters. In order to allow the coordinate change to be prescribed conveniently, I decompose the coordinate transformation into

$$T = \text{Rot} \circ \text{Slow} \circ \text{Dfrm} \circ \text{Cshn} \circ \text{Shear} \circ \text{Bst} \circ \text{Vel} \quad (6.42)$$

where

**Rot** is a rotation of the spatial components,

**Slow** is a slowdown, i.e. a scaling of the lapse,

**Dfrm** is a deformation of the spatial components, i.e. a rescaling of the coordinate axes,

**Cshn** is a cushion deformation of the spatial components,

**Shear** is a shear transformation of the spatial components,

<sup>2</sup>Currently I implemented this only for the Kerr–Schild solution.

## 6 Initial data

Bst is a Lorentz boost, and

Vel is a change to a moving coordinate system.

Of the above, Bst is not really necessary and could be replaced by a combination of the other transformations, but I keep it for convenience. The individual transformation operators are defined as

$$\text{Rot}_j^i = \delta_j^i - \Omega_k^i \Omega_j^k (\cos 2\pi\alpha - 1) \quad (6.43)$$

$$+ \Omega_j^i \sin 2\pi\alpha \quad (6.44)$$

$$\text{with } \Omega_j^i = \epsilon_{ijk} \text{rot}^k / \alpha \quad (6.45)$$

$$\text{and } \alpha = |\mathbf{rot}| \quad (6.46)$$

$$\text{Slow}_0^0 = \text{slow} \quad (6.47)$$

$$\text{Dfrm}_j^i = \text{diag}(\text{dfrm}^k) \quad (6.48)$$

$$\text{Cshn}_j^i = \delta_j^i + |\epsilon_{ijk}| \text{cshn}^k \quad (6.49)$$

$$\text{Shear}_j^i = \delta_j^i + \epsilon_{ijk} \text{shear}^k \quad (6.50)$$

$$\text{Bst}_0^0 = \gamma \quad (6.51)$$

$$\text{Bst}_0^i = \text{Bst}_i^0 = \text{bst}^i \gamma \quad (6.52)$$

$$\text{Bst}_j^i = \delta_j^i + \frac{\gamma^2}{\gamma + 1} \text{bst}^i \text{bst}^j \quad (6.53)$$

$$\text{with } \gamma = \frac{1}{\sqrt{1 - |\mathbf{bst}|^2}} \quad (6.54)$$

$$\text{Vel}_0^i = \text{vel}^i \quad (6.55)$$

where the remaining components of these four-tensors are set to  $\delta_\nu^\mu$ . The lower-case three-vectors  $\text{rot}^i$ ,  $\text{dfrm}^i$ ,  $\text{cshn}^i$ ,  $\text{shear}^i$ ,  $\text{bst}^i$ ,  $\text{vel}^i$ , and the scalar  $\text{slow}$  parameterise these transformations with 19 (instead of the necessary 16) free parameters. Additionally there are the 4 translation parameters  $C^\mu$ .

A rotation is described by a three-vector  $\text{rot}^i$ . Its direction is the axis of rotation, and its length the angle, where a length of 1 means one full rotation. A cushion transformation changes a square into a cushion- or a barrel-shaped object, where the components of the three-vector  $\text{cshn}^k$  describe the distortion factors along the diagonals. A shear transformation changes a square into a rhomboid, where the components of the three-vector  $\text{shear}^k$  describe the shear factor along the corresponding coordinate axis.

Rotations are useful e.g. to point the spin of an object in an arbitrary direction. Deformations and shears can be used e.g. to create coordinates where the contravariant and covariant three-vectors differ (for testing purposes). A velocity transformation can be used to cancel effects of a boost, e.g. to create a stationary boosted black hole (which differs from a non-boosted black hole). Rotations and boosts together form the proper Lorentz transforms.

From the transformed four-metric I then calculate the ADM quantities, i.e. the three-metric, the extrinsic curvature, lapse, and shift. The extrinsic curvature is defined via the time derivative of the three-metric using equation (A.5). The necessary partial derivatives can easily be calculated numerically to any given accuracy, much more accurately than to the grid spacing accuracy.

When lapse and shift are later, during the time evolution, determined through elliptic equations, one needs boundary conditions for them. I often use the boundary values from the initial data as Dirichlet boundary conditions. This makes the method used to initially calculate lapse and shift actually important.

## 6.3 Multiple black hole data

### 6.3.1 Brill–Lindquist data

Brill–Lindquist data [Coo02, section 3.1.2] can contain arbitrarily many black holes. The black holes are described by their coordinate location and by a mass parameter. This solution is also only valid on a single time slice. It is time-symmetric and conformally flat:

$$\psi = 1 + \sum_n \frac{\mu_n}{2|\mathbf{x} - \mathbf{x}_n|} \quad (6.56)$$

$$\gamma_{ij} = \psi^4 \delta_{ij} \quad (6.57)$$

$$K_{ij} = 0 \quad (6.58)$$

$$\alpha = 1 \quad (6.59)$$

$$\beta^i = 0 \quad (6.60)$$

where  $\mathbf{x}_n$  are the positions of the black holes, and  $\mu_n$  are their mass parameters.

If there is only one black hole, then the convention to write  $\mu/2$  instead of  $2\mu$  means that the event horizon is at  $r = \mu/2$  instead of at  $r = 2\mu$ . In this case, the black hole still has the mass  $M = \mu$ .

### 6.3.2 Superposed Kerr–Schild data

For multiple black hole runs I prefer superposed Kerr–Schild data. They were to my knowledge first proposed by Mazner et al. [MHS99] and have recently been refined by Moreno et al. [MNS02]. They follow a rather intuitive approach. One views a single black hole as the sum of a flat space metric and a black hole metric contribution. This view is motivated by the form of equation (6.23) in which the Kerr–Schild four-metric can be written. One then combines two black holes by adding two different black hole contributions to a flat space metric. This combined metric does, however, not satisfy the constraints any more, so that a constraint solving step has to follow.

The black holes can be combined in two ways. In the first way, one combines the three-metrics and the extrinsic curvatures; in the second way, one combines the four-metrics and their time derivatives. Both ways are equally “valid” in principle. Note, however, that the second way breaks down when the black holes are close to each other.<sup>3</sup> It can be convenient to attenuate the combined solutions as one gets close to one of the black holes, regaining a single black hole solution near the individual holes.

When superposing the three-metrics and the extrinsic curvatures of  $n$  black holes, one uses

$$\gamma_{ij} = \delta_{ij} + \sum_n \left[ \gamma_{ij}^{(n)} - \delta_{ij} \right] \quad (6.61)$$

<sup>3</sup>The combined four-metric then does not have a  $(-, +, +, +)$  signature any more. This cannot happen when superposing the three-metrics and extrinsic curvatures.

## 6 Initial data

$$K_{ij} = \sum_n K_{ij}^{(n)} \quad (6.62)$$

$$\alpha = 1 + \sum_n [\alpha^{(n)} - 1] \quad (6.63)$$

$$\beta^i = \sum_n \beta^{(n)i} \quad (6.64)$$

The quantities  $\cdot^{(n)}$  are the corresponding quantities from the to-be-superposed black holes. Note that the way in which the extrinsic curvatures are superposed means that the superposition of two black holes at the same position does not give a single black hole with the combined mass, and does not satisfy the constraint equations any more.

When superposing the four-metric and its time derivative, one uses

$$g_{\mu\nu} = \eta_{\mu\nu} + \sum_n [g_{\mu\nu}^{(n)} - \eta_{\mu\nu}] \quad (6.65)$$

and then calculates three-metric, extrinsic curvature, lapse, and shift from this four-metric and its time derivatives. In both cases, one can also use a different lapse and shift than calculated here, but this will lead to a different extrinsic curvature with the second method. When attenuating, one attenuates the contributions from the individual black holes.

As mentioned above, the resulting spacetime will in general not satisfy the constraints. One has to use the combined metric as background metric and initial guess to explicitly solve the constraint equations (see chapter 4). I usually use the conformal factor  $\psi$  resulting from the superposition and vector potential  $V_i = 0$  as boundary conditions for this. It is also possible to use a Robin boundary condition for  $\psi$ . In order to verify that this procedure does indeed lead to black holes, one has to locate the apparent horizons (see section 7.6).

## 7 Code

The computer code that is used by us numerical physicists is of utmost importance to us. It is our experimental setup, the testbed for our ideas, the centre about which our group assembles in the morning, and the equipment that we check upon even on weekends. Small codes might be written on rainy afternoons or on lazy weekends; they come a dime a dozen and are quickly forgotten. The large codes take several people and several months or years to assemble and fine-tune, and correspondingly one has to put a lot of effort into keeping a code maintainable and understandable to others.

Yet a code is never, at least not to us numerical physicists, an end in itself. It is a tool; it is an important one, but yet only a tool.

### 7.1 The Tiger code

I created and used the *Tiger code*<sup>1</sup> to test the ideas presented in the previous chapters. It descended from the Maya code [Pen], written in 2000 at Penn State under Pablo Laguna, which in turn descended from the Agave code [Col], which in turn was one of the results of the Binary Black Hole Coalescence Grand Challenge [All].

The Tiger code is written in the Cactus framework [ABD<sup>+</sup>01, ABG<sup>+</sup>01, Cac], which relieves the programmer of many merely software-engineering related problems, and which is also supposed to make easier the sharing of code modules. At the time of this writing, the sharing still has to happen. The main obstacles seem to be rather mundane things such as e.g. differing variable names. A promising standardisation effort for ADM-like evolution codes was started in the spring of 2002 by the home institution of Cactus, the Albert–Einstein–Institut in Golm near Potsdam.

When writing a numerical code for a complicated system of equations, there is always the issue of how to translate the equations into code. One can either create the code semi-automatically with a symbolic algebra package such as Maple [Map], or one can code the equations by hand. Both approaches have their advantages. I chose to code the equations by hand. In doing that, I strove for clarity, relying on the compiler to produce efficient code. Appendix B.4 shows some example code.

The Tiger code has the standard structure found in time evolution codes. (This structure is also mandated by Cactus.) It consists of five large components: initial data, constraint solving, time evolution, boundary conditions, and analysis routines. Each of these components is described below.

---

<sup>1</sup>TGR, pronounced “Tiger”: the Tübingen General Relativity Code. (Codes apparently have to have names.) The pronunciation “Tiger” was suggested by Gabrielle Allen.

## 7.2 Initial data

In order to facilitate exchanging initial data routines and initial data themselves, it is customary in numerical general relativity to create initial data in the ADM variables (see chapter 6), i.e. for the three-metric  $\gamma_{ij}$  and the extrinsic curvature  $K_{ij}$ . While these are sufficient as initial data, it is also often customary to additionally provide the initial lapse  $\alpha$  and shift  $\beta^i$ . With lapse and shift included, the whole four-metric  $g_{\mu\nu}$  can be reconstructed on the initial time slice.

The Tiger code contains initial data routines for several analytic solutions and background data. Among these are the Minkowski spacetime (flat space, see section 6.1.1), weak Bondi waves (linear planar gravitational waves, see section 6.1.2), the background data for Brill waves (see section 6.1.4), and black holes in Kerr–Schild coordinates (see section 6.2.1), Painlevé–Gullstrand coordinates (see section 6.2.2), and harmonic coordinates (see section 6.2.3), as well as Brill–Lindquist black holes (see section 6.3.1). The Kerr–Schild data can have generic coordinate transformations applied (see section 6.2.4), and they can also be used as background data to superpose black holes (see section 6.3.2).

The background data mentioned above do not satisfy the constraints. They can be used as background and as initial guess to solve the constraint equations numerically (see below), which is necessary to obtain a solution to Einstein’s equations from them.

Sometimes it is convenient to create initial data e.g. in spherical or cylindrical coordinates, and then transform these into Cartesian coordinates. For this, the initial data are still calculated at the grid points forming the Cartesian grid, but the tensors have their components in another coordinate system. A coordinate transformation into Cartesian tensor components is then a linear transformation according to the usual  $T^i = (\partial x^i / \partial x^j) T^j$ .

After creating initial data in the ADM variables, these are converted to the TGR variables (see chapter 4), which form the primary variables in the Tiger code.

## 7.3 Constraint solvers

After creating initial data in the TGR variables, and after every time step, these data are used as background and as initial guess to enforce the gauge and the constraints, and to calculate the lapse and shift. This is the part that distinguishes the Tiger code from other codes that evolve unconstrained and without fixing the gauge.

Enforcing the gauge condition for  $F_i$ , enforcing the constraints, and calculating lapse and shift requires solving nonlinear coupled elliptic equations. This is currently done using the thorn TATelliptic in Cactus. This thorn is an interface to generic nonlinear elliptic solvers. The only currently available reasonable solvers are TATPETSc, which is an interface to the PETSc library [BBG<sup>+</sup>01, BGMS97, BGMS01], and TATMG, which is a full approximation storage multigrid solver [Wes92] that is currently being written by me.

Enforcing the gauge condition  $F_i$  yields the traceless conformal metric  $\bar{h}_{ij}$ . In order to calculate  $\tilde{\gamma}_{ij}$  from this, one has to choose trace  $\tilde{\gamma}_{ij}$  such that  $\det \tilde{\gamma}_{ij} = 1$ . This is a nonlinear equation that does not involve derivatives. I solve it with the `zridr` routine of Numerical Recipes [PTVF92].

## 7.4 Time integration

The evolution equations are the equations for the time derivatives of the primary variables. In the Tiger code, these are  $\psi$ ,  $\tilde{\gamma}_{ij}$ , and  $\tilde{A}_{ij}$  (see chapter 4). Evaluating these equations is straightforward but tedious (see appendix A.2.2, eqns. (A.21), (A.22), and (A.27)). One usually introduces the Christoffel symbols  $\Gamma_{jk}^i$  and/or  $\tilde{\Gamma}_{jk}^i$  and the Ricci tensor  $R_{ij}$  as explicit intermediate quantities.

The time evolution equation for  $\psi$  is not strictly necessary during time evolution, but is there nonetheless for analysis purposes. The Tiger code contains additionally the time evolution equations for the gauge variables  $K$  and  $F_i$ , which are needed to determine the lapse  $\alpha$  and the shift  $\beta^i$  (see appendix A.2.2).

The time evolution equations for the Hamiltonian and momentum constraints are not implemented. One could theoretically use them to verify the Bianchi identities at run time, and thus gather an additional measure for discretisation errors.

The time integrator proper uses the iterative Crank–Nicholson scheme [Teu00] (see appendix B.2). This is an explicit second-order scheme that can be used to introduce some diffusion in order to obtain a stable discretisation for advection terms. As the name suggests, this diffusion is introduced via additional iterations. I often run with just a single iteration, so that the scheme is identical to the midpoint rule (see appendix B.2) and does not add any artificial diffusion. Instead, I add explicit artificial diffusion terms to the time evolution equations (see appendix B.2.1).

## 7.5 Boundary conditions

Boundary conditions are necessary for enforcing the constraints and gauge conditions, and for the time evolution.

### 7.5.1 Outer boundary

For the constraint, gauge condition, and coordinate condition solvers, there are Dirichlet and Robin boundary conditions available on the outer boundary. Dirichlet boundaries are kept constant while solving, but they do not have to be constant in space. Robin boundary conditions enforce a certain falloff towards infinity (see section 5.1.2). They are readily available in Cactus [Cac].

For the time evolution, there are Dirichlet and radiative boundary conditions available. Dirichlet boundary conditions are kept constant in time, but they do not have to be constant in space. Radiative boundary conditions assume that the evolved quantity is an outgoing spherical radial wave (see section 5.1.2). They, too, are available in Cactus.

Additionally, certain symmetry conditions can be enforced at the boundaries, e.g. to restrict the simulation domain to a quadrant or an octant of space, or to enforce periodicity.

For the robust stability tests (see section 8.2), noise can be introduced at the boundary.

### 7.5.2 Excision boundary

For the constraint, gauge condition, and coordinate condition solvers, there are only Dirichlet boundary conditions available on the excision boundary. These Dirichlet boundaries are kept constant while solving, but may vary in space.

For the time evolution, there are Dirichlet and extrapolation boundary conditions available on the excision boundary. Dirichlet boundaries are kept constant in time, but may vary in space. The extrapolation boundaries apply an  $n$ -th order polynomial extrapolation ( $n \in [0 \dots 3]$ ) towards the excision boundary. They are applied along the normals of the excision boundary. The high order of extrapolation is necessary because it is applied close to the singularity, where the shape of the extrapolated functions is not anywhere near flat. It is quite possible that a non-polynomial extrapolation (e.g. in terms of  $1/r$ ) would perform better.

## 7.6 Analysis routines

After every time step, the ADM variables are calculated from the TGR variables. The ADM variables by themselves are important analysis quantities, because they allow comparisons to analytic solutions, or to results from other codes. However, because the coordinate system that is used to represent the ADM variables is generally not known, the three-metric and the extrinsic curvature alone do not provide much insight into the result of a simulation. While they are, together with the lapse and shift, sufficient to extract the four-metric and therefore theoretically all information about the spacetime, these quantities are basically impossible to interpret when visualised on their own.

The Tiger code provides, as analysis quantities, also all the intermediate quantities that are calculated during the time evolution. These are the three-Ricci tensor, the time derivatives of the TGR variables, the constraints, the gauge variables and their time derivatives, and the gauge violations. It also provides the time derivatives of the ADM variables, and the constraints as calculated from the ADM variables. Additionally it calculates the four-Weyl tensor, which can be used to extract information about gravitational radiation from a simulation, although I did not attempt this in my test runs.

Apparent horizons [Tho93, chapter 4], [Tho96, Shi97, SU00, HCM00, SHM00, Sch02] are the only locally (in time) detectable structures that are present in vacuum spacetimes. Event horizons are global structures and cannot be detected during a time evolution. The Tiger code can locate and track multiple apparent horizons. It reports the area and irreducible mass of the horizon. If the horizon is isolated [DKSS], it calculates also the spin and total mass.



## 8 Results

In this chapter I present results from example runs with the Tiger code, using the formalism laid out in the previous chapters. I begin with some convergence tests demonstrating that the Tiger code is second-order convergent apart from artificial diffusion, and also showing the typical magnitude of the discretisation errors. A section about runs with added noise then supports my claim that the formalism and its implementation are robustly stable in the sense of Szilágyi et al. [SGBW00, SSW02]. Two sections on Brill waves and Kerr–Schild black holes show that the code works well in the presence of strong field dynamics and black holes.

### 8.1 Convergence tests

#### 8.1.1 Static and stationary tests: black holes

Here I present a series of convergence tests for highly nonlinear but static or stationary spacetimes. By calculating the time derivatives of several quantities, essentially the whole right hand side evaluation subsystem of the code is tested. The tests here contain no time evolution (but all the following tests do). All time derivatives should converge to zero to second order as the numerical resolution is increased.

As test cases I use black holes in several coordinates, namely Kerr–Schild (see section 6.2.1), Painlevé–Gullstrand (see section 6.2.2), and harmonic coordinates (see section 6.2.3). In all cases, the mass of the black hole is  $M = 1$ . For Kerr–Schild coordinates, the spin is  $a = 0.9$ , and for the other two cases, the spin is zero. These are stationary or static solutions, meaning that the analytic values of the time derivatives are all zero. The time derivatives of certain primary quantities are shown, as well as some constraints. All shown quantities should be zero. The absolute values of the numerical values along the  $x$  axis are plotted, where the results from the finer resolutions have been scaled by factors of 4 and 16, respectively. The dips in the graphs indicate places where the numerical error vanishes because it changes sign.

The fact that the graphs for the different resolutions in figures 8.1, 8.2, and 8.3 do overlap indicates second order convergence. Nevertheless, the errors of some of these quantities are surprisingly large. Note that the coarsest resolution that I present here is  $dx = 1/16$ , which is already considered to be a rather fine resolution for a typical black hole collision simulation.

The  $L_2$  norms of the convergence factors for the resolutions  $dx = 1/32$  and  $dx = 1/64$  and for the three coordinate systems (cs) Kerr–Schild (KS), Painlevé–Gullstrand (PG), and harmonic coordinates (hc) are given below. The fact that the factors are so close to 4 indicates near-perfect second order convergence of the code:

cs	$\partial_t \psi$	$\partial_t K$	$\partial_t h_{xx}$	$\partial_t A_{xx}$	$H$	$M_x$
KS	3.99554	4.00827	4.00078	4.00763	3.99803	3.99002
PG	3.99958	4.00089	3.99852	4.0006	(n/a)	3.99987
hc	3.99976	3.99453	(4.59489)	4.00214	3.99408	3.99923

## 8 Results

The convergence factor for the Hamiltonian constraint  $H$  for Painlevé–Gullstrand coordinates is ill-defined because the metric is flat, and hence the Hamiltonian constraint is exactly zero everywhere. The convergence factor for  $\partial_t h_{xx}$  for harmonic coordinates is larger than 4 because the discretisation error changes sign at  $x = 2$  and hence the convergence factor is ill-defined there. Excluding this grid point, the  $L_2$  norm of this convergence factor is 4.00058.

## 8.1 Convergence tests

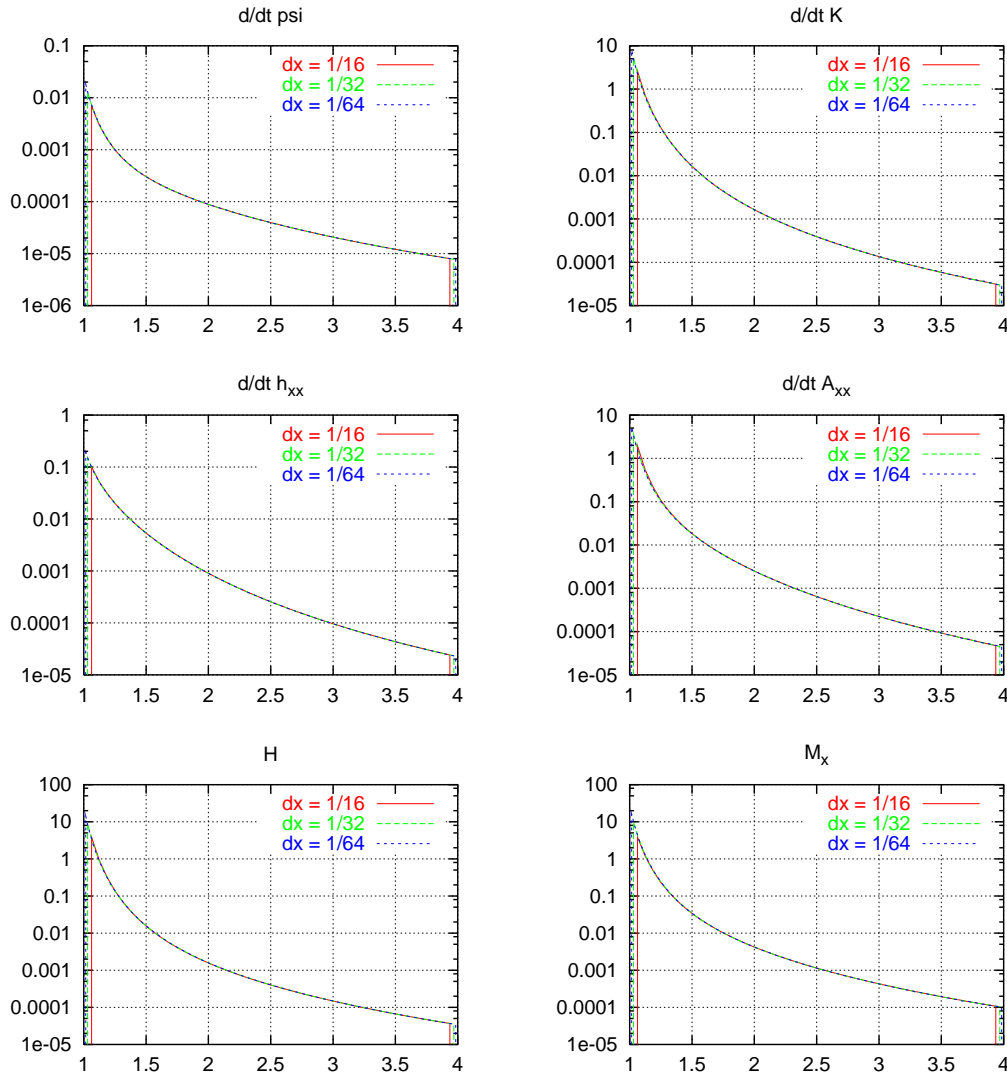


Figure 8.1: Convergence test with Kerr–Schild coordinates. The graphs show the errors in the time derivatives of various quantities for three resolutions. The errors for the finer resolutions have been scaled by the factors 4 and 16, respectively. The coinciding graphs show that there is second order convergence towards zero.

## 8 Results

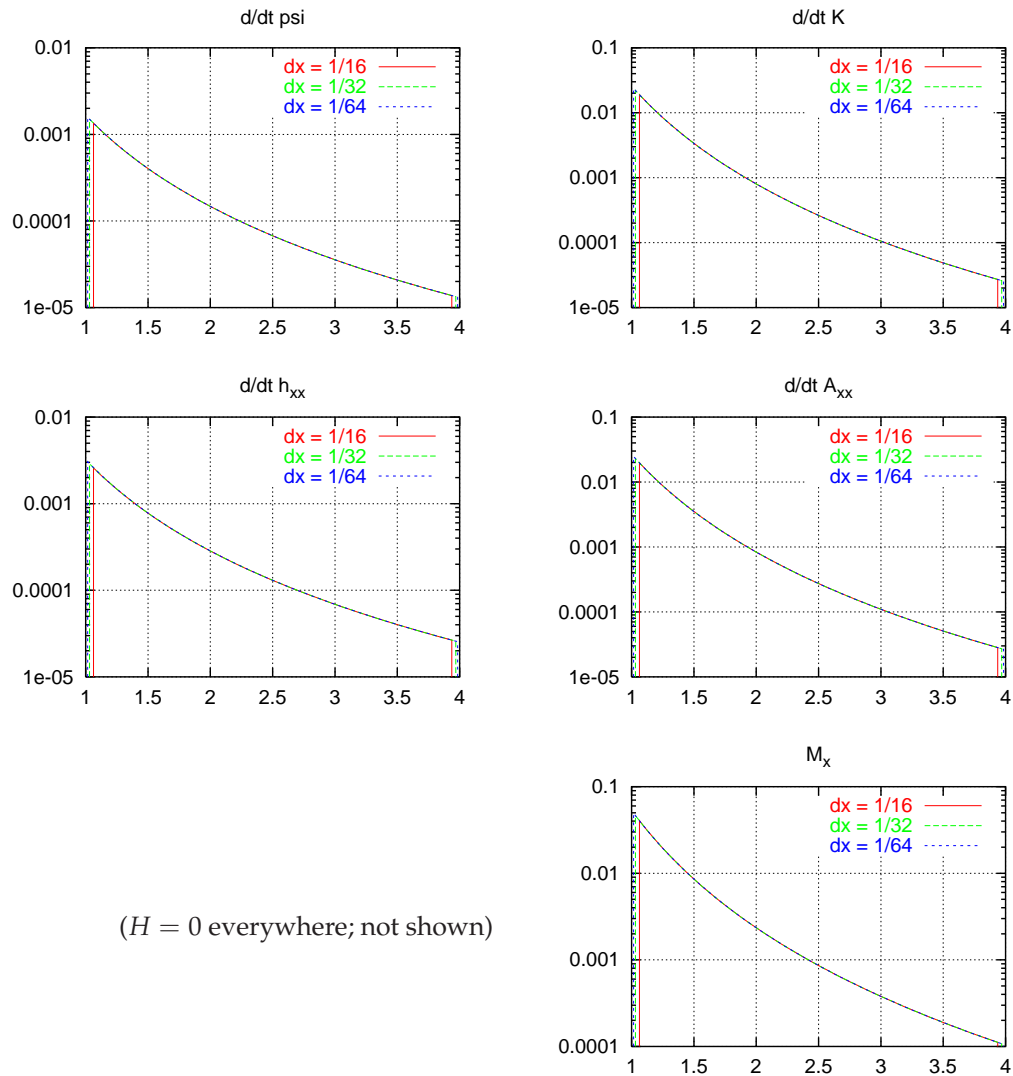


Figure 8.2: Convergence test with Painlevé–Gullstrand coordinates. The graphs show the errors in the time derivatives of various quantities for three resolutions. The errors for the finer resolutions have been scaled by the factors 4 and 16, respectively. The coinciding graphs show that there is second order convergence towards zero.

## 8.1 Convergence tests

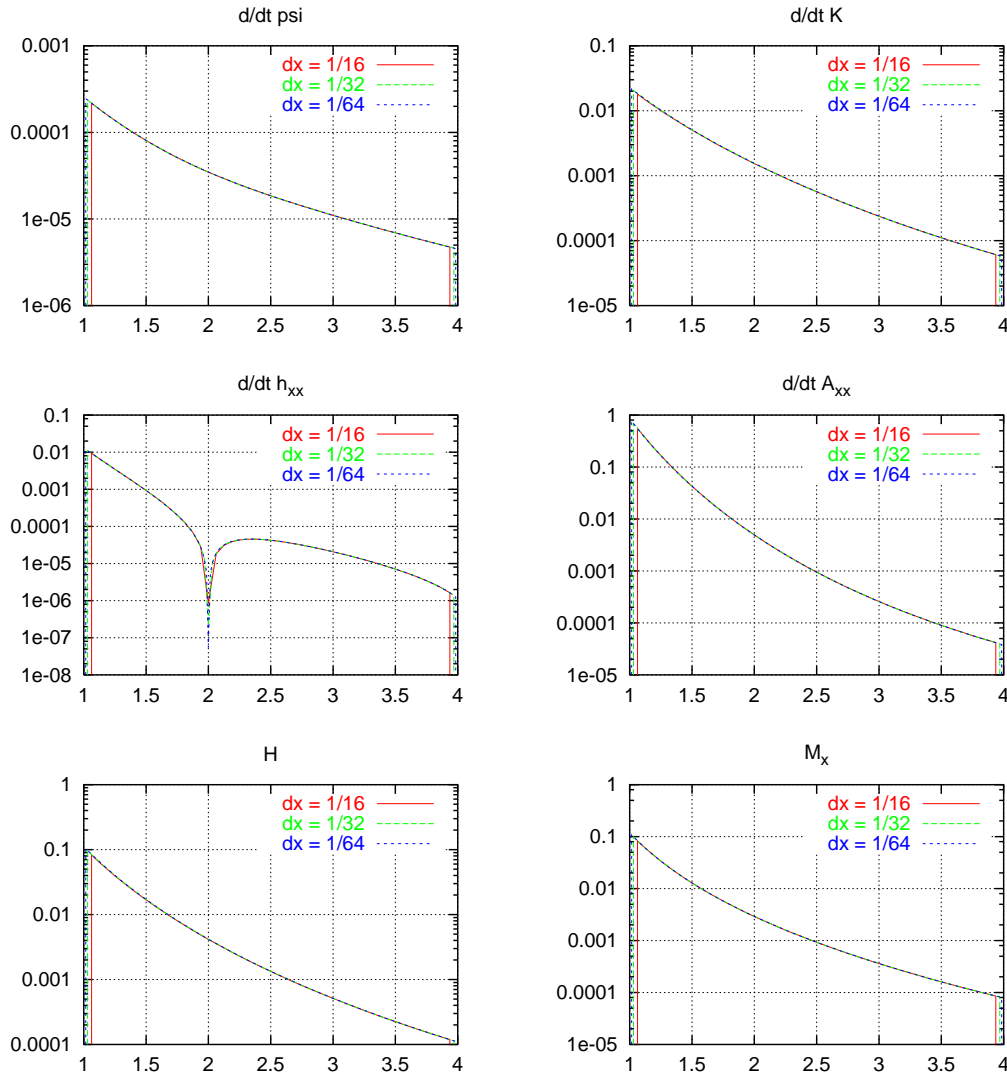


Figure 8.3: Convergence test with harmonic coordinates. The graphs show the errors in the time derivatives of various quantities for three resolutions. The errors for the finer resolutions have been scaled by the factors 4 and 16, respectively. The coinciding graphs show that there is second order convergence towards zero.

### 8.1.2 Dynamic linear test: weak Bondi wave

As a test of the dynamic behaviour in the linear regime I use weak Bondi waves (see section 6.1.2). Because a periodicity boundary condition is not possible when solving the elliptic constraint and gauge equations, I decided to use standing waves with Dirichlet boundary conditions instead. It is also possible to use Dirichlet boundaries for a travelling wave, but they would continuously inject the analytic solution into the simulation domain, which I want to avoid. By putting the Dirichlet boundaries at nodes of the standing wave, the boundary values are constant in time, which is a stronger test of the code.

I use  $K = 0$  and  $F_i = 0$  as gauge conditions. This is consistent with the analytic solution.

I use an effectively one-dimensional simulation domain, which corresponds to having a translational symmetry in two directions. My simulation domain extends only into the  $z$  direction with  $z \in [-0.5; +0.5]$ . I use a wave length  $L = 1$  and an amplitude of  $A = 10^{-6}$ . I choose a resolution of  $dx = 1/100$  and add artificial diffusion with a coefficient  $C_{SM} = 1/4$  (see appendix B.2.1). I use the midpoint rule (see appendix B.2) for time integration.

Figure 8.4 shows the result of this simulation. The phase of the wave stays correct, which is to be expected for a standing wave. The amplitude decreases with time, which is also to be expected due to numerical and artificial diffusion. The quantities  $g_{zz}$ ,  $F_z$ , and the constraints  $H$  and  $M_z$  are all correct up to floating point accuracy.

The amplitude decay is exponential in time. It can be empirically described by the expression  $A(t) = A(0) e^{-\tau t}$  with a resolution and wave length dependent decay rate  $\tau$ . The table below shows decay rates for several example resolutions and wave lengths:

$dx$	$L$	$A(t=1)/A(t=0)$	$\tau$	$\tau/\tau_0$
1/100	1	0.906	0.0987 (= $\tau_0$ )	1
1/200	1	0.952	0.0493	0.500
1/100	1/2	0.673	0.3964	4.017
1/100	1/4	0.207	1.5764	15.98

This table indicates that the decay rate  $\tau$  is proportional to the resolution  $dx$  and inversely proportional to the square of the wave length  $L$ .

This rate can be explained by the kind of artificial diffusion that I use: Given initial data with  $A \ll 1$  as described in section 6.1.2, gauge conditions as described above, and including artificial viscosity with  $C_{SM} \neq 0$  as described in section B.2.1, the set of equations governing the time evolution of  $g_{xx}$  is

$$\partial_t g_{xx} = -2 K_{xx} + C_{SM} dx \partial_{zz} g_{xx} \quad (8.1)$$

$$\partial_t K_{xx} = -\frac{1}{2} \partial_{zz} g_{xx} + C_{SM} dx \partial_{zz} K_{xx} + O(A^2) \quad (8.2)$$

Neglecting the terms in  $O(A^2)$ , these equations can be combined into

$$\partial_{tt} g_{xx} = \partial_{zz} g_{xx} + 2 C_{SM} dx \partial_{tzz} g_{xx} + O(dx^2) \quad (8.3)$$

Neglecting again the terms in  $O(dx^2)$ , the ansatz

$$g_{xx}(t, z) = \exp(-k^2 C_{SM} dx t) \sin(kt) \cos(kz) \quad (8.4)$$

## 8.1 Convergence tests

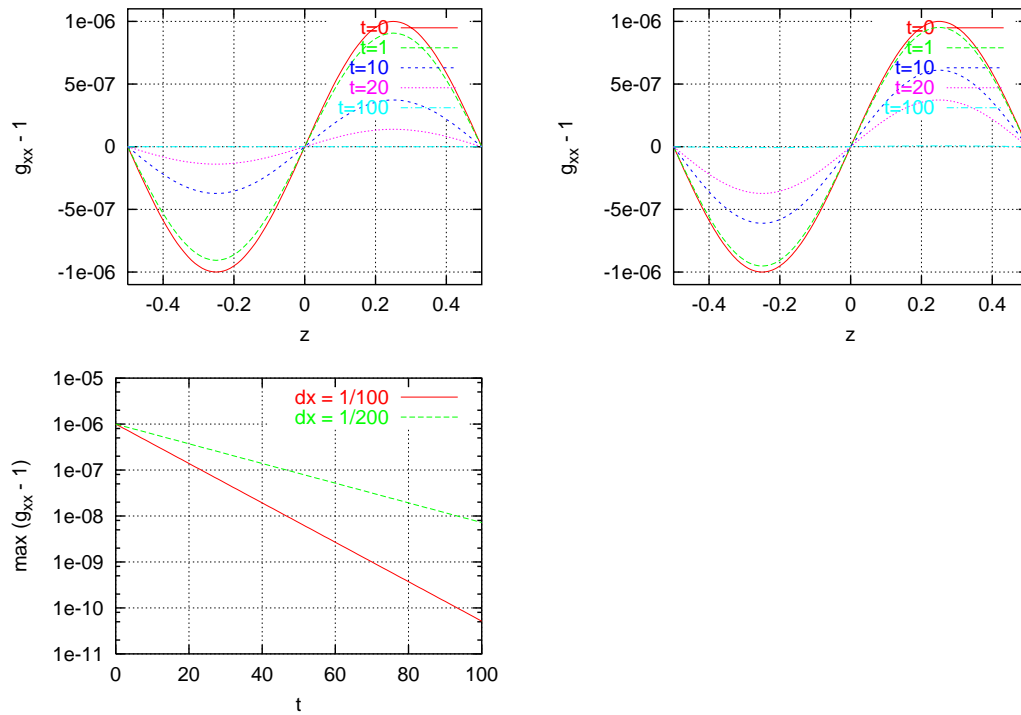


Figure 8.4: Performance test with a weak Bondi wave for the resolutions  $dx = 1/100$  (top left) and  $dx = 1/200$  (top right). Shown are the wave forms at certain times during the evolution. The bottom graph compares the amplitude decay for the two resolutions.

## 8 Results

which is motivated by the form of the initial data, solves this equation. That means that the decay rate  $\tau$  caused by the artificial diffusion should be

$$\tau = \frac{C_{\text{SM}} dx}{L^2} \quad (8.5)$$

with  $L = 1/k$ , and this is indeed the case in the table above. It is therefore reasonable to assume that the amplitude decay is due to the artificial diffusion.

Although an amplitude loss of 10% per crossing time seems large, it is actually acceptable for a binary black hole collision simulation. Scaling the resolution to typical values for such a run, I arrive at a simulation domain with  $x^i \in [0; 20]$ , a resolution of  $dx = 1/5$ , and a wave length of  $L = 20$ . This wave length is close to the quasi-normal mode of a black hole with a mass of  $M = 2$ , the result of a collision of two  $M = 1$  black holes. In this case, it takes a time  $T = 20$  for the numerical amplitude to decrease to 90% of its real, physical value. This is about the time scale in which the wave reaches the outer boundary. That means that the code is not perfect, but the performance<sup>1</sup> is acceptable for a realistic run.

---

<sup>1</sup>I use the term “performance” as measuring the quality of the numerical result. This performance depends on the magnitude of the numerical errors, not on the speed of an implementation on some hardware.



### 8.1.3 Dynamic nonlinear test: gauge pulse

As a test of the dynamic behaviour in the nonlinear regime I present a nonlinear gauge pulse (see section 6.1.3). For the same reason as in the previous section, a periodicity boundary condition is not possible. Again, I therefore use a standing gauge pulse with Dirichlet boundary conditions that are constant in time.

I use the analytically known (time and space dependent) values of  $K$  and  $F_i$  as gauge conditions. This is permissible, because these are gauge quantities only, and one is free to specify the gauge condition in advance — indeed, one has to. It is certainly possible to use a different gauge condition, but one then cannot compare the result to this analytic solution any more.

I use an effectively one-dimensional simulation domain, which corresponds to a translational symmetry in two directions. My simulation domain extends only into the  $z$  direction with  $z \in [-0.5; +0.5]$ . I use a wave length  $L = 1$  and an amplitude of  $A = 1$ . I choose a resolution of  $dx = 1/100$  and add artificial diffusion with a coefficient  $C_{SM} = 1/4$  (see appendix B.2.1). I use the midpoint rule (see appendix B.2) for time integration. Except for the wave amplitude, these parameters are the same as in the previous section.

Figure 8.5 shows the result of this simulation. The phase stays correct, which is to be expected for a standing wave. The amplitude does not decrease, it stays constant in time. The simulation result does not deviate from the analytic solution in any significant manner.

This test case contains a pure gauge wave, and is therefore a pathologically well suited<sup>2</sup> case for my formulation. Because I explicitly enforce the gauge condition at every time step, the nontrivial part of the evolution for these data is prescribed. The gravitational wave degrees of freedom are not prescribed, but those stay zero all the time.

---

<sup>2</sup>The term “pathologically well suited” was coined by Ed Seidel in spring 2002 in Mexico.

## 8 Results

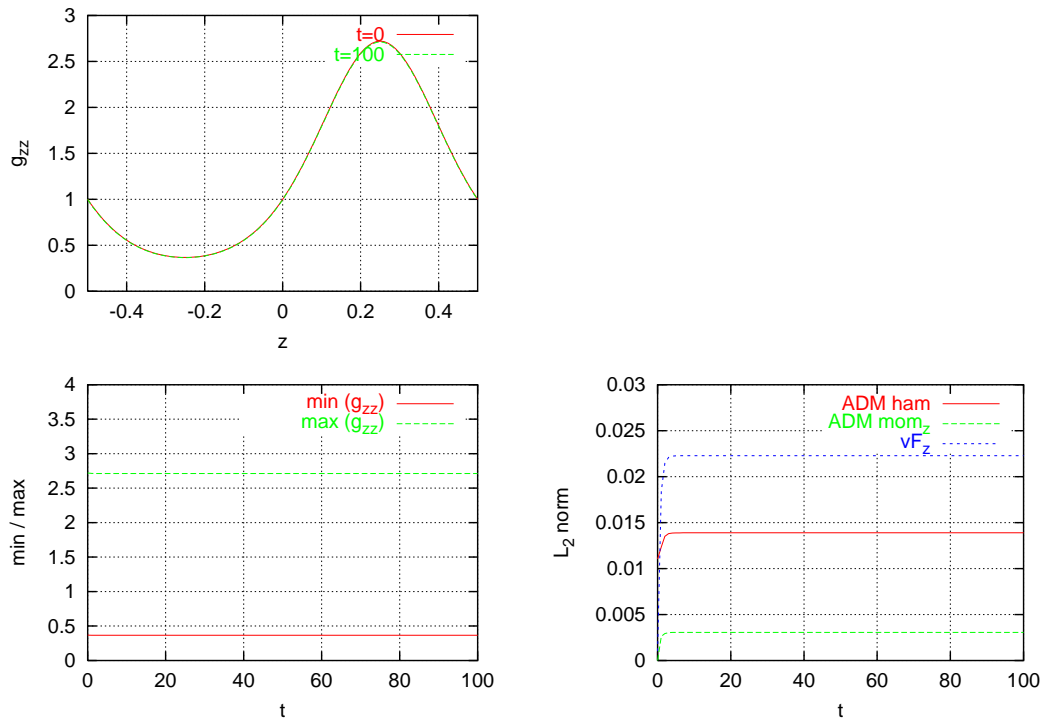


Figure 8.5: Performance test with a gauge pulse. The top graph compares the initial wave form and the wave form after 100 crossing times. The bottom graphs show the wave amplitude (left) and constraint and gauge violations (right) vs. time.

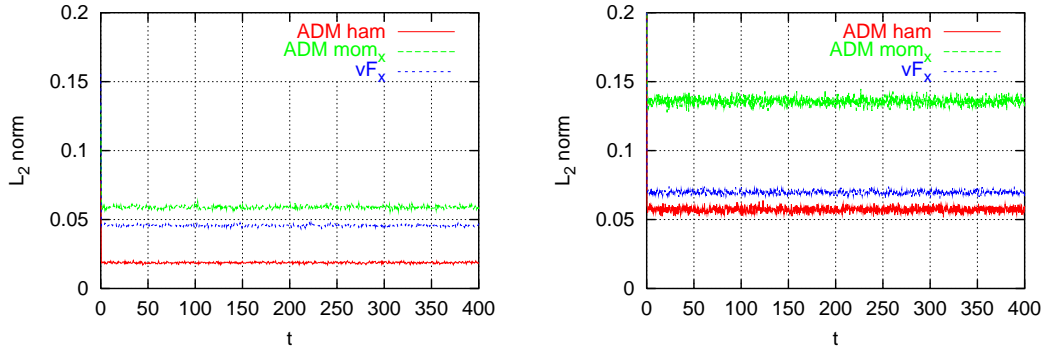


Figure 8.6: Robust stability test. Plotted are the violations of the constraints and of the gauge condition versus time for the resolutions  $dx = 1/4$  (left) and  $dx = 1/8$  (right).

## 8.2 Stability test

Szilágyi et al. [SGBW00, SSW02] define the notion of *robust stability* of a code. This definition is not an analytic, but rather an experimental one, which means that it can be tested rather easily. The basic idea is to add noise to the initial data, and also to add noise to the values provided by the boundary conditions. A code that behaves gracefully, i.e. does not show exponential growth, is called *robustly stable*.

The robust stability test, as proposed by Szilágyi et al., comes in four stages of increasing difficulty. Stages I and II include periodicity, which is not a valid boundary condition for my elliptic equations. I therefore concentrate on stage III, which uses a rectangular domain without periodicity. Stage IV requires a spherical outer boundary, which I did not test.

For this test, I use Minkowski flat space (see section 6.1.1) as background to which the noise is added. I use  $K = 0$  and  $F_i = 0$  as gauge conditions and Dirichlet boundary conditions.

I run this test in two configurations with different resolutions  $dx = 1/4$  and  $dx = 1/8$ . I use a cubic box with a length of  $L = 4$ , and run the code up to  $T = 400$ , which is equivalent to  $T/L = 100$  crossing times. I use a noise amplitude of  $A = 0.1$  on the initial data and on the boundaries. I add an artificial diffusion with a coefficient of  $C_{SM} = 0.1$  (see appendix B.2.1). I use the midpoint rule (see appendix B.2) for time integration.

The result of this test is that the formulation of Einstein's equations as implemented in the Tiger code is robustly stable.<sup>3</sup> The constraints and the gauge violations, which are shown in figure 8.6, do not increase with time after an initial transient. Similarly, all components of the three-metric and of the extrinsic curvature stay bounded.

I assume that the artificial diffusion is the reason for the fact that there seems to be no growth at all. I assume that the levels at which the individual metric and extrinsic curvature components remain are defined by the noise on the boundary, which inserts energy into the system, and the artificial viscosity, which removes energy.

Note that the finer run is not just a higher-resolution version of the coarser run. The two space-times are different, in that the finer run contains noise with a higher spatial frequency. For that

<sup>3</sup>A longer run time would have been preferable, but was not possible because of the large computational resource requirements.

## *8 Results*

reason the errors in the fine run cannot be expected to be smaller than those in the coarse run. The two runs do not form a convergence test.

## 8.3 Brill wave

A Brill wave (see section 6.1.4) tests the dynamic nonlinear behaviour in a realistic situation. Although the initial data that I use are axially symmetric, I perform a full three-dimensional evolution. Due to the Cartesian grid in the simulation domain the setup loses its axial symmetry.

There is no complete analytic solution for the Brill wave initial data; the conformal factor has to be determined numerically from the Hamiltonian constraint. In addition, there is no analytic solution at all for the evolution of Brill waves at times  $t \neq 0$ . It is thus difficult to gauge the correctness and performance of a code.

The Albert–Einstein–Institut in Golm also has a code, called *Einstein code*, that solves Einstein’s equations. This code is publicly available from the Cactus web pages [Cac]. I used both their and the Tiger code, and tried to compare the results for Brill waves. This is unfortunately very difficult, because the codes use different gauge conditions during the evolution. While both codes can use maximal slicing, i.e.  $K = 0$ , they differ in their shift conditions. The Tiger code uses a metric gauge condition  $F_i = \text{const}$  or  $F_i = 0$ , and derives a shift condition from that. The Einstein code cannot impose a gauge condition on the metric, and one has to specify the shift condition directly. For Brill waves one usually uses normal coordinates, i.e.  $\beta^i = 0$ . This difference leads to very different time evolutions, although the spacetimes should (barring implementation errors) be identical up to the discretisation error.

I simulate Brill waves with initial data as described in section 6.1.4. I use an amplitude  $A = 4$ , which makes the Brill wave highly nonlinear, but still subcritical, i.e. it does not form a black hole. I also use  $C = 0$  and  $\omega = 1$ . I use maximal slicing, i.e. the gauge condition  $K = 0$  on the extrinsic curvature. I use an iterative Crank–Nicholson time integrator with 2 iterations after the initial Euler step (see appendix B.2).

I run the Tiger code with two different gauge conditions. The first, which I call here “ $F_i = \text{const}$ ”, keeps the gauge variable  $F_i$  constant in time at the values from the initial data. The second, called “ $F_i = 0$ ”, sets  $F_i$  to zero at all times. Thus only the case  $F_i = \text{const}$  uses the same initial data as the Einstein code. The case  $F_i = 0$  evolves a different (but closely related) spacetime. This gauge condition has the advantage that it, together with  $K = 0$ , enforces a Minkowski metric when the spacetime is flat (and with suitable boundary conditions).

It turns out that the cases  $F_i = \text{const}$  and  $F_i = 0$  show very similar behaviour. This indicates that my way of enforcing the gauge leaves the physical degrees of freedom mostly unchanged. This is also confirmed by the time evolution of the ADM mass, as shown in figure 8.7. Strangely, the behaviour of the Einstein code using a zero shift differs greatly, as can also be seen in the following.

Traditionally, one of the most interesting quantities to look at in maximal slicing is the lapse  $\alpha$ , or its minimum. With maximal slicing, the lapse drops to zero near a singularity; thus the minimum of the lapse indicates heuristically whether a singularity is forming. The Brill wave that I look at is subcritical, i.e. there is no singularity in the spacetime. Consequently, although the lapse drops initially, it later “recovers” and ends up as  $\alpha = 1$  everywhere at late times.

These time evolutions of the minimum of the lapse are shown in figure 8.8 for four resolutions from  $dx = 1/4$  to  $dx = 1/8$ , run with the Tiger code. Finer resolutions would have been desirable, but would have required much longer run times. (The PETSc elliptic solver (see section 7.3) that I used does not scale well on multiple processors.) As the resolutions are, they form only a weak convergence test. The same figure also shows a run with the Einstein code with a resolution of  $dx = 1/6$ . Figures 8.9 and 8.10 show the time evolution of the lapse along the  $x$  axis.

All three evolutions show qualitatively the same features: the lapse first drops sharply down

## 8 Results

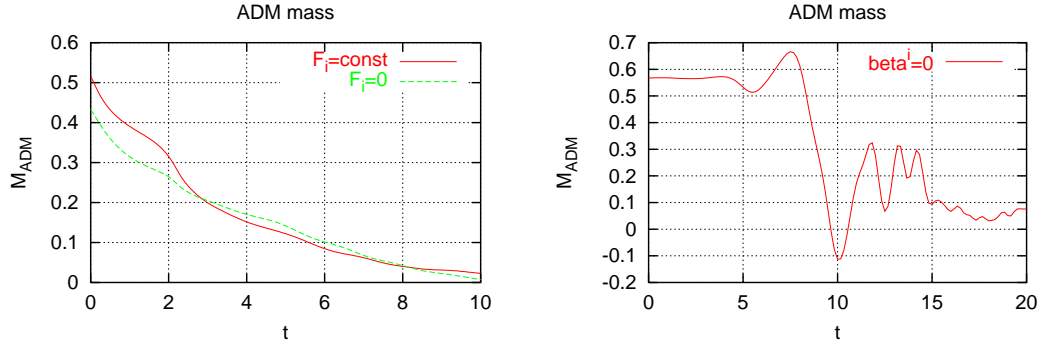


Figure 8.7: Brill wave runs: ADM mass vs. time for different gauge and coordinate conditions. Note the different time scales.

from  $\alpha = 1$ , bounces back up two times, and then drifts back towards  $\alpha = 1$ . At late times, the Brill wave has radiated away, and the spacetime becomes flat. The largest and maybe most puzzling difference is that it takes about twice as much coordinate time until the lapse has recovered for the zero shift coordinate condition than for the two other gauge conditions.

This difference in coordinate time seems to be caused by a combination of two effects. First, due to the different shift values, the lapse near the origin has different values. This is because the shift enters into the  $\partial_t K$  equation (A.23) that determines the lapse. (The shifts are shown in figure 8.11.) A smaller lapse leads to a larger ratio between coordinate time and proper time. However, this explains only a part of the difference, as can be seen when integrating proper time along the geodesic formed by the origin (see figure 8.12).

The second reason is that the lapse is a pure coordinate quantity, and by comparing the lapse one cannot directly make a statement about the location of gravitational waves. That is, the Brill wave might have radiated away before the lapse has fully recovered. A better (but still not perfect) quantity to look at is  $g_{yy}$  along the  $x$  axis. This is a metric component which is orthogonal to the direction in which the Brill wave radiates, and hence is connected to the transverse gravitational wave degrees of freedom in the system.

Figures 8.13 and 8.14 show the evolution of  $g_{yy}$  vs. time. One can see that for the gauges  $F_i = \text{const}$  and  $F_i = 0$  there are two wave trains that leave the simulation domain at  $x = 6$  at about  $t = 10$ . With the coordinate condition  $\beta^i = 0$ , there are also two wave trains, but it is clear from the graph that they arrive at  $x = 6$  substantially earlier than at  $t = 20$ . Hence there was not really a factor of two difference between the coordinate times at which the Brill wave has radiated away to begin with.

Figure 8.15 compares then initial (at  $t = 0$ ) and late time (at  $t = 10$  and  $t = 20$ , resp.) behaviour of several quantities, namely the conformal factor  $\psi$ , the Ricci scalar  $R$ , and the transverse metric component  $g_{yy}$ . All quantities are plotted vs. the  $x$  coordinate.

By construction, the conformal factor  $\psi$  is initially the same for  $F_i = \text{const}$  and  $\beta^i = 0$ . With  $K = 0$  and  $\beta^i = 0$ , it is  $\partial_t \psi = 0$  (see eqn. (A.21)), so that the final  $\psi$  is the same as the initial one in this case. For  $K = 0$  and  $F_i = 0$ , flat space has a Minkowski metric, so that  $\psi = 1$  in this case. (This state has not yet completely been reached at  $t = 10$ .) Note that the cases  $F_i = \text{const}$  and  $\beta^i = 0$  go to different static coordinate systems of flat space.

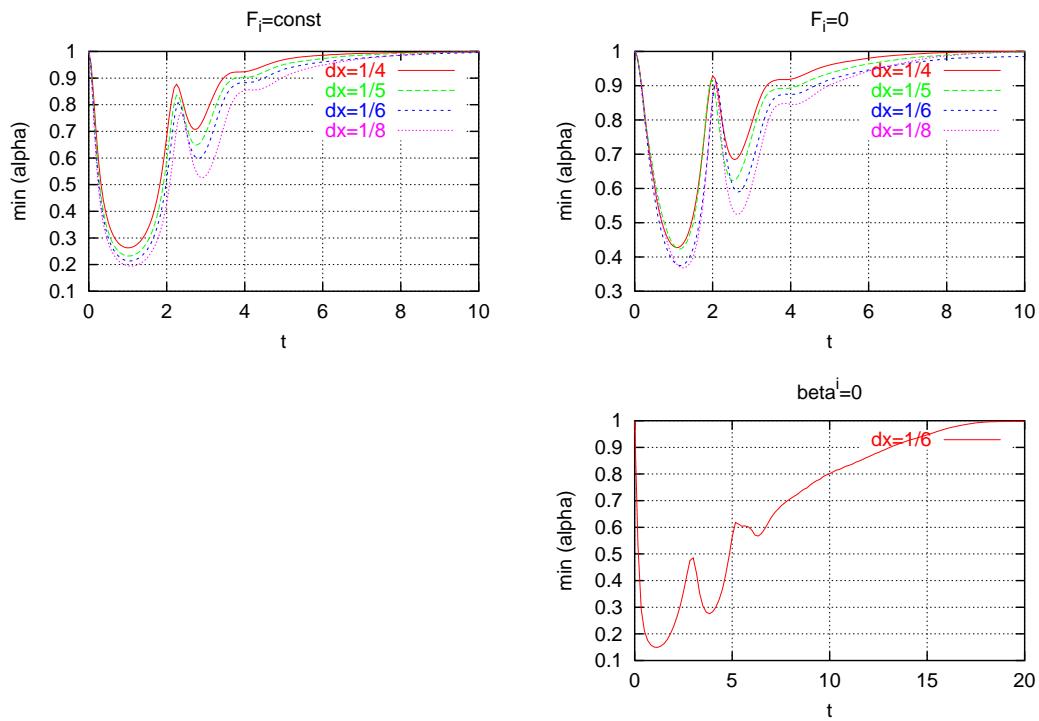


Figure 8.8: Brill wave runs: Minimum of the lapse  $\alpha$  vs. time for different gauge and coordinate conditions. (This is always the value of the lapse at the origin.) All cases use maximal slicing, i.e.  $K = 0$  everywhere. Note the different time scales.

## 8 Results

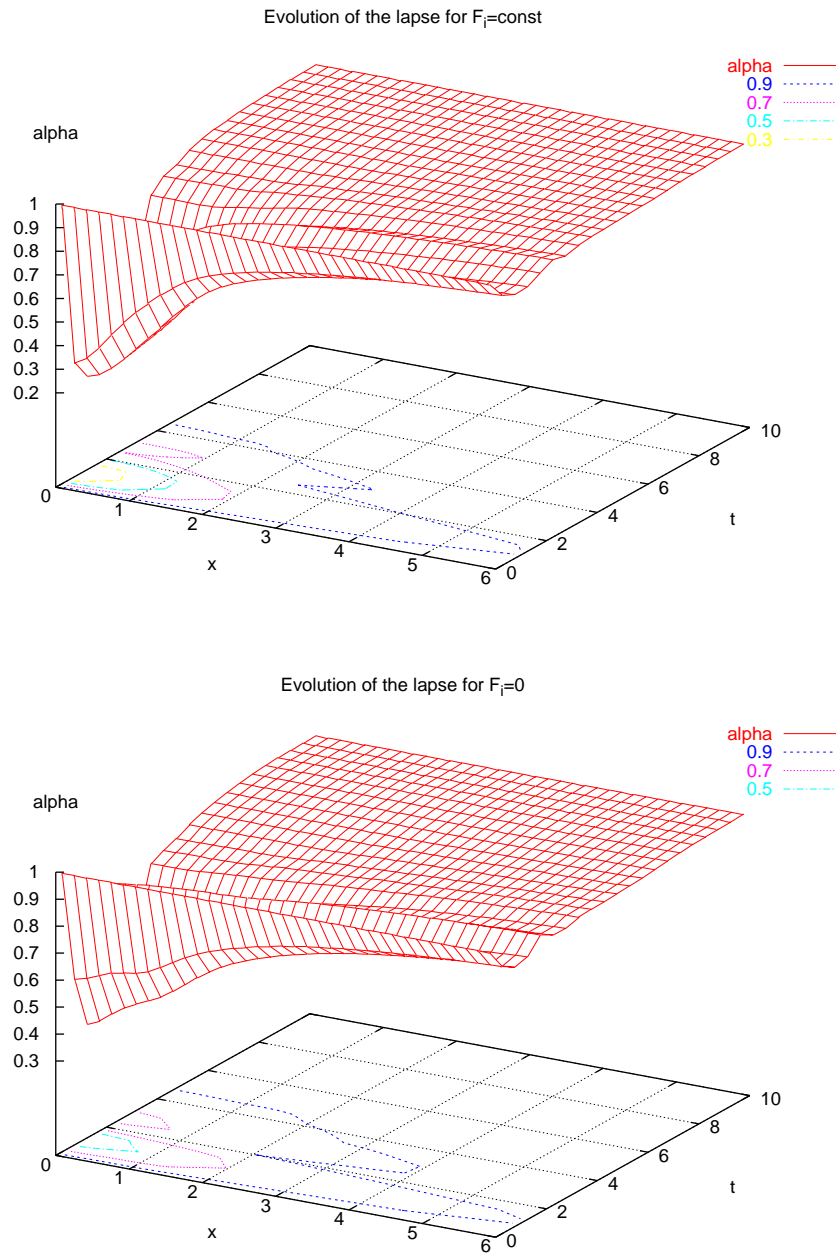


Figure 8.9: Brill wave runs: Lapse  $\alpha$  vs. radius (along the  $x$  axis) and time for different gauge conditions. Note that also  $K = 0$  everywhere.



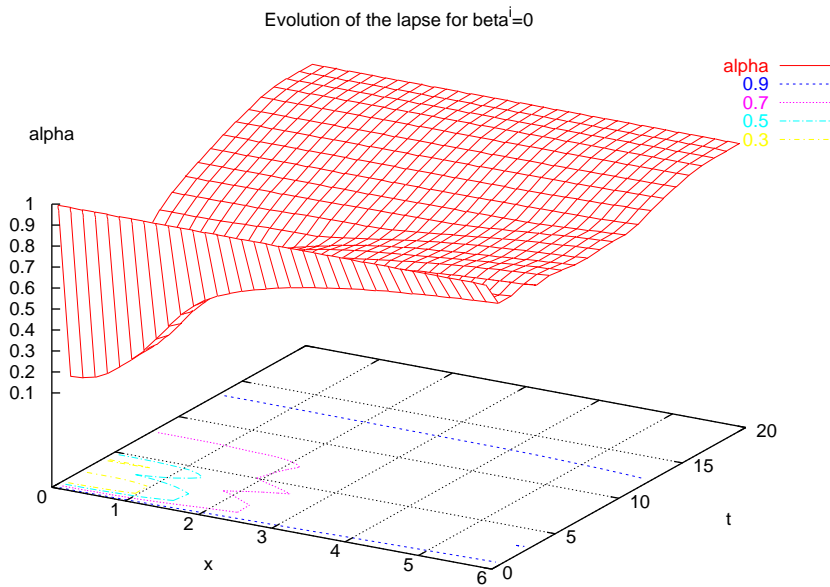


Figure 8.10: Brill wave runs: Lapse  $\alpha$  vs. radius (along the  $x$  axis) and time for zero shift. Note that also  $K = 0$  everywhere.

## 8 Results

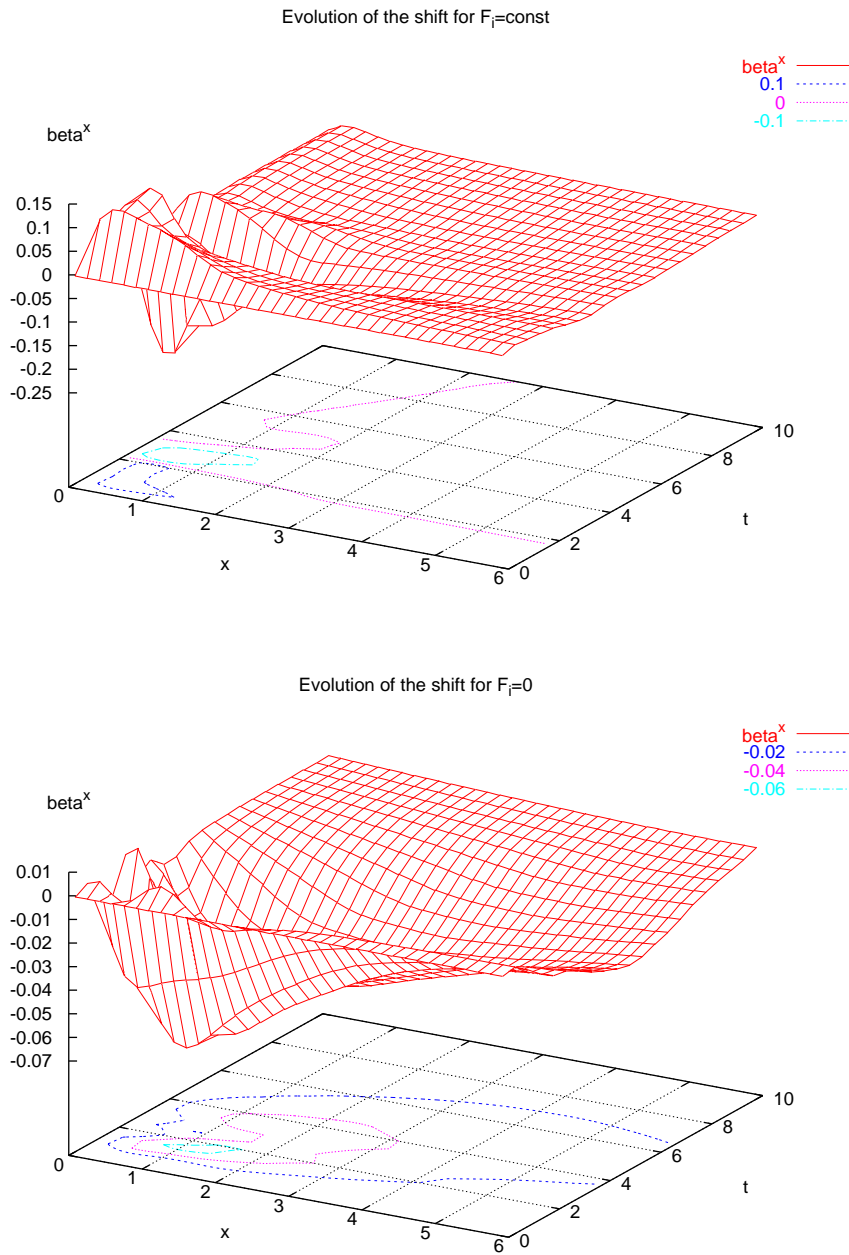


Figure 8.11: Brill wave runs: Shift component  $\beta^x$  vs. radius (along the  $x$  axis) and time for different gauge conditions. Note that also  $K = 0$  everywhere.

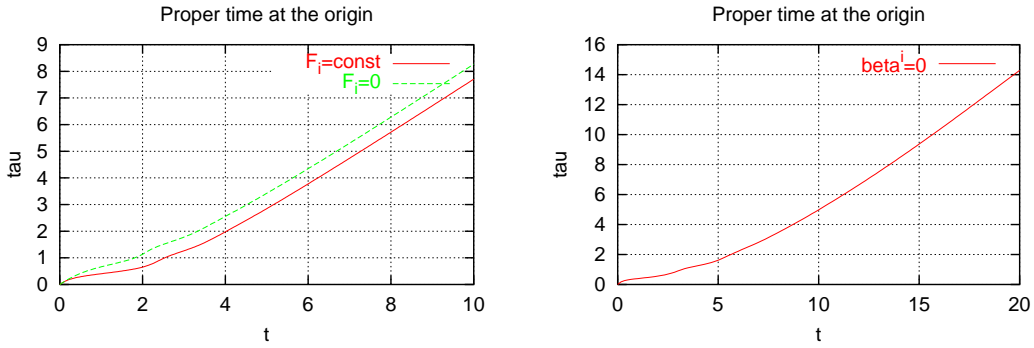


Figure 8.12: Brill wave runs: Proper time vs. coordinate time at the origin for different gauge and coordinate conditions.

The Ricci scalar should be zero initially, due to the Hamiltonian constraint and time symmetry. The Ricci scalar is nonzero because of discretisation errors. The final Ricci scalar should be zero for the  $F_i = 0$  case.

Again, by construction the initial values of  $g_{yy}$  are the same for  $F_i = \text{const}$  and  $\beta^i = 0$ . The case  $F_i = 0$  differs, because it has a different gauge condition enforced onto it. At late times,  $g_{yy}$  tends to its Minkowski value of one for  $F_i = 0$ .

A “real” comparison between the two  $F_i = \text{const}$  and  $\beta^i = 0$  runs would involve finding a four-coordinate transformation between the two four-metrics. The two spacetimes are identical if and only if such a coordinate transformation exists (up to numerical errors). This would be a difficult undertaking, not only because it involves a huge amount of data (namely two complete spacetimes). I know of no proven numerical method to find such a transformation. The Lazarus project [BCL02] tries to solve a similar problem; they compare e.g. curvature invariants.

## 8 Results

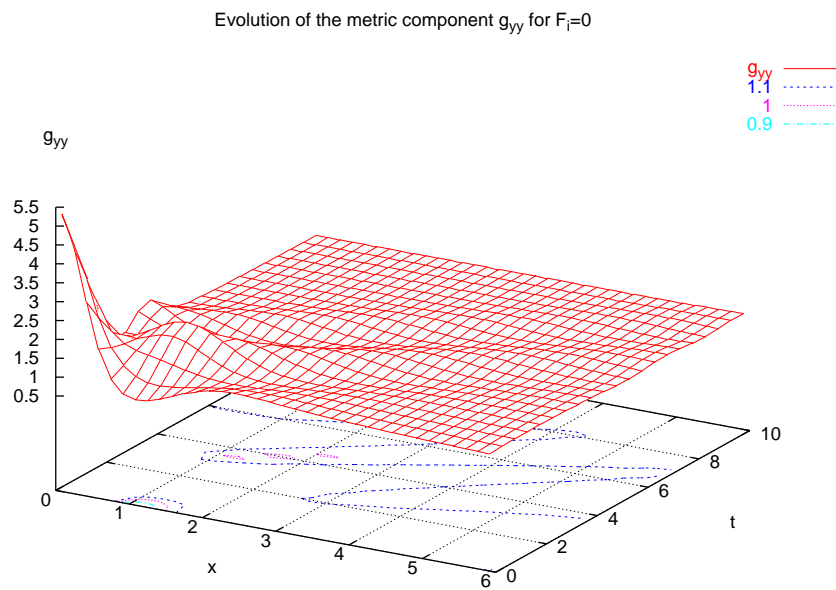
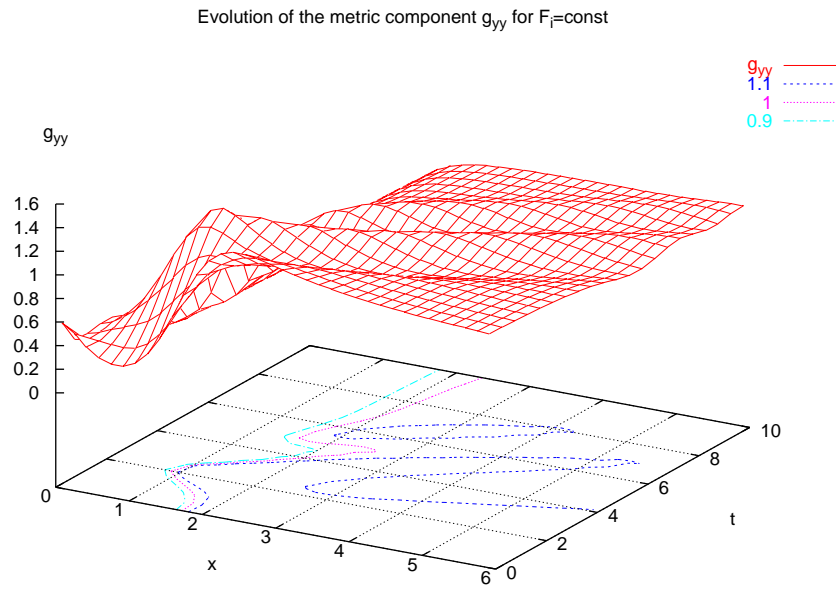


Figure 8.13: Brill wave runs: Metric component  $g_{yy}$  vs. radius and time for different gauge conditions. Note that also  $K = 0$  everywhere.

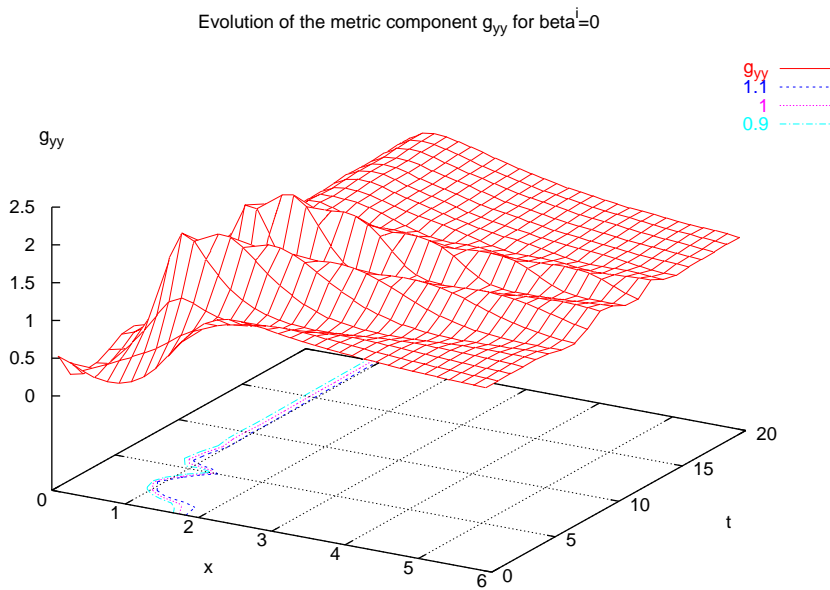


Figure 8.14: Brill wave runs: Metric component  $g_{yy}$  vs. radius and time for zero shift. Note that also  $K = 0$  everywhere.

## 8 Results

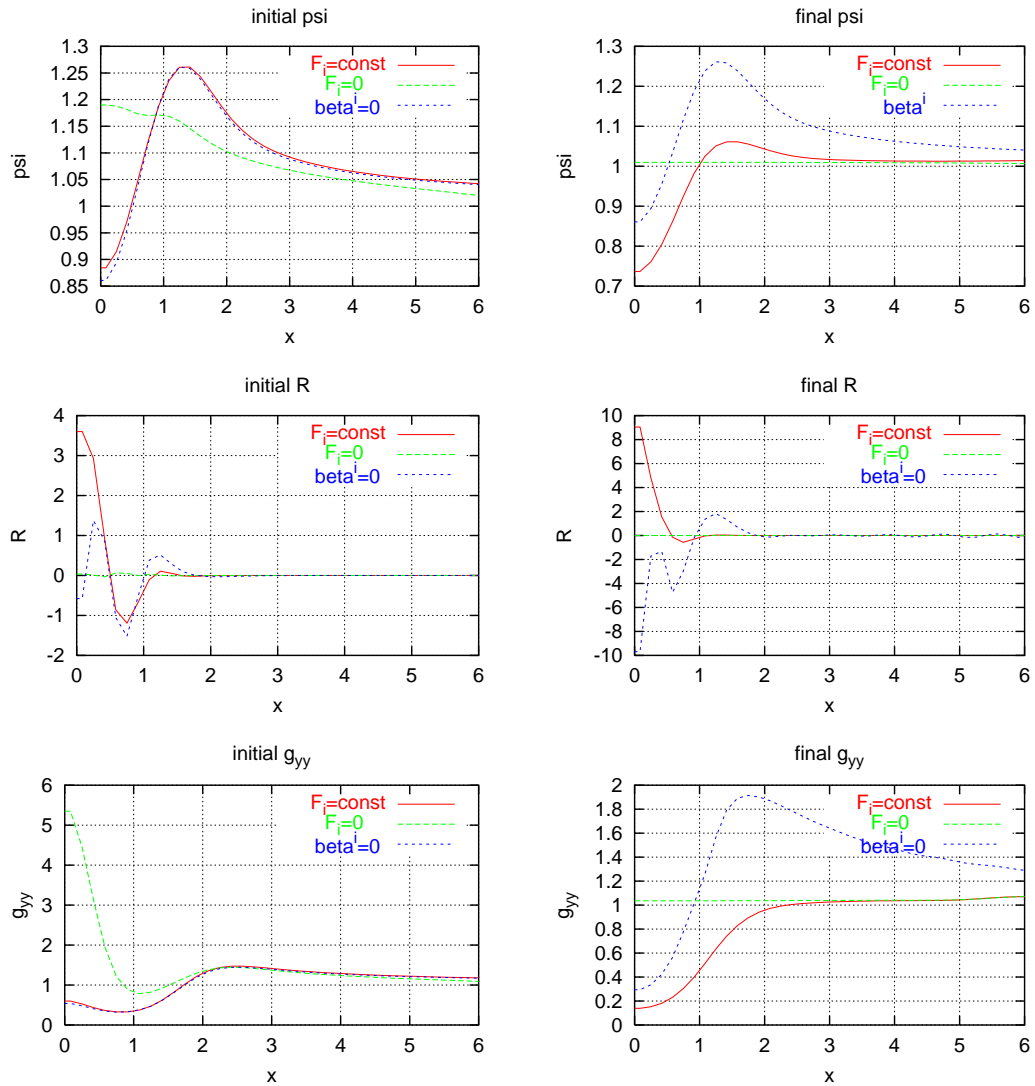


Figure 8.15: Brill wave runs: Conformal factor  $\psi$ , Ricci scalar  $R$ , and metric component  $g_{yy}$  vs. radius along the  $x$  axis at  $t = 0$  and at  $t = late$ . Note that for all shown cases  $\alpha = 1$  and  $\beta^i = 0$ . The initial Ricci scalar  $R$  should be identically zero; it shows the magnitude of the discretisation errors.

## 8.4 Kerr–Schild black hole

One of the most basic tests of a nonlinear evolution code is a static or stationary black hole. I already tested the right hand side of the evolution equations in various coordinate systems in section 8.1.1 above. Here I want to continue these tests by performing time evolutions with different numerical configurations, i.e. with different resolutions, outer boundary locations, and different enforced grid symmetries.

I consider the following configurations:

title	resolution	spin	location of outer bnd.	symmetries
std	1/4	0	4	octant
dx8	1/8	0	4	octant
ob8	1/4	0	8	octant
full	1/4	0	4	none
spin	1/4	1/2	4	octant

In all cases, the mass of the black hole is  $M = 1$ . I excise a region with radius  $r = 1$  around the singularity. I use Dirichlet inner and outer boundary conditions, and I add artificial diffusion with a coefficient of  $C_{SM} = 0.1$  (see appendix B.2.1). I use an iterative Crank–Nicholson time integrator with 2 iterations after the initial Euler step (see appendix B.2). I run these configuration up to  $t = 100$ .

With octant symmetry, only one octant of the spacetime is simulated. The boundary conditions at the zero coordinate planes are given by the symmetry conditions. Using these symmetries reduces the memory and run time requirements by a factor of eight, which is considerable. However, using or not using these symmetries can influence the stability of the code, and therefore has to be tested.

I also use other, more physical boundary conditions. For these runs, I use radiative outer boundary conditions, or (third-order, or cubic) extrapolated inner boundary conditions, or both.<sup>4</sup> Otherwise, these runs are identical to the std run above:

title	outer bc	excision bc
std	Dirichlet	Dirichlet
rad	radiative	Dirichlet
extrap	Dirichlet	extrapolated
extrap-rad	radiative	extrapolated

I show in figure 8.16 the  $L_2$  norms of the Hamiltonian and the momentum constraints and of the gauge violation. The time evolutions of the above configurations std, dx8, ob8, full, and spin show an initial transient, and then settle down close to the initial data, i.e. close to the analytic solution. They are all stable in the sense that no growth is visible during the examined time scale. Because the code is robustly stable, I do not expect instabilities at later times, although I have no proof for that.

The configurations rad and extrap-rad, which have a radiative outer boundary condition, pick up a slowly decaying global breathing mode. This error has an amplitude of about 1% in the ADM and apparent horizon masses, as shown in figure 8.17. This mode has not yet decayed at  $t = 100$ .

<sup>4</sup>However, the inner boundary condition for the conformal factor  $\psi$  was always Dirichlet.

## 8 Results

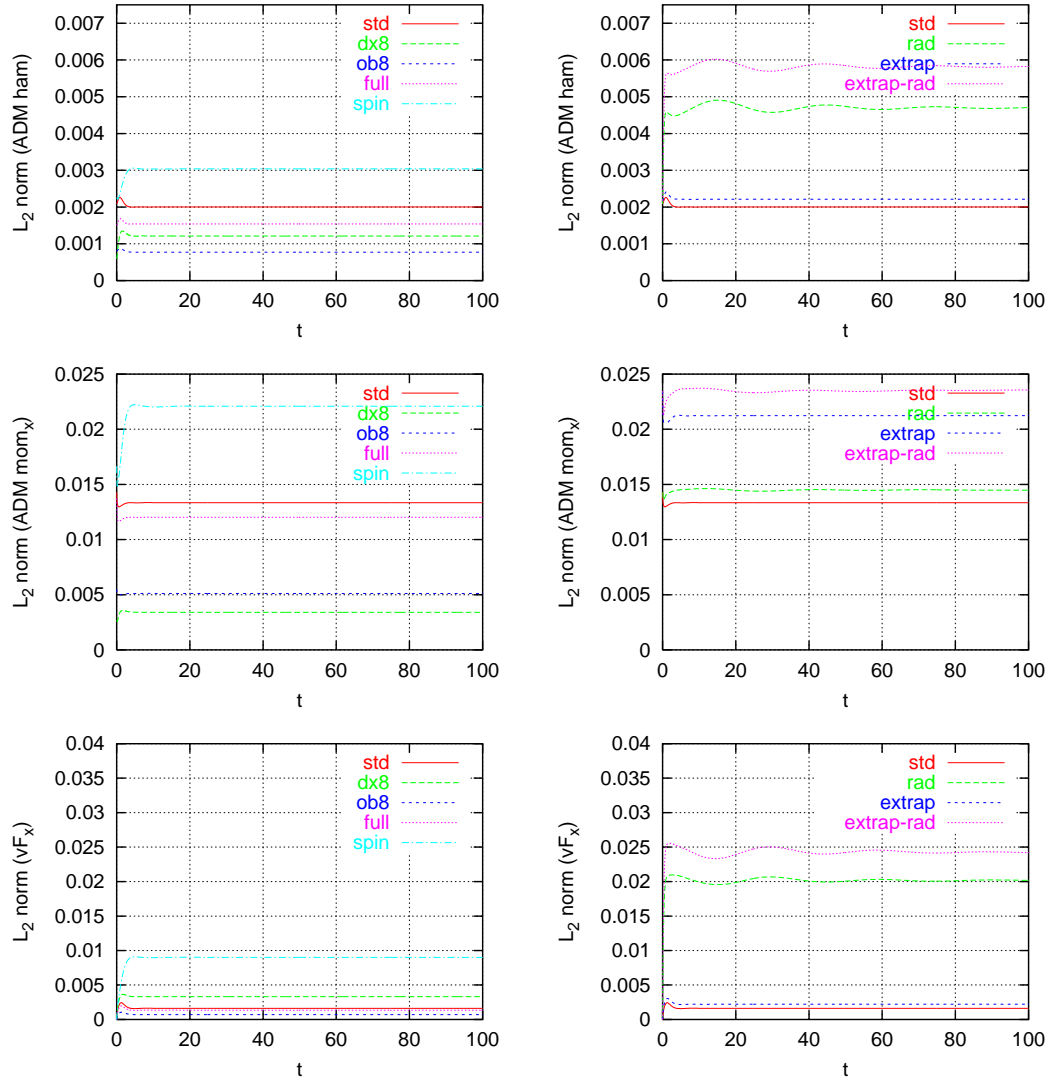


Figure 8.16: Kerr–Schild black hole time evolution:  $L_2$ -norms of the constraint and gauge violations for various configurations and boundary conditions. *std*=standard, *dx8*=higher resolution, *ob8*=larger domain, *full*=without symmetries, *spin*=with spin, *rad*=radiative outer boundary, *extrap*=extrapolated inner boundary



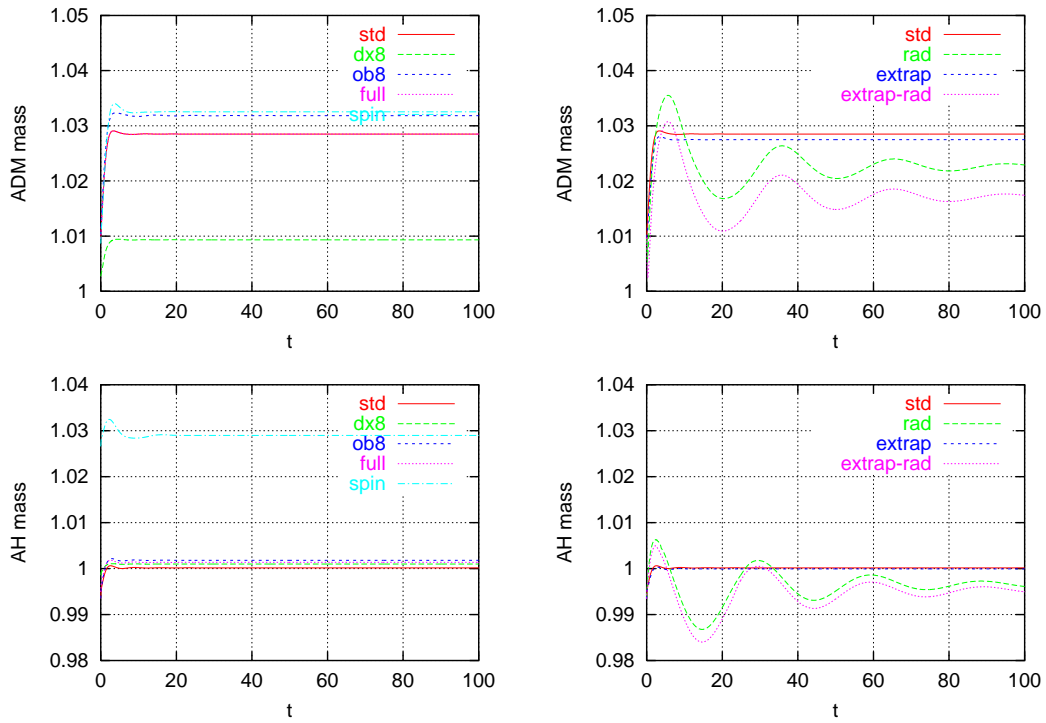


Figure 8.17: Kerr–Schild black hole time evolution: ADM masses and apparent horizon masses. *std*=standard, *dx8*=higher resolution, *ob8*=larger domain, *full*=without symmetries, *spin*=with spin, *rad*=radiative outer boundary, *extrap*=extrapolated inner boundary

## 8 Results

When comparing simple (std) Kerr–Schild runs with the resolutions  $dx = 1/4$ ,  $dx = 1/6$ , and  $dx = 1/8$  at  $t = 100$  along the  $x$  axis, I get following convergence factors (cf):

$x$	1.5	2.0	2.5	3.0	3.5
cf	2.26687	2.71461	2.74507	2.73848	2.73511

A factor of  $(1/4^2 - 1/6^2)/(1/6^2 - 1/8^2) \approx 2.85714$  in the above would indicate second order convergence. The numbers suggest that the TGR system is able to evolve static black holes in Kerr–Schild coordinates with excision in a stable and convergent manner. The stability of the evolution is independent of the resolution, the location of the outer boundaries, the symmetries that are imposed, and the kind of boundary conditions that are used.

## 9 Conclusion

In this thesis, I set out to find a way to arrive at some more understanding of the instabilities that one encounters in today's black hole evolution simulations. I looked at gauge conditions and classified them into gauge evolution and gauge fixing conditions, assuming that gauge modes do play an important role in the instabilities. I proposed a gauge fixing condition and an implementation for it, and examined it in various test problems and some applications.

Gauge fixing seems to lead to very stable evolutions. The Tiger code is robustly stable, and has also sufficient accuracy to treat more complex configurations. It remains to be shown that this system also works for two coalescing black holes. The computational resources required by the current implementation do unfortunately not allow such a test; further algorithmic improvements (the implementation of a parallel multigrid solver) will probably be necessary for that.

## 9 Conclusion

# A Equations

Many of the equations in this appendix are only a repetition of well-known literature. They serve mostly as a quick reference, and to define the sign conventions. For other equations, I give a short derivation. I restrict myself to the vacuum case everywhere.

## A.1 The ADM formalism

The ADM formalism is one way to transform the Einstein equations into a system of time evolution equations.

### A.1.1 Variables

The ADM variables [ADM62] are the three-metric  $\gamma_{ij}$ , the extrinsic curvature  $K_{ij}$ , the lapse  $\alpha$  and the shift  $\beta^i$ . The four-metric can be written as

$$g_{\mu\nu} = \left( \begin{array}{c|c} -\alpha^2 + \beta^2 & \beta_j \\ \hline \beta_i & \gamma_{ij} \end{array} \right) \quad (\text{A.1})$$

where  $\beta_i = \gamma_{ij}\beta^j$ , and  $\beta^2 = \beta_j\beta^j$ . This metric is equivalent to the line element

$$ds^2 = -\alpha^2 dt^2 + \gamma_{ij} (dx^i + \beta^i dt) (dx^j + \beta^j dt) \quad (\text{A.2})$$

$$= (-\alpha^2 + \gamma_{ij}\beta^i\beta^j) dt^2 + 2\gamma_{ij}\beta^j dx^i dt + \gamma_{ij} dx^i dx^j \quad (\text{A.3})$$

The inverse metric is then

$$g^{\mu\nu} = \frac{1}{\alpha^2} \left( \begin{array}{c|c} -1 & \beta^i \\ \hline \beta^i & \alpha^2 \gamma^{ij} - \beta^2 \end{array} \right) \quad (\text{A.4})$$

The three-metric and extrinsic curvature on a time slice are enough to completely specify the physics in the whole spacetime. Lapse  $\alpha$  and shift  $\beta^i$  can be chosen freely during time evolution and determine only the coordinate system. The extrinsic curvature is defined via the time derivative of the three-metric by eqn. (A.5) below.

## A Equations

### A.1.2 Time evolution

The time evolution of the three-metric (which is also definition of the extrinsic curvature  $K_{ij}$ ) is given by

$$\partial_t \gamma_{ij} = -2\alpha K_{ij} + \gamma_{lj} \beta^l_{,i} + \gamma_{il} \beta^l_{,j} + \beta^l \gamma_{ij,l} \quad (\text{A.5})$$

The time evolution of the extrinsic curvature is given by

$$\begin{aligned} \partial_t K_{ij} = & -\nabla_i \nabla_j \alpha + \alpha \left[ R_{ij} - 2K_{il} K^l_j + K K_{ij} \right] \\ & + K_{lj} \beta^l_{,i} + K_{il} \beta^l_{,j} + \beta^l K_{ij,l} \end{aligned} \quad (\text{A.6})$$

### A.1.3 Ricci tensor

The connection coefficients to the three-metric are given by

$$\Gamma^i_{jk} = \frac{1}{2} \gamma^{il} \left[ \gamma_{lj,k} + \gamma_{lk,j} - \gamma_{jk,l} \right] \quad (\text{A.7})$$

The three-Ricci tensor is e.g. given by

$$R_{ij} = \Gamma^k_{ij,k} - \Gamma^k_{ik,j} + \Gamma^k_{jl} \Gamma^l_{ik} - \Gamma^k_{lk} \Gamma^l_{ij} \quad (\text{A.8})$$

It is a bad idea to calculate it in this way numerically, as this would involve taking derivatives of derivatives. Instead, one has to explicitly take second derivatives of the three-metric.

### A.1.4 Constraints

The Hamiltonian constraint is usually written as

$$H = R + K^2 - K_{ij} K^{ij} \quad (\text{A.9})$$

The momentum constraint is usually written as

$$M_i = \nabla^j (K_{ij} - \gamma_{ij} K) \quad (\text{A.10})$$

As these constraints have to be zero for a physical spacetime, one can multiply them by an arbitrary nonzero function to arrive at other formulations for the constraints. This especially leaves scaling freedoms, so that a statement saying the constraints are smaller than a certain value is only meaningful if this is with respect to a certain given length scale.

One can introduce normalised constraints e.g. as

$$H^{(N)} = \frac{H}{|R| + |K^2| + |K_{ij} K^{ij}|} \quad (\text{A.11})$$

$$M_i^{(N)} = \frac{M_i}{|\nabla^j K_{ij}| + |\nabla_i K|} \quad (\text{A.12})$$

where the absolute value of a vector  $x^i$  is calculated as  $|x^i|^2 = \gamma_{ij} x^i x^j$ . These normalised constraints have a range of  $[0;1]$  and are thus scaling invariant. They have the disadvantage of being ill-defined e.g. in the Minkowski spacetime, and are meaningless in perturbations thereof.

## A.2 The TGR system

The TGR system is a conformal traceless ADM (ctADM) formalism that is derived from the ADM formalism by introducing two additional scalar quantities  $\psi$  and  $K$ , which represent the determinant of the three-metric and the trace of the extrinsic curvature, respectively. This also leads to two new constraints, namely just these conditions.

### A.2.1 Variables

The variant of conformal traceless ADM formalism (compare [SN95, BS99]) that I use has the following five variables:

The conformal factor

$$\psi^4 = (\det \gamma_{ij})^{1/3} \quad (\text{A.13})$$

The conformal metric

$$\tilde{\gamma}_{ij} = \psi^{-4} \gamma_{ij} \quad (\text{A.14})$$

$$\text{where thus } \det \tilde{\gamma}_{ij} = 1 \quad (\text{A.15})$$

The trace of the extrinsic curvature:

$$K = K_i^i \quad (\text{A.16})$$

The traceless extrinsic curvature (this is only an intermediate quantity):

$$A_{ij} = K_{ij} - \frac{1}{3} \gamma_{ij} K \quad (\text{A.17})$$

$$\text{where thus } A_i^i = 0 \quad (\text{A.18})$$

The conformal traceless extrinsic curvature:

$$\tilde{A}_{ij} = \psi^2 A_{ij} \quad (\text{A.19})$$

$$\text{where thus } \tilde{A}_i^i = 0 \quad (\text{A.20})$$

Quantities with a tilde  $\tilde{\cdot}$  have their indices raised and lowered using the conformal metric  $\tilde{\gamma}_{ij}$ . Equations (A.15) and (A.20) form two additional, algebraic constraints.

### A.2.2 Time evolution

The time evolution equations for the ctADM quantities follow in a straightforward way from their definitions, and from the time evolution equations of the ADM quantities.

The time evolution of the conformal factor is given by

$$\partial_t \psi = -\frac{1}{6} \alpha \psi K + \beta^l \psi_{,l} + \frac{1}{6} \psi \beta^l_{,l} \quad (\text{A.21})$$

## A Equations

The time evolution of the conformal metric is given by

$$\begin{aligned} \partial_t \tilde{\gamma}_{ij} &= -2\alpha\psi^{-6}\tilde{A}_{ij} \\ &\quad + \tilde{\gamma}_{lj}\beta^l_{,i} + \tilde{\gamma}_{il}\beta^l_{,j} + \beta^l\tilde{\gamma}_{ij,l} - \frac{2}{3}\tilde{\gamma}_{ij}\beta^l_{,l} \end{aligned} \quad (\text{A.22})$$

The time evolution of the trace of the extrinsic curvature is given by

$$\partial_t K = -\Delta\alpha + \alpha [R + K^2] + \beta^l K_{,l} \quad (\text{A.23})$$

Here  $\Delta$  denotes the covariant Laplace operator  $\nabla^l\nabla_l$ .

The time evolution of the traceless extrinsic curvature (an intermediate quantity) is given by

$$\partial_t A_{ij} = \partial_t K_{ij} - \frac{1}{3}\partial_t (\gamma_{ij}K) \quad (\text{A.24})$$

$$= -\nabla_i\nabla_j\alpha + \alpha [R_{ij} - 2K_{il}K^l_j + KK_{ij}] \quad (\text{A.25})$$

$$+ K_{lj}\beta^l_{,i} + K_{il}\beta^l_{,j} + \beta^l K_{ij,l}$$

$$- \frac{1}{3} [-2\alpha K_{ij} + \gamma_{lj}\beta^l_{,i} + \gamma_{il}\beta^l_{,j} + \beta^l\gamma_{ij,l}] K$$

$$- \frac{1}{3}\gamma_{ij} [-\Delta\alpha + \alpha [R + K^2] + \beta^l K_{,l}]$$

$$= -(\nabla_i\nabla_j\alpha)^{\text{TF}} + \alpha (R_{ij})^{\text{TF}} \quad (\text{A.26})$$

$$+ \alpha [-2A_{il}A^l_j]$$

$$+ A_{lj}\beta^l_{,i} + A_{il}\beta^l_{,j} + \beta^l A_{ij,l}$$

Here  $(X_{ij})^{\text{TF}}$  denotes the tracefree part of  $X_{ij}$  with respect to the physical metric, i.e.  $X_{ij} - \frac{1}{3}\gamma_{ij}\gamma^{lm}X_{lm}$ .

The time evolution of the conformal traceless extrinsic curvature is given by

$$\partial_t \tilde{A}_{ij} = \partial_t (\psi^2 A_{ij}) \quad (\text{A.27})$$

$$= 2\psi \left( -\frac{1}{6}\alpha\psi K + \beta^l\psi_{,l} + \frac{1}{6}\psi\beta^l_{,l} \right) A_{ij} \quad (\text{A.28})$$

$$+ \psi^2 \left( -(\nabla_i\nabla_j\alpha)^{\text{TF}} + \alpha (R_{ij})^{\text{TF}} \right)$$

$$+ \psi^2 \left( \alpha \left[ -2A_{il}A^l_j + \frac{1}{3}A_{ij}K \right] \right)$$

$$+ \psi^2 \left( A_{lj}\beta^l_{,i} + A_{il}\beta^l_{,j} + \beta^l A_{ij,l} \right)$$

$$= -\psi^2 (\nabla_i\nabla_j\alpha)^{\text{TF}} + \alpha\psi^2 (R_{ij})^{\text{TF}} \quad (\text{A.29})$$

$$- 2\alpha\psi^{-6}\tilde{A}_{il}\tilde{A}^l_j$$

$$+ \tilde{A}_{lj}\beta^l_{,i} + \tilde{A}_{il}\beta^l_{,j} + \beta^l\tilde{A}_{ij,l} + \frac{1}{3}\tilde{A}_{ij}\beta^l_{,l}$$



### A.2.3 Constraints

The conformal Hamiltonian constraint can be written as

$$\tilde{H} = \tilde{\Delta}\psi - \frac{1}{8}\psi\tilde{R} - \frac{1}{12}\psi^5K^2 + \frac{1}{8}\psi^{-7}\tilde{A}_{ij}\tilde{A}^{ij} \quad (\text{A.30})$$

The conformal momentum constraint can be written as

$$\tilde{M}_i = \tilde{\nabla}^j\tilde{A}_{ij} - \frac{2}{3}\psi^6\tilde{\nabla}_iK \quad (\text{A.31})$$

Note that that these two constraints contain different scaling factors than the ADM constraints (A.9) and (A.10). These two formulations of the constraints cannot readily be compared to each other.

### A.2.4 Enforcing the constraints

In order to enforce the constraints, one can extend the system of ctADM variables with a vector potential  $V_i$  for the conformal traceless extrinsic curvature [Coo02, section 2.2.1]. This leads to the modified conformal traceless extrinsic curvature

$$\tilde{A}_{ij} = \tilde{A}_{ij}^* + (\tilde{L}V)_{ij} \quad (\text{A.32})$$

where the operator  $\tilde{L}$  is the longitudinal derivative with respect to the conformal metric, defined by

$$(\tilde{L}V)_{ij} = \tilde{\nabla}_iV_j + \tilde{\nabla}_jV_i - \frac{2}{3}\tilde{\gamma}_{ij}\tilde{\nabla}^kV_k \quad (\text{A.33})$$

which makes the gradient  $(\tilde{L}V)_{ij}$  symmetric and tracefree.

Given a conformal metric  $\tilde{\gamma}_{ij}$ , a mean curvature  $K$  and a background conformal traceless extrinsic curvature  $\tilde{A}_{ij}^*$ , one can enforce the constraints by solving the constraint equations for the conformal factor  $\psi$  and the vector potential  $V_i$ . This vector potential and the background conformal traceless extrinsic curvature then define the real conformal traceless extrinsic curvature  $\tilde{A}_{ij}$  through (A.32).

### A.2.5 Gauge condition

I introduce the traceless conformal metric

$$\bar{h}_{ij} = \tilde{\gamma}_{ij} - \frac{1}{3}\delta_{ij}\delta^{kl}\tilde{\gamma}_{kl} \quad (\text{A.34})$$

The bar  $\bar{\cdot}$  is used to indicate that the indices are to be raised and lowered using the coordinate metric  $\delta_{ij}$ .

The gauge variable is

$$F_i = \bar{h}_{ij,j} \quad (\text{A.35})$$

which is close to what Shibata and Nakamura use in [SN95].

## A Equations

The gauge condition should constrain the conformal metric, and the conformal metric already has to satisfy the constraint  $\det \tilde{\gamma}_{ij} = 1$ . Enforcing the gauge condition will change the conformal metric, but one has to make sure that it does not change its determinant. By making the gauge condition independent of the trace of the conformal metric, one can later change the trace to adjust its determinant to one.

### A.2.6 Enforcing the gauge condition

Enforcing the gauge condition on the trace of the extrinsic curvature  $K$  is trivial.

The method that I use to enforce the gauge on the conformal metric is similar to the method used to enforce the constraints. I extend the system of ctADM variables with a vector potential  $W_i$  for the traceless conformal metric. This leads to the modified traceless conformal metric

$$\bar{h}_{ij} = \bar{h}_{ij}^* + (\bar{L}W)_{ij} \quad (\text{A.36})$$

where the operator  $\bar{L}$  is the longitudinal derivative with respect to the coordinate metric, i.e. using partial derivatives. It is defined by

$$(\bar{L}W)_{ij} = W_{j,i} + W_{i,j} - \frac{2}{3}\delta_{ij}W_{k,k} \quad (\text{A.37})$$

which makes the gradient  $(\bar{L}W)_{ij}$  symmetric and tracefree.

The gauge condition is then

$$F_i = \bar{h}_{ij,j}^* + W_{i,jj} + \frac{1}{3}W_{j,ij} \quad (\text{A.38})$$

Given a background traceless conformal metric  $\bar{h}_{ij}^*$ , one can enforce the gauge condition on the metric by solving the gauge equation (A.38) for the vector potential  $W_i$ . This vector potential and the background traceless conformal metric, together with the constraint  $\det \tilde{\gamma}_{ij} = 1$  from which the trace of the conformal metric is calculated, then define the real conformal metric  $\tilde{\gamma}_{ij}$  through (A.36).

### A.2.7 Determining lapse and shift

The gauge condition implicitly determines the lapse and shift.

One differentiates the gauge conditions with respect to time, and then uses the time evolution equations for the trace of the extrinsic curvature  $\partial_t K$  and for the conformal metric  $\partial_t \tilde{\gamma}_{ij}$  to arrive at a set of coupled elliptic equations for the lapse and shift.

The equation for the lapse  $\alpha$  is immediately given by (A.23). The equation for the shift  $\beta^i$  is largish, but not very enlightening, and I omit most of it here. The fact that it is so complicated seems to point to the fact that there should be a more elegant gauge condition. The terms containing second derivatives of the shift are

$$\partial_t F_i \simeq \tilde{\gamma}_{ik}\beta_{,jj}^k + \frac{1}{3}\tilde{\gamma}_{jk}\beta_{,ij}^k - \frac{2}{3}\tilde{\gamma}_{ij}\beta_{,jk}^k + \frac{2}{9}\tilde{\gamma}_{jj}\beta_{,ik}^k \quad (\text{A.39})$$

$$= \tilde{\gamma}_{ik}\beta_{,jj}^k + \frac{1}{3}\tilde{\gamma}_{jk}\beta_{,ij}^k - \frac{2}{3}\bar{h}_{ij}\beta_{,jk}^k \quad (\text{A.40})$$

These terms look sufficiently close to being elliptic that one can hope that the equation is well-posed. The numerical experiment shows that this seems to be the case.

# B Numerics

## B.1 Spatial discretisation

I discretise the quantities on a Cartesian grid. I approximate the partial derivatives by second order centred derivatives. This is among the most simple possible discretisation methods.

## B.2 Time integration

I integrate in time with an explicit second order integrator, using the iterative Crank–Nicholson scheme [Teu00]. For that I usually use two iterations after the initial Euler step. For some experiments I use only one iteration after the Euler step, which turns this scheme into the midpoint rule, or a second order Runge–Kutta. This is one of the most simple possible second-order time integrators.

Given the ordinary differential equation

$$\frac{d}{dt}f(t) = u[t, f(t)] \quad (\text{B.1})$$

the midpoint rule uses the time stepping scheme

$$f_n^{(1)} := f_{n-1} + h u[t_{n-1}, f_{n-1}] \quad (\text{B.2})$$

$$f_n^{(2)} := f_{n-1} + h u\left[\frac{1}{2}(t_{n-1} + t_n), \frac{1}{2}(f_{n-1} + f_n^{(1)})\right] \quad (\text{B.3})$$

$$f_n := f_n^{(2)} \quad (\text{B.4})$$

to advance from  $f_{n-1}$  to  $f_n$  with the step size  $h$ .  $f_n^{(1)}$  is an intermediate quantity.

Similarly, the iterative Crank–Nicholson method uses the time stepping scheme

$$f_n^{(1)} := f_{n-1} + h u[t_{n-1}, f_{n-1}] \quad (\text{B.5})$$

$$f_n^{(i)} := f_{n-1} + h u\left[\frac{1}{2}(t_{n-1} + t_n), \frac{1}{2}(f_{n-1} + f_n^{(i-1)})\right] \quad (\text{B.6})$$

$$f_n := \lim_{i \rightarrow \infty} f_n^{(i)} \quad (\text{B.7})$$

where the limes is usually only taken up to  $i = 3$ . The first step is a simple Euler step. All other right hand sides are evaluated at the half-time  $t_{n-1} + \frac{h}{2}$ .

### B.2.1 Artificial viscosity

The advection terms in the time derivatives, i.e. those terms involving the shift  $\beta^i$ , are unstable when discretised as above and integrated with the midpoint rule. I therefore add artificial diffusion to the right hand sides of the time evolution equations. I implement two kinds of artificial diffusion, of which one depends on the shift:

$$(\partial_t f)_{\text{AD}} = \sum_i \left( C_{\text{ADV}} \frac{|\beta^i|}{2} + C_{\text{SM}} \right) dx^i f_{,ii} \quad (\text{B.8})$$

with  $0 \leq C_{\text{ADV}} \lesssim 1$  and  $0 \leq C_{\text{SM}} \lesssim 1$ . The quantity  $dx^i$  is the grid spacing. These two viscosities are explained below.

The first kind, ADV, which depends on the shift, transforms the centred differencing advection terms into first order upstream differencing terms when  $C_{\text{ADV}} = 1$ . In one dimension this follows as follows:

$$\beta \partial_x^{\text{us}} f \equiv \Theta(\beta) \beta \frac{f(x+h) - f(x)}{h} + \Theta(-\beta) \beta \frac{f(x) - f(x-h)}{h} \quad (\text{B.9})$$

$$= (\beta + |\beta|) \frac{f(x+h) - f(x)}{2h} \quad (\text{B.10})$$

$$- (-\beta + |-\beta|) \frac{f(x) - f(x-h)}{2h} \quad (\text{B.11})$$

$$= \beta \frac{f(x+h) - f(x-h)}{2h} + |\beta| \frac{f(x+h) - 2f(x) + f(x-h)}{2h} \quad (\text{B.12})$$

$$= \beta \partial_x f + \frac{|\beta|}{2} h \partial_{xx} f \quad (\text{B.13})$$

where  $h$  is the grid spacing. The first line is the first order upstream difference. I use the Heaviside-function  $\Theta(x)$  which has the value 0 for  $x < 0$  and 1 for  $x > 0$ . It is also  $2|x|\Theta(x) = x + |x|$ .

The second kind of artificial diffusion, SM, is a generic smoothing operator, and is independent of the shift. It is necessary in some simulations. I found that, without this diffusion, the system of equations is unstable against high frequency noise, and the amplification rate depends on the grid resolution. This points to either a bad discretisation scheme, or an ill-posed problem already at the physical level. I did not want to examine this kind of instability any further, so I decided to remove it by using some suitable artificial diffusion.

Both kinds of artificial diffusion terms remove high frequency modes, making the simulation stable against such noise. They also dissipate energy, dampening the amplitude of gravitational waves. They introduce a second order error into the system, turning it into a first order correct system only.

### B.3 Elliptic integration

In order to transform the constraints and the gauge conditions into elliptic equations, I add vector potentials to the set of equations. That means that enforcing the constraints requires going back and forth between different representations, and that introduces discretisation errors.

### B.3.1 Variable transformations

The step of introducing the vector potentials does not introduce errors, as the vector potentials are set to zero initially. However, going back to the original system then does introduce discretisation errors. This can be demonstrated by using the prototype of a constraint equation

$$F_i = \partial_j h_{ij} \quad . \quad (\text{B.14})$$

I first introduce a vector potential  $W_i$ , leading to

$$h_{ij} = h_{ij}^* + \partial_j W_i \quad . \quad (\text{B.15})$$

This turns the constraint equation into

$$F_i' = \partial_j h_{ij}^* + \partial_{jj} W_i \quad , \quad (\text{B.16})$$

which is now elliptic in  $W_i$ . It can be solved to arbitrary accuracy. Note that  $F_i$  and  $F_i'$  have fundamentally different properties.

After solving  $F_i'$  for  $W_i$ , one calculates the new  $h_{ij}$  from its definition (B.15). This requires taking a first derivative of  $W_i$ . In order to evaluate the original constraint  $F_i$ , one has to take a first derivative of  $h_{ij}$ , which contains then two successive first derivatives of  $W_i$ . This is, on the discrete level, quite different from the constraint  $F_i'$ , which involves taking one second derivative of  $W_i$ . Both these steps introduce different discretisation errors. That means, even after solving  $F_i'$  to very high accuracy,  $F_i$  will still contain an error of the order of the discretisation error. Furthermore, taking two successive first derivatives tends to introduce a high frequency noise.

This problem might be eliminated by using staggered grids. On a staggered grid, two consecutive first derivatives are the same as one second derivative.

#### Double first derivatives

Using two consecutive first derivatives for solving the equations would be unstable. A second order centred first derivative has the stencil weights

$$-\frac{1}{2} \quad 0 \quad +\frac{1}{2} \quad (\text{B.17})$$

while a second derivative has the weights

$$+1 \quad -2 \quad +1 \quad (\text{B.18})$$

Taking two consecutive first derivatives leads to an effective stencil with the weights

$$+\frac{1}{4} \quad 0 \quad -\frac{1}{2} \quad 0 \quad +\frac{1}{4} \quad (\text{B.19})$$

Stencil (B.19) contains two zeros. If one calculates the derivative of e.g. an even-numbered grid point, then only other even-numbered grid points contribute. This decouples odd- and even-numbered grid points. If one uses this stencil while solving an elliptic equation, then one obtains effectively two independent solutions, namely one for the odd, and one for the even grid points. These solutions are coupled through their initial data and boundary conditions only and will differ slightly. Going from one grid point to the next, one jumps between these two solutions, and that is equivalent to a high frequency mode.

### B.3.2 Elliptic solvers

Solving elliptic equations is expensive. The elliptic solver needs the majority (more than 90%) of the total computing time in the Tiger code. This is partly my fault, as I use methods that are known to be subideal and very slow.

Currently I use PETSc [BBG<sup>+</sup>01, BGMS01, BGMS97] to solve the elliptic equations. PETSc uses a Newton-like method to reduce the nonlinear equations to linear ones, and then uses Krylov-subspace methods to solve these. I calculate the Jacobian that is necessary for the Newton-like method numerically. This is known to be a very expensive operation; it is about ten to twenty times slower than a hand-coded Jacobian. On the other hand, hand-coded Jacobians would need to be written and debugged.

I also have a simple iterative Jacobi solver for testing purposes. This solver is only a toy, and is only usable for very small problems.

I estimate that a nonlinear multigrid solver would be several orders of magnitude faster than the way I (ab)use PETSc, as it does not need to calculate the Jacobian. An experimental implementation of a nonlinear full approximation storage multigrid solver for the two-dimensional Poisson equation with excision shows promising results.

## B.4 Coding equations

As mentioned in section 7.1, I chose to code the equations by hand instead of using a symbolic algebra package. This only makes sense because it is possible to make the computer code look sufficiently close to an explicit mathematical notation. The standard mathematical notation used in general relativity is full of context-sensitive abbreviations, such as the Einstein sum convention, that cannot be used in an unambiguous notation.

One of the key points to obtain a readable source code is to make use of the local character of the equations, leading to a *pointwise* programming style. A tensor such as  $K_{ij}$  is really a tensor field  $K_{ij}(x^k)$ , which becomes a grid function  $K_{ij}(x, y, z)$  after discretisation. Dealing with a set of five indices ( $i, j, x, y, z$ ) at the same time leads to an awkward notation. Hence I chose to deal with one grid point at a time only.

As an example, I present the code for one of the more complicated equations, namely the time evolution equation of the extrinsic curvature. It is given in appendix A.1.2 as:

$$\begin{aligned} \partial_t K_{ij} = & -\nabla_i \nabla_j \alpha + \alpha \left[ R_{ij} - 2K_{il}K_j^l + KK_{ij} \right] \\ & + K_{lj}\beta_{,i}^l + K_{il}\beta_{,j}^l + \beta^l K_{ij,l} \end{aligned} \quad (\text{B.20})$$

When translated into a Fortran subroutine for Cactus, this equation becomes

```
subroutine calc_extcurv_dot &
  (gu, ri, kk, dkk, alfa, ggalfa, beta, dbeta, kk_dot)
  CCTK_REAL, intent(in)  :: gu(3,3)
  CCTK_REAL, intent(in)  :: ri(3,3)
  CCTK_REAL, intent(in)  :: kk(3,3), dkk(3,3,3)
  CCTK_REAL, intent(in)  :: alfa, ggalfa(3,3)
  CCTK_REAL, intent(in)  :: beta(3), dbeta(3,3)
  CCTK_REAL, intent(out) :: kk_dot(3,3)
```

```

integer :: i,j,k,l
! K_ij,t = - D_i D_j alpha
!           + alpha [ R_ij - 2 K_ik K^kj + K K_ij ]
!           + K_kj d_i beta^k + K_ik d_j beta^k + beta^k d_k K_ij
do i=1,3
  do j=1,3
    kk_dot(i,j) = - ggalfa(i,j) + alfa * ri(i,j)
    do k=1,3
      do l=1,3
        kk_dot(i,j) = kk_dot(i,j) &
          - 2*alfa * gu(k,l) * kk(i,k) * kk(j,l) &
          +   alfa * gu(k,l) * kk(k,l) * kk(i,j)
      end do
      kk_dot(i,j) = kk_dot(i,j) &
        + kk(k,j) * dbeta(k,i) + kk(i,k) * dbeta(k,j) &
        + beta(k) * dkk(i,j,k)
    end do
  end do
end do
end subroutine calc_extcurv_dot

```

In the above routine, the variables  $gu$ ,  $ri$ , etc. represent the corresponding tensors at a single point in the time slice only. This routine is called once for every grid point for every right hand side evaluation. Such a coding convention needs powerful compilers and optimisers to yield good performance, and likely cannot be used on vector machines. This also shows that programming styles are heavily influenced by the current software and hardware technology. However, I strove for clarity and simplicity rather than for performance.

*B Numerics*



# C Definitions

## C.1 Glossary of terms

**Agave:** A numerical code for the vacuum Einstein equations, descending from the Grand Challenge

**Cactus:** A framework for solving three-dimensional time-dependent systems of partial differential equations, see [ABD<sup>+</sup>01, ABG<sup>+</sup>01, Cac]

**coordinate condition:** A condition that determines lapse  $\alpha$  and shift  $\beta^i$  (equivalent to the term *gauge condition*)

**excision:** A method to treat singularities. One cuts a region of the spacetime that contains the singularity out of the simulation domain, introducing an inner boundary. This is possible as long as the boundary is located within the event horizon. As no physical information can propagate out of the event horizon, the details of how the excision boundary is handled cannot influence the simulation outside the event horizon

**gauge condition:** A condition that determines lapse  $\alpha$  and shift  $\beta^i$  (equivalent to the term *coordinate condition*)

**gauge evolution condition:** A choice of lapse  $\alpha$  and shift  $\beta^i$  that imposes no restrictions on the three-metric  $\gamma_{ij}$  and extrinsic curvature  $K_{ij}$ . For example, geodesic slicing ( $\alpha = 1$ ) is a gauge evolution condition

**gauge fixing condition:** A condition on the three-metric  $\gamma_{ij}$  and extrinsic curvature  $K_{ij}$  that also leads to a prescription for lapse  $\alpha$  and shift  $\beta^i$  via the ADM time evolution equations. For example, maximal slicing ( $K = 0$ ) is a gauge fixing condition

**Maya:** A numerical code, descending from Agave, see [Pen]

**performance:** (of a code) the quality of the result of a simulation, i.e. a measure of the magnitude of the numerical errors. This has nothing to do with the speed of the code on a particular hardware

**punctures:** A method to treat singularities. The singularity is contained in a conformal factor  $\psi$ , and all other quantities can be chosen so that they remain finite. This is the case e.g. for Brill–Lindquist black holes (see section 6.3.1). The singularity is placed in between grid points. The conformal factor and its derivatives are known analytically. With maximal slicing ( $K = 0$ ) and normal coordinates ( $\beta^i = 0$ ), the conformal factor is then constant in time

**robust stability:** A practical definition for the notion of stability of a code that can be tested empirically. See [SGBW00, SSW02]

## C Definitions

**Tiger:** A numerical code, descending from Maya

**time slice:** Another term for a spacelike hypersurface

## C.2 Abbreviations

**ADM:** Arnowitt–Deser–Misner. An initial–boundary–value formulation for the Einstein equations, see [ADM62]

**AEI:** the Albert–Einstein–Institut in Golm near Potsdam, Germany

**BH:** black hole

**BSSN:** Baumgarte–Shapiro–Shibata–Nakamura. An ADM-like initial–boundary–value formulation for the Einstein equations, see [NOK87, NO89, SN95, BS99]

**ctADM:** conformal traceless ADM system

**KST:** the Kidder–Scheel–Teukolsky system; see [KST<sup>+</sup>00]

**MPI:** Max–Planck–Institut, e.g. the AEI, which is also called the Max–Planck–Institut für Gravitationsphysik

**MTW:** the book *Gravitation* by Misner, Thorne, and Wheeler; see [MTW73]

**NS:** neutron star

**PSU:** Penn State University

**TAT:** Theoretische Astrophysik Tübingen, the Abteilung für Theoretische Astrophysik in the Institut für Astronomie und Astrophysik of the Fakultät für Mathematik und Physik at the Eberhard–Karls–Universität Tübingen (yes, this is in Germany)

**TGR:** the name of the Tübingen General Relativity (Tiger) code

## C.3 Symbols

It goes without saying that Greek letters denote four-vector indices  $0 \dots 3$ , while Latin letters denote three-vector indices  $1 \dots 3$ . I follow the sign conventions of MTW [MTW73].

### Four-quantities:

$\eta_{\mu\nu}$  Minkowski metric.  $\eta_{\mu\nu} = \text{diag}(-1, +1, +1, +1)$

$g_{\mu\nu}$  four-metric

$G_{\mu\nu}$  Einstein tensor

$T_{\mu\nu}$  energy density tensor

### Three-quantities:

$\delta_{ij}$  identity tensor.  $\delta_{ij} = \text{diag}(+1, +1, +1)$   
 $\gamma_{ij}$  three-metric, see appendix A.1.1  
 $K_{ij}$  extrinsic curvature, see appendix A.1.2  
 $\alpha$  lapse, see appendix A.1.1  
 $\beta^i$  shift, see appendix A.1.1  
 $\Gamma_{jk}^i$  connection coefficients, see appendix A.1.3  
 $\Gamma^i$  contracted connection coefficients.  $\Gamma^i = \gamma^{jk}\Gamma_{jk}^i$   
 $R_{ij}$  Ricci tensor, see appendix A.1.3  
 $H$  Hamiltonian constraint, see appendix A.1.4  
 $M_i$  momentum constraint, see appendix A.1.4

**Conformal quantities:**

$\tilde{\phantom{x}}$  a tilde denotes a conformal quantity, which has its indices raised and lowered with the conformal metric  
 $\psi$   $\psi^4$  is the conformal factor, see appendix A.2.1  
 $\tilde{\gamma}_{ij}$  conformal three-metric, see appendix A.2.1  
 $K$  trace of the extrinsic curvature, see appendix A.2.1  
 $A_{ij}$  traceless extrinsic curvature, see appendix A.2.1  
 $\tilde{A}_{ij}$  conformal traceless extrinsic curvature, see appendix A.2.1  
 $V_i$  vector potential for the extrinsic curvature, see appendix A.2.4

**Coordinate quantities:**

$\bar{\phantom{x}}$  a bar denotes a coordinate quantity, which has its indices raised and lowered with the coordinate metric (i.e.  $\delta_{ij}$  for Cartesian coordinates)  
 $\bar{h}_{ij}$  traceless conformal three-metric, see appendix A.2.5  
 $F_i$  gauge condition for the metric, akin to a constraint variable, see appendix A.2.5  
 $W_i$  vector potential for the traceless three metric, see appendix A.2.6

## *C Definitions*

# Bibliography

- [ABD<sup>+</sup>01] Gabrielle Allen, Werner Bengler, Thomas Dramlitsch, Tom Goodale, Hans-Christian Hege, Gerd Lanfermann, André Merzky, Thomas Radke, and Edward Seidel, *Cactus grid computing: Review of current development*, Euro-Par 2001: Parallel Processing, Proceedings of the 7th International Euro-Par Conference (R. Sakellariou, J. Keane, J. Gurd, and L. Freeman, eds.), Springer, 2001.
- [ABG<sup>+</sup>01] Gabrielle Allen, Werner Bengler, Tom Goodale, Hans-Christian Hege, Gerd Lanfermann, André Merzky, Thomas Radke, Edward Seidel, and John Shalf, *Cactus tools for grid applications*, Cluster Computing **4** (2001), 179–188.
- [ACM<sup>+</sup>95] Peter Anninos, Karen Camarda, Joan Massó, Edward Seidel, Wai-Mo Suen, and John Towns, *Three-dimensional numerical relativity: The evolution of black holes*, Phys. Rev. D **52** (1995), 2059–2082.
- [ADM62] R. Arnowitt, S. Deser, and C. W. Misner, *The dynamics of general relativity*, Gravitation: an introduction to current research (Louis Witten, ed.), John Wiley & Sons, Inc., 1962.
- [All] The Binary Black Hole Grand Challenge Alliance, *The binary black hole coalescence grand challenge*, <http://www.npac.syr.edu/projects/bh/>.
- [app] *Comparing apples with apples*, web site (in preparation), <http://www.appleswithapples.org/>.
- [BB97] Steven Brandt and Bernd Brügmann, *A simple construction of initial data for multiple black holes*, Phys. Rev. Lett. **78** (1997), 3606–3609.
- [BBG<sup>+</sup>01] Satish Balay, Kris Buschelman, William D. Gropp, Dinesh Kaushik, Lois Curfman McInnes, and Barry F. Smith, *PETSc home page*, <http://www.mcs.anl.gov/petsc>, 2001.
- [BCG<sup>+</sup>00] Steve Brandt, Randall Correll, Roberto Gomez, Mijan Huq, Pablo Laguna, Luis Lehner, Pedro Marronetti, Richard A. Matzner, David Neilsen, Jorge Pullin, Erik Schnetter, Deirdre Shoemaker, and Jeffrey Winicour, *Grazing collisions of black holes via the excision of singularities*, Phys. Rev. Lett **85** (2000), 5496–5499.
- [BCL02] John Baker, Manuela Campanelli, and Carlos Lousto, *The Lazarus project: A pragmatic approach to binary black hole evolutions*, Phys. Rev. D **65** (2002), 044001.
- [BGMS97] Satish Balay, William D. Gropp, Lois Curfman McInnes, and Barry F. Smith, *Efficient management of parallelism in object oriented numerical software libraries*, Modern Software Tools in Scientific Computing (E. Arge, A. M. Bruaset, and H. P. Langtangen, eds.), Birkhauser Press, 1997, pp. 163–202.

## Bibliography

- [BGMS01] ———, *PETSc users manual*, Tech. Report ANL-95/11 - Revision 2.1.1, Argonne National Laboratory, 2001.
- [BM88] Charles Bona and Joan Massó, *Harmonic synchronization of spacetime*, Phys. Rev. D **38** (1988), 2419–2422.
- [Bri59] Dieter R. Brill, *On the positive definite mass of the Bondi-Weber-Wheeler time-symmetric gravitational waves*, Ann. Phys. **7** (1959), 466–483.
- [BS99] Thomas W. Baumgarte and Stuart L. Shapiro, *On the numerical integration of Einstein's field equations*, Phys. Rev. D **59** (1999), 024007.
- [Cac] The Cactus Team, *The Cactus computational toolkit*, <http://www.cactuscode.org/>.
- [Cho91] Matthew W. Choptuik, *Consistency of finite-difference solutions of Einstein's equations*, Phys. Rev. D **44** (1991), 3124–3135.
- [Col] The Agave Collaboration, *The Agave code*, (outdated, no known references).
- [Coo02] Gregory B. Cook, *Initial data for numerical relativity*, Living Reviews in Relativity **3** (2000 [Online article: cited on 10 Jun 2002]), no. 5, <http://www.livingreviews.org/Articles/Volume3/2000-5cook/>.
- [DKSS] Olaf Dreyer, Badri Krishnan, Deirdre Shoemaker, and Erik Schnetter, *Introduction to Isolated Horizons in Numerical Relativity*, Phys. Rev. D (to be published).
- [Eva89] Charles R. Evans, *Enforcing the momentum constraints during axisymmetric spacelike simulations*, Frontiers in numerical relativity (Charles R. Evans, Lee S. Finn, and David W. Hobill, eds.), Cambridge University Press, 1989, pp. 194–205.
- [Fra98] Jörg Frauendiener, *Numerical treatment of the hyperboloidal initial value problem for the vacuum Einstein equations. I. The conformal field equations*, Phys. Rev. D **58** (1998), 064002.
- [Haw02] Scott Hawley, *Notes from the Mexico meeting*, web pages, 2002, <http://www.aei.mpg.de/~shawley/Mexico/>.
- [HCM00] Mijan F. Huq, Matthew W. Choptuik, and Richard A. Matzner, *Locating boosted Kerr and Schwarzschild apparent horizons*, gr-qc/0002076, 2000.
- [KLL<sup>+</sup>01] Bernard Kelly, Pablo Laguna, Keith Lockitch, Jorge Pullin, Erik Schnetter, Deirdre Shoemaker, and Manuel Tiglio, *A cure for unstable numerical evolutions of single black holes: adjusting the standard ADM equations*, Phys. Rev. D **64** (2001), 084013.
- [KST<sup>+</sup>00] Lawrence E. Kidder, Mark A. Scheel, Saul A. Teukolsky, Eric D. Carlson, and Gregory B. Cook, *Black hole evolution by spectral methods*, Phys. Rev. D **62** (2000), 084032.
- [LS02] Pablo Laguna and Deirdre Shoemaker, *Numerical stability of a new conformal-traceless 3 + 1 formulation of the Einstein equation*, Class. Quantum Grav. **19** (2002), 3679–3686.
- [Map] *Maple*, Birkhauser, 175 Fifth Ave, New York, NY 10010.
- [MC96] Robert L. Marsa and Matthew W. Choptuik, *Black-hole–scalar-field interactions in spherical symmetry*, Phys. Rev. D **54** (1996), 4929–4943.

- [MHS99] Richard A. Mazner, Mijan F. Huq, and Deirdre Shoemaker, *Initial data and coordinates for multiple black hole systems*, Phys. Rev. D **59** (1999), 024015.
- [MNS02] Claudia Moreno, Darío Núñez, and Olivier Sarbach, *Kerr-schild type initial data for black holes with angular momenta*, To appear in Class. Quantum Grav., 2002.
- [MTW73] Charles W. Misner, Kip S. Thorne, and John Archibald Wheeler, *Gravitation*, W. H. Freeman and Company, 1973.
- [NO89] T. Nakamura and K. Oohara, *Methods in 3D numerical relativity*, Frontiers in Numerical Relativity (Charles R. Evans, Lee S. Finn, and David W. Hobill, eds.), Cambridge University Press, 1989, pp. 254–280.
- [NOK87] T. Nakamura, K. Oohara, and Y. Kojima, *General relativistic collapse to black holes and gravitational waves from black holes*, Prog. Theor. Phys. Suppl. **90** (1987), 1–218.
- [O’B75] Richard O’Brien, *The rocky horror picture show*, Motion picture by 20th Century Fox, 1975.
- [Pen] Penn State Numerical Relativity Group, *The Maya project: Computational infrastructure to solve Einstein’s equations*, <http://www.astro.psu.edu/nr/research.html>.
- [Pol01] Denis Pollney, *Gauge techniques for numerical relativity*, <http://www.aei.mpg.de/~koppitz/proceedings/talks.html> (Am Mühlenberg 5, 14476 Golm, Germany), Max-Planck-Institut für Gravitationsphysik, 2001.
- [PTVF92] William H. Press, Saul A. Teukosky, William T. Vetterling, and Brian P. Flannery, *Numerical recipes in FORTRAN*, Cambridge University Press, Cambridge, 1992 (english).
- [Sal02] Marcelo Salgado, *Taller de rel. num.*, web pages, 2002, [http://www.nuclecu.unam.mx/~gravit/main\\_rn.html](http://www.nuclecu.unam.mx/~gravit/main_rn.html).
- [Sch02] Erik Schnetter, *A fast apparent horizon algorithm*, gr-qc/0206003, 2002.
- [SGBW00] Béla Szilágyi, Roberto Gómez, Nigel T. Bishop, and Jeffrey Winicour, *Cauchy boundaries in linearized gravitational theory*, Phys. Rev. D **62** (2000), 104006.
- [Shi97] M. Shibata, *Apparent horizon finder for a special family of spacetimes in 3d numerical relativity*, Phys. Rev. D **55** (1997), 2002.
- [SHM00] Deirdre M. Shoemaker, Mijan F. Huq, and Richard A. Matzner, *Generic tracking of multiple apparent horizons with level flow*, Phys. Rev. D **62** (2000), 124005.
- [SN95] Masaru Shibata and Takashi Nakamura, *Evolution of three-dimensional gravitational waves: Harmonic slicing case*, Phys. Rev. D **52** (1995), 5428–5444.
- [SSW02] Béla Szilágyi, Bernd Schmidt, and Jeffrey Winicour, *Boundary conditions in linearized harmonic gravity*, Phys. Rev. D **65** (2002), 064015.
- [SU00] M. Shibata and K. Uryu, *Apparent horizon finder for general three-dimensional spaces*, Phys. Rev. D **62** (2000), 087501.

## Bibliography

- [SY78] Larry Smarr and James W. York, Jr., *Kinematical conditions in the construction of spacetime*, Phys. Rev. D **17** (1978), 2529–2551.
- [SY02] Hisa-aki Shinkai and Gen Yoneda, *Re-formulating the Einstein equations for stable numerical simulations*, gr-qc/0209111, 2002.
- [Teu00] Saul A. Teukolsky, *On the stability of the iterated Crank-Nicholson method in numerical relativity*, Phys. Rev. D **61** (2000), 087501.
- [Tho93] Jonathan Thornburg, *Numerical relativity in black hole spacetimes*, Ph.D. thesis, University of British Columbia, 3 1993.
- [Tho96] ———, *Finding apparent horizons in numerical relativity*, Phys. Rev. D **54** (1996), 4899–4918.
- [Wal84] Robert M. Wald, *General relativity*, The University of Chicago Press, 1984.
- [Wei72] Steven Weinberg, *Gravitation and cosmology*, John Wiley & Sons, 1972.
- [Wes92] Pieter Wesseling, *An introduction to multigrid methods*, John Wiley & Sons, 1992.
- [Win02] Jeffrey Winicour, *Characteristic evolution and matching*, Living Reviews in Relativity **4** (2001 [Online article: cited on 26 Oct 2002]), no. 3, <http://www.livingreviews.org/Articles/Volume4/2001-3winicour/>.
- [Yor73] J. W. York, Jr., *Conformally invariant orthogonal decomposition of symmetric tensors on Riemannian manifolds and the initial-value problem of general relativity*, J. Math. Phys. **14** (1973), 456–464.
- [Yor74] ———, *Covariant decompositions of symmetric tensors in the theory of gravitation*, Ann. Inst. Henri Poincaré A **21** (1974), 319–332.



And crawling on the planet's face  
Some insects called the human race  
Lost in time, and lost in space  
And meaning.

RHPS [O'B75]